HIGH TEMPERATURE PHASE EQUILIBRIA IN THE Fe-Co-Cu-Si SYSTEM PERTINENT TO SLAG CLEANING

by

WEZI BANDA

Dissertation presented for the Degree

of

DOCTOR OF PHILOSOPHY

(EXTRACTIVE METALLURGICAL ENGINEERING)

in the Department of Process Engineering

at the University of Stellenbosch

PROMOTERS

Prof. J. J. Eksteen (University of Stellenbosch)

Prof. C. Lang (University of Cape Town)

Prof. L. Lorenzen (University of Stellenbosch)

Stellenbosch
December 2006

DECLARATION

I, the undersigned, declare that this dissertation is my own original work, except where specifically acknowledged in text. Neither the present dissertation nor any part thereof has been submitted previously at any other university.

_____

W Banda

SUMMARY

In the smelting of copper waste slags to recover cobalt and copper, the prediction of the metal liquidus temperature and the associated superheat for liquid metal handling for subsequent treatments cannot be done with certainty, making the management of furnace integrity very difficult. By studying the phase equilibria and solution thermodynamics in liquid ferrocobalt new experimental data on the liquidus temperature and phase equilibria of the quaternary system can contribute to the improvement of existing copper slag smelting processes. This will alleviate the operational uncertainties and difficulties associated with ferrocobalt production in electric arc furnaces.

There is no specific literature available that describes the physicochemical and thermochemical properties of the ferrocobalt produced from smelting of waste copper slags. Therefore, the quaternary system Fe-Co-Cu-Si has been characterised by studying and reviewing the binary and ternary subsystems with respect to the high temperature phase equilibria.

The ferrocobalt metal has been modelled on the Fe-Co-Cu-Si quaternary system. The liquidus temperatures and phase equilibria in the Fe-Co-Cu-Si system, within the composition and temperature regimes pertinent to smelting of slag, were investigated by differential thermal analysis and metallography. Drop-quench techniques coupled with scanning electron microscopy were used to study the phase equilibria. The activity of silicon in liquid Fe-Co-Cu-Si at 1450 °C was calculated from gas-alloy-silica equilibrium experiments conducted in controlled oxygen partial pressure atmospheres at 10^{-13}, 10^{-14}, and 10^{-15} atmosphere (absolute) corresponding to the conditions found in the industrial application.

The liquidus temperature of the quaternary Fe-Co-Cu-Si is influenced by the content of silicon in the system. When silicon is added to the Fe-Co-Cu ternary the liquidus temperature is lowered in the new system (Fe-Co-Cu-Si). In the range of silicon content studied $(0 < X_{Si} \leq 0.1)$, the liquidus temperature decreased by over 70 °C. The liquidus temperature profiles of the subsystems of the quaternary Fe-Co-Cu-Si, show large composition dependence too, except in the Fe-Co system. In the ternary Fe-Co-Cu, the liquidus temperature decreases with increasing copper content and is characteristic of the profiles of the liquidus lines in the binary subsystems Fe-Cu and Co-Cu.

In the dilute concentrations of silicon, it is shown that the phase equilibria in the quaternary system have attributes of the Fe-Si and Fe-Cu-Si systems. Silicon is associated more with the iron rich phase than it is with the copper rich phase. It stabilises the metastable liquid immiscibility when added to the Fe-Cu, Co-Cu, and Fe-Co-Cu in the corresponding ternary systems Fe-Cu-Si, Co-Cu-Si and quaternary Fe-Co-Cu-Si system.

The activity of silicon in liquid Fe-Co-Cu-Si at 1450 °C, in the composition range 1 to 5 wt. %Si exhibits a negative deviation from ideal liquid solution behaviour. The activity coefficient approaches a constant value of 0.2×10^{-3}, with pure liquid silicon as reference state, as the silicon concentration approaches zero implying a Henrian solution behaviour. This information should be useful in the thermodynamic modelling of the system.

OPSOMMING

Die smelting van afval koper slakke om kobalt en koper te herwin, word gekenmerk deur ‘n tekort aan inligting om die smeltpuntskromme temperatuur van die gevormde legering te voorspel, asook die gepaardgaande legering superverhitting, wat die bestuur van die oondintegriteit belemmer. Deur die fase-ewewigte en oplossingstermodinamika van gesmelte ferrokobalt te bestudeer, maak nuwe eksperimentele data oor die smeltpuntskromme temperature en fase ewewigte ‘n beduidende bydrae om huidige koper slak smeltingsprosesse te verbeter, en om van die bedryfsonsekerhede en probleme wat gepaard gaan met elektriese boogoonde te verminder.

Daar is geen spesifieke literatuur beskikbaar oor die fisies-chemiese en termochemiese eienskappe van industriële ferrokobalt nie, met spesifieke verwysing na die smelting van afval koperslakke. Vervolgens is die Fe-Co-Cu-Si kwaternêre sisteem gekarakteriseer deur die binêre en têrnêre subsisteme te bestudeer met betrekking tot hul hoë temperatuur fase ewewigte.

Die industriële ferrokobalt is gebaseer op die vereenvoudigde Fe-Co-Cu-Si kwaternêre sisteem. Die smeltpuntskromme temperature en fase-ewewigte in die Fe-Co-Cu-Si sisteem, binne die samestelling- en temperatuurgebiede van belang tot afval slak smelting, was bestudeer deur differensiële termiese analise (DTA) en metallografiese tegnieke. Die fase-ewewigte was ook bestudeer bet behulp van die hoë tempo blus van die gesmelte legerings gevolg deur ‘n skanderingselektronmikroskopie-studie van die legerings. Verder is die termodinamiese aktiwiteit van silikon in gesmelte Fe-Co-Cu-Si legerings bepaal by 1450 °C gebaseer op gas-metaal-silika ewewigseksperimente gedoen onder beheerde suurstof parsiële druk omgewings van 10^{-13}, 10^{-14}, en 10^{-15} atmosfeer ooreenstemmend met die kondisies van industriële toepassing.

Die smeltpuntskromme temperature van die kwaternêre Fe-Co-Cu-Si legerings word primêr beïnvloed deur die silikon-inhoud van die sisteem. Wanneer silikon tot die Fe-Co-Cu têrnêre sisteem toegevoeg word, verlaag dit die smeltpuntskromme temperature beduidend om die nuwe Fe-Co-Cu-Si sisteem te vorm. In die samestellingsgebied van silikon wat bestudeer is, $(0 < X_{Si} \leq 0.1)$, het die smeltpuntskromme temperature tipies met meer as 70°C gedaal. Verder toon die smeltpuntskromme temperature profiele van die Fe-Co-Cu-Si legerings en al sy onderliggende binêre en têrnêre sisteme ‘n sterk samestellingsafhanklikheid, met uitsondering

van die Fe-Co binêre sisteem. In die têrnêre Fe-Co-Cu sisteem, daal die smeltpuntskromme temperature met toenemende koperinhoud en toon dit ooreenstemmings met die binêre Fe-Cu en Co-Cu sisteme.

Vir lae konsentrasies silikon, is daar gevind dat die fase ewewig van die kwaternêre sisteem ooreenkomste toon met die Fe-Si en Fe-Cu-Si sisteme. Silikon assosieer tipies meer met die ysterryke fase as met die koperryke fase. Verder stabiliseer silikon die metastabiele vloeistyof onmengebaarheid van die Fe-Cu-, Co-Cu en Fe-Co-Cu sisteme in die ooreenstemmende têrnêre sisteme Fe-Cu-Si, Co-Cu-Si en die kwaternêre sisteem Fe-Co-Cu-Si.

Die termodinamiese aktiwiteit van silikon in gesmelte Fe-Co-Cu-Si by 1450°C, in die samestellingsgebied van 1 tot 5 gewig % Si toon ‘n negatiewe afwyking van ideale oplossing gedrag. Die aktiwiteitskoëffisiënt benader ‘n konstante waarde van 0.2×10^{-3} relatief tot suiwer vloeistof Si soos die silikon konsentrasie streef na oneindige verdunning, en dus Henriaanse oplossingsgedrag toon. Hierdie inligting is dan van nut in die termodinamiese modellering van die sisteem.

To my parents,

Washington Kamutumba Malimba Banda (late) and Lyness Skambayao Khonje

For their wise advice

ACKNOWLEDGEMENTS

First and foremost I would like to acknowledge Mintek for the financial support towards this study and Prof. Jacques Eksteen for according me the opportunity to study under his supervision. I further acknowledge Professors Jacques Eksteen and Leon Lorenzen for their support and advice during the course of the degree.

The support and encouragement I received from Prof. Candy Lang was unprecedented. The cooperation and support of the members of staff and fellow students at the materials engineering department of University of Cape Town was enabling made it possible for me to accomplish the experimental objectives needed for the differential thermal analysis and the necessary metallography.

I am indebted to Dr. Johan Nell of Mintek for his guidance and genuine interest in the study. His critique and technical advice during our lengthy meetings and discussions improved the scope of the subject for the dissertation.

The technical aspect of analytical analyses was achieved with the help of Mr. Mark Reid and Prof. Riaan Dipenaar of the University of Wollongong for the analysis of the ternary alloys using HLSCM techniques and MTData calculations. Mr Bernard Joja of Mintek and Ms. Esmé Spicer of the Geology Department of the University of Stellenbosch, helped with the SEM/EDS techniques.

Lastly but not the least I would like to thank my wife, Tebogo, for her patience, endurance and trust during the long and demanding period of studying, and for taking care of matters in my absence. To my mother whose parenting I cherish and is the reason of my being here today, to Thomas for his encouragement and support, and the family as a whole for believing in me.

To all my friends who got off their tight schedules to assist me and in a way contributed to this work, I say thank you.

TABLE OF CONTENTS

CHAPTER 1

INTRODUCTION

Back in time in the early 20th century, the cost of copper production by smelting and converting justified it to be produced preferentially to the by-product cobalt. This meant that metals like cobalt ended up in the slag and discarded. The development of technology for recovering metals from the slag was then costly as well as challenging because of the high operating temperatures required to smelt the slag to recover cobalt (Whyte *et al.* 1977). Advancements in the construction of smelting furnaces and new refractory materials have overcome the past challenges albeit with newer challenges (Curr *et al*. 1983). The challenges associated with the recent technologies relate to the optimisation of the recovery of cobalt and copper at high operating temperatures and aggressive acidic slag that affect the integrity of the furnace refractory lining. An industrial application of this technology is the electric furnace at Chambishi in Zambia. It is a direct current (dc) single electrode furnace that is used to recover cobalt and copper from a blend of old reverbaratory and converter slags.

The production of copper from copper-containing minerals in the reverbaratory furnace is a smelting and settling principle followed by matte converting to remove sulphur. The matte phase (Cu-Fe-S) is immiscible with the slag and settles to the bottom upon formation. To maintain the immiscibility between matte and slag, silica (SiO_2) is added as a flux to near silica saturation of slag without which, the matte phase is completely miscible in the iron oxide slag. The losses of the matte to the slag would result in cobalt alongside copper partitioning to the slag and can only be recovered by recycling of the slag. Subsequent treatment of the matte is the conversion to blister copper in a converter furnace where the sulphide matte is converted to oxide blister copper and the iron oxide report to the slag. Losses of copper at this stage are due to the depleted iron sulphide (FeS) in the matte resulting in the formation of magnetite and conversion of the white metal (Cu_2S) to copper oxide. As a consequence cobalt ends up in the waste slag which is high in iron and almost saturated with silica. An extensive discussion on how these losses occur has been presented by Imriš (1982) who particularly investigated the distribution of cobalt during the smelting of copper ore concentrates in the Nkana (formerly Rokana) smelter.

The advancements in pyrometallurgical technology have facilitated the recovery of pay metals from slags by high temperature reduction smelting processes known as slag cleaning. During the

slag cleaning of copper slags, cobalt and copper are recovered in an iron-rich alloy[1] called ferrocobalt. The behaviour of this ferrocobalt at high operating temperatures and the phase equilibria associated with it is not established let alone fully understood.

In most smelting furnaces and particularly open arc electric furnaces, operations are carried out at superheat conditions above the liquidus temperatures of both slag and metal phases (Kongoli *et al*. 1998). The slag liquidus temperature being lower than that of the metal phase in the smelting of waste slags, makes it to possesses a relatively higher superheat during the smelting process, which exacerbates the problems associated with management of the furnace integrity. As a result demand on managing the energy to the furnace increases and failure of which leads to losses of refractory lining. Such incidents are the causes of the "runaway" losses of molten furnace contents, reduced furnace campaigns and raise the costs of production.

Operating the furnace at such conditions therefore, requires a good knowledge of the reaction mechanisms of the smelting process in general, and the thermodynamic data of the liquid slag phase and the corresponding liquid metal phase. It is worthy emphasising here that the reaction mechanisms that describe the smelting processes are kinetics driven and their derivation requires an initial understanding of the thermodynamic properties such as activities and energies of formation and mixing of the involved phases. An understanding of the influence of changes in composition of both the slag and the metal phases on liquidus temperatures is important in the operation of smelting units and can contribute to the effective use of energy in the smelting process, resulting in reduced production costs and prolonged furnace campaigns.

1.1 Scope of the Study

The scope of the study is outlined in the following paragraphs. The description of the occurrence of metals in the slag and the methods of recovering these metals, particularly cobalt and copper in an iron rich phase is presented first. It is followed by the description of the behaviour of cobalt during slag cleaning based on the available literature.

[1] In this study the term *alloy* refers to metallic product from the smelting of waste copper slags, particularly the Fe-Co-Cu-Si system, and not its usual meaning.

1.1.1 Recovery of Valuable Metals from Slags

Metals in slag are generally encountered as a dispersed phase of entrained metal phases (matte or pure metal) or as dissolved species in the form of sulphide or oxide existing in a single homogeneous phase (Imriš 1982). The latter form is prevalent in slags from processes involving high-grade mattes typical of converter slags and is only recoverable by chemical reduction. Other methods such as settling can be employed to recover copper and nickel when they are not entrained and dispersed finely in slag.

During converting of matte, cobalt follows iron and invariably partitions to the converter slag or to the smelter slags if converter slags are returned to the smelter. From these slags, cobalt can be recovered as an alloy or a matte by reductive smelting in an electric furnace. Recent studies (Banda *et al*. 2002; Banda *et al*. 2004; Jones *et al*. 2001; Yucel *et al*. 1992) on the subject of slag cleaning show that carbothermic reduction smelting in DC plasma-arc furnaces can be applied as a post treatment of copper smelter slags to recover cobalt and copper metals. The past studies focused on the slag chemistry and the modification of it to maximise the recovery of cobalt from the slag. They do not address the behaviour of cobalt in the product alloy.

1.1.2 Thermodynamic Behaviour of Cobalt in Slag Cleaning

Teague *et al.* (1999) studied the thermodynamic properties of cobalt oxide in slags and within the same work, a review of activity and activity coefficient of cobalt oxide at controlled oxygen partial pressures was reported. The focus of their work was on the distribution of cobalt between metal and slag. They calculated the activity coefficient of cobalt oxide in slag and in relation to the calcium-ferrite slags and iron-silicate slags. Kongoli and Pelton (1999) studied the cobalt behaviour between matte and slag in copper making. However, the past studies do not address the thermodynamics in the ferrocobalt alloy.

1.2 Hypothesis of the Study

Despite the extensive research carried out on the behaviour of cobalt, iron and copper during the smelting of copper concentrates and the converting of the matte as well as the recovery of these metals from the waste slag, no experimental data on ferrocobalt alloy is available. However, from the published resources on the binary and ternary alloy systems of the Fe-Co-Cu-Si one can develop an understanding of the thermodynamics in the ferrocobalt alloy.

It is suggested that in smelter operations where cobalt is recovered from copper waste slags, the unpredictable thermal behaviour of liquid metal can be attributed to a lack of experimental data on the physical and thermodynamic properties of the Fe-Co-Cu-Si system. Even if it is obvious from temperature-composition studies of metallic alloys that the liquidus temperature of the ferrocobalt alloy can be affected by variations in alloy composition, it is not obvious what difference this change in composition would make between having a wide or narrow temperature range of the liquidus and solidus temperatures. The physical state of ferrocobalt system can be liquid over a wide temperature range but could solidify over a narrow range of composition change due to impurity contamination such as silicon, or increased copper, cobalt or iron content influenced by the changing furnace conditions.

Since the ferrocobalt alloy is rich in iron and contains silicon as an impurity among others such as sulphur and carbon, a lower liquidus temperature would be indicative of high silicon (impurity) content. On the other hand, if no contamination was assumed, then the lower liquidus temperature may imply lower iron content and higher copper content in the system. The distribution of silicon, which originates from silica-rich fayalite slag, between the iron rich phase and copper rich phase is another important factor to consider because of its effect on the solubility of copper in iron and its effect on stabilising miscibility gaps in the transition group metal alloys. If the activity of silica increases in the molten slag the presence of silicon in alloy increases too. Apart from affecting the liquidus temperature of the ferrocobalt its presence would influence the phase equilibria due to the increased activity, depending on how it partitions between the iron-rich phase and the copper rich phase.

1.3 Objectives of the study

The objectives listed below were set up and studied by experiments in the iron rich section of the Fe-Co-Cu-Si system to characterise the ferrocobalt alloy with respect to composition and temperature.

- Determine the liquidus and solidus temperatures of ferrocobalt over the composition range pertinent to smelting of copper slags.
- Determine the phase equilibria in Fe-Co-Cu-Si system at high temperatures pertinent to smelting,
- Investigate the behaviour of silicon in ferrocobalt during slag cleaning in relation to extent of reducing conditions and temperature.

1.4 Outline of Thesis

A background on copper making, how copper and the co-products (cobalt) are lost to the slag during smelting and converting of copper bearing minerals is compiled in chapter 2. In this chapter the recovery of the metals from the slag by slag cleaning is presented. The experimental techniques used in the study are described in chapter 3 followed by the results and discussions in chapter 4. Conclusions drawn from the study are summarised in chapter 5.

CHAPTER 2
LITERATURE REVIEW

This chapter examines the binary and ternary subsystems of the quaternary Fe-Co-Cu-Si system for the published thermodynamic data and phase diagrams. Also presented are the solution thermodynamic models essential to the description of the phase equilibria in multicomponent systems. A general background is presented on the process of copper smelting and matte converting in the reverbaratory furnace and convertor. The first section in this chapter is a general background on the process of copper making discussing the critical stages at which metals are lost to the slag. The subsequent treatment of waste slag by high temperature smelting to recover cobalt is presented and discussed. The fundamental thermodynamics governing the process of slag cleaning are reviewed as well.

The methods of studying phase equilibria are discussed on the basis of their merits, particularly on thermal analysis. The review of literature includes phase diagram calculations and derivation of thermodynamic information from published data. The applicability of these methods to the current study regarding the underlying theory of phase equilibria is considered.

2.1 An overview of metal losses during copper making

Imriš (1982) addressed the distribution of metals in slags at the smelting and converting stages of copper making. The losses occur at two stages of copper making; smelting in a reverbaratory furnace which is mainly a settling unit and in convertor furnace during matte conversion to blister copper. In the reverbaratory furnace the losses are mainly of matte phases and pure metals whereas in the convertor furnace the losses are in the form of oxides due to extensive air blowing to remove sulphur from the matte.

Teague *et al.* (1999) studied the activity and activity coefficients of cobalt oxide in calcium ferrite and iron silicate slags, after Grimsey and Toguri (1988). They found that the losses of metals to the slag during smelting and converting can be reduced by minimising the content of silica in the slag and the formation of magnetite. The activity coefficient of solid cobalt oxide decreases with increasing silica content in iron silicate slags.

The occurrence of metals in the slag influences the methods selected for their subsequent recovery. The metals of interest to this study are cobalt and copper which are contained as chemically dissolved metals and/or mechanically entrained in the slag as metallic prills (Imriš 1982; Pirard 1991). In the high temperature (pyrometallurgy) route using electric furnaces these metals are recovered by a carbothermic reduction process into an iron-rich metallic phase.

The literature on the subject of slag cleaning is focussed on slag manipulation to optimise the recovery of metals as discussed in the following section.

2.2 Recovery of cobalt and copper from slags

The literature on the subject of slag cleaning focuses on slag chemistry manipulation by using carbonaceous reductants and a suite of fluxes to selectively recover cobalt and copper. An iron-rich alloy; referred to as ferroalloy (or ferrocobalt when referring to the valuable metal cobalt) is produced from the slag cleaning process. Jones *et al.* (2001) studied the recovery of cobalt in a direct current (DC) arc furnace. They reported a mechanism of cobalt reduction in which iron oxide (magnetite) is reduced by carbon to iron and then cobalt oxide reduced by iron to cobalt metal. This mechanism was based on the occurrence of cobalt as an oxide in that the magnetite form of iron was present in the slag besides the iron in the fayalite structure. Even if the work by Jones *et al.* (2001) is not specific on the association of cobalt oxide with the fayalite phase as observed in the work by Banda *et al.* (2004), it is worth noting that slag chemistry modification plays an important role in the selective recovery cobalt.

The rate of reduction of fayalite slags by carbonaceous materials (coal) follows a rate-limiting step controlled by the Bourdouard reaction resulting from the carbon monoxide to carbon dioxide (CO/CO_2) gas ratio (Warczok and Utigard 1997). The evolution of the CO and CO_2 gases is dependent on the availability of magnetite (or iron oxide) in the slag for a continuous supply of oxygen (O_2) for carbon to react with. The extent of slag reduction to optimally recover cobalt is accompanied by slag chemistry manipulation to increase the activity of cobalt oxide in the slag as well as to control the activity of iron oxide so that iron is retained in the slag as much as possible (Banda *et al.* 2002). Increased activity of silica and iron oxide in the slag is inevitable at this stage and results in increased dissolution of silicon in the ferroalloy.

The physical properties of the slag have been reported extensively, including the liquidus temperatures of the slags estimated on the major components constituting the process slag (Mackey 1982). Contrary to this is that there is no experimental data available on the physical properties of the ferrocobalt. The report by Jones *et al.* (2001) does not give the liquidus temperature but uses an assumed value between 1500 and 1600 °C based on the melting point of the individual metallic elements iron, cobalt, and copper. The other reported value of the liquidus temperature of the ferrocobalt is 1370 °C (Nelson *et al.* 2004). How this value was determined is not reported, especially the composition relating to this temperature. The lack of published information relating the composition of ferrocobalt and the liquidus temperatures makes it difficult to quantify the values given by Jones *et al.* (2001) and Nelson *et al.* (2004).

Nelson *et al.* (2004) have reported operational problems in DC arc furnace that are related the slag and alloy superheat and that put the furnace integrity at risk. This problem causes increased heat flux on the side walls of the furnace causing thermal stress on the refractory lining and subsequent premature loss of the lining. Again it can be observed that the operating temperatures of furnace are based on temperatures that are supposed to be the liquidus temperatures of the alloy and slag. The operating philosophy of the furnace is to operate above these liquidus temperatures inducing a superheat in the slag of about 400 °C in order to keep the alloy liquid. Now, in a case where the thermodynamics of the alloy and slag are not well understood, the energy supplied to the melt might be overestimated resulting in such problems mentioned by Nelson *et al.* (2004). In the post tap hole operations of slag cleaning the metal fluidity must be sustained. Plasma arcing is used for the purpose of maintaining the ferrocobalt temperatures above the liquidus. The temperature reported by Jones (2001) of 1650 °C to achieve this, is again based on a guess value by assuming the melting temperatures of the individual metallic elements.

A study of the transformation temperatures in the ferrocobalt over a range of composition pertinent to the slag cleaning can resolve the issue of liquidus temperatures and let alone the required superheat at both smelting and reheating stages. The following section describes how the ferrocobalt alloy is characterised on the basis of its components.

2.3 Characterisation of Ferrocobalt

There is no literature specifically describing the physicochemical properties of the ferrocobalt produced in the smelting of the waste slags. The ferrocobalt system is a multicomponent mixture with iron, cobalt, and copper as the major components and the minor components include silicon, carbon and sulphur. The chart in Figure 2.1, constituted from the smelter plant data shows the typical distribution by proportion of the ferrocobalt alloy components. Based on this distribution, the constitution of the quaternary Fe-Co-Cu-Si system has been defined. The system can then be characterised from its subsystems by studying the properties of the binary systems Fe-Co, Fe-Cu, Co-Cu, Fe-Si, Cu-Si, and Co-Si; and the ternary systems Fe-Co-Cu, Fe-Cu-Si, Fe-Co-Si, and Co-Cu-Si.

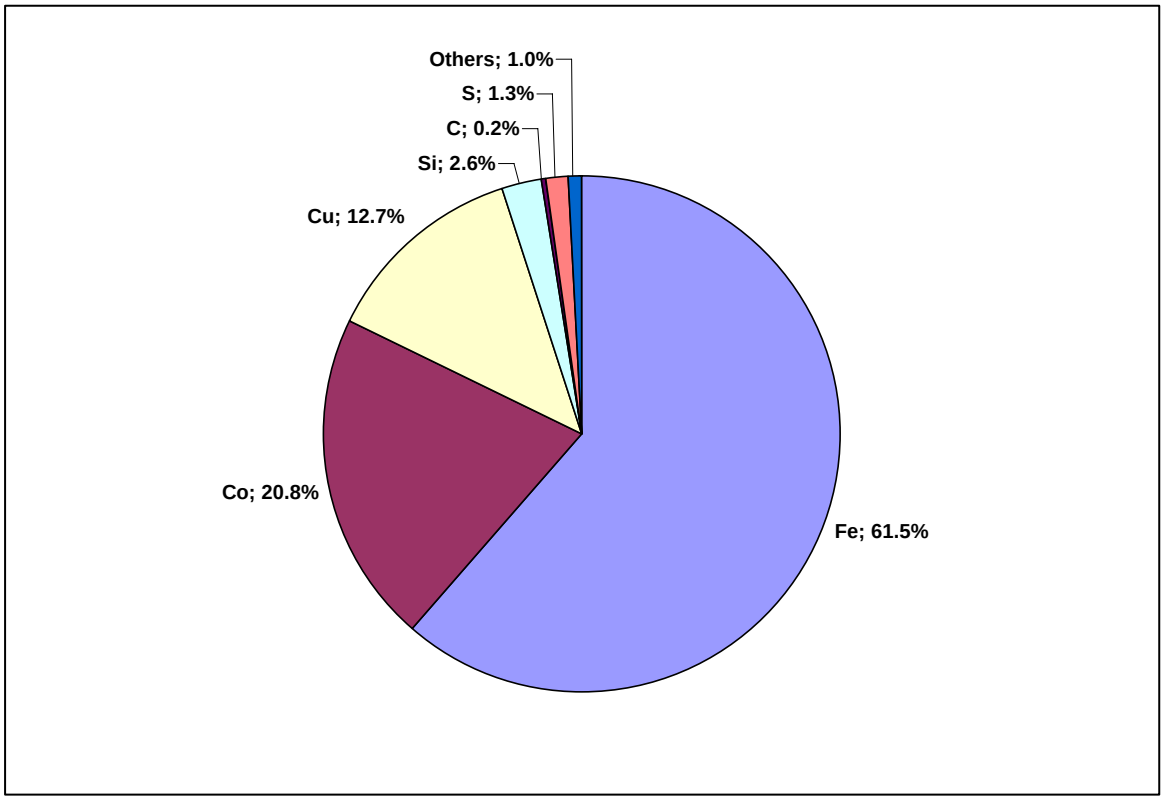

Figure 2.1 The distribution of components in the ferrocobalt alloy ***Source: Chambishi Metals Plc, 2002***

The properties for this system are characterised on the basis of physical transformations of the alloy such as the liquidus and solidus temperatures, phase equilibria, enthalpies of transformation, and activities of the components of the system. This information is derived from published phase diagrams and thermodynamic data where available. Otherwise, experiments are conducted to generate the necessary data. The calculation of phase diagrams on the other hand involves complex mathematical formulations and numerical methods to solve the thermodynamic relations of Gibbs energy minimisation for the description of phases.

Fortunately, the pioneering extensive work by Kaufman and Bernstein (1970) has led to development of computer thermochemistry software that handles the mathematical aspect of this subject. Nevertheless, some experimental data are inconsistent and continued evaluation of the reported phase diagrams forms a huge part in the development of computation thermochemistry (Chang *et al*. 2004) as pointed out in their work and (discussed in Chapter 4) on the calculated liquidus temperatures.

2.4 Methods for studying phase diagrams

Construction of phase diagrams is an art developed as early as the first quarter of the twentieth century. Experiments conducted in the early works included thermal techniques like quenching and electromagnetic methods. However, in the latter part of the twentieth century, mathematical methods using experimental data emerged and have evolved along with the development of computer technology. A comprehensive review covering the principles of phase equilibria in metallic systems has been compiled by Kaye *et al.* (2003). They reviewed the mathematical concept of equilibrium that underlies binary phase diagram construction, and examined the possible methods that provide experimental data useful to modelling. Even if the calculation of phase diagrams has advanced with time, it is still imperative to have access to experimental data to validate some of the calculated phase diagrams (Kaye *et al*. 2003).

In the following sections some of the methods applied in the determination of phase diagrams are discussed and emphasis rendered to the ones used in the current study.

2.4.1 Microscopic phase examination

When the alloys are quenched from elevated temperatures the evolved microstructures can be detected by microscopic methods. The number and identity of the phases in the evolved microstructures can be established (Kuo *et al*. 1990). The compositional information is obtained by using scanning electron microscopy (SEM) coupled with electron dispersive spectroscopy (EDS) or electron probe microanalyser (EPMA). It can be used to locate the ends of the tie lines on the phase diagram. The relative proportions of phases can be determined by using the compositional information obtained by applying the principles of lever rule (West 1982). A complement to this method is X-ray diffraction spectroscopy (XRD) by which metallic phases and crystals can be determined. In phase transformations where there is a change in lattice

parameter with a change in proportions of atoms of different elements, XRD techniques are used to determine the type of lattice present.

2.4.2 Thermal Analysis

Thermal analysis (TA) is a method in which chemical or physical properties of an alloy are measured as a function of temperature or time at controlled supply of heat. Details of how this is used in the current study are described in Chapter 3. Differential thermal analysis (DTA) is a form of TA in which the temperature difference between the specimen and a known reference material is recorded as heat flow[2] that can be plotted against time or temperature. When a solid specimen melts it absorbs heat which is used to promote phase transformation. This causes the specimen to remain at the same temperature whilst the temperature of the reference specimen rises. This transformation is indicated as an endotherm on a plot of differential temperature (ΔT) versus time or temperature, if the specimen and reference are exposed to a constant heating rate. The advantage of DTA over normal TA is that it does not yield slopes on the temperature-time curves, Figure 2.2. The normal TA measures a single temperature. The evaluation of the exotherm and endotherm peaks is easier on the DTA curve than on normal TA curve (Schwendt 1997).

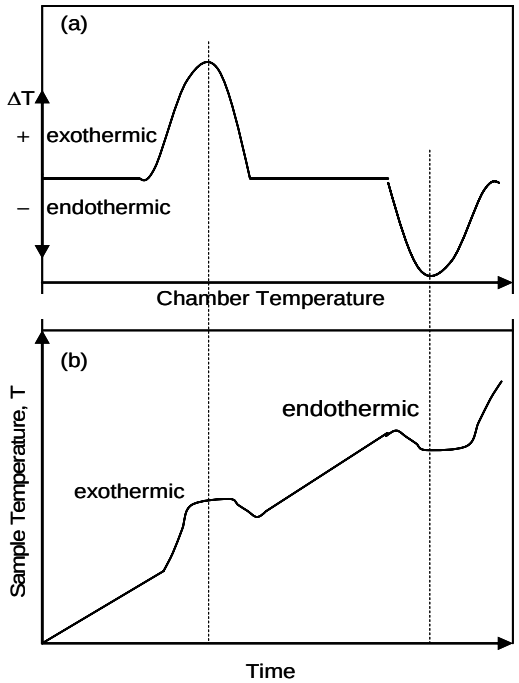

Figure 2.2 Comparison of (a) DTA and (b) normal TA. After Schwendt (1997)

[2] The relationship between heat and temperature follows ohm's law for a steady-state one-dimensional conductive heat flow; $dQ/dt = k'(T_2 - T_1) = k'\Delta T$, *k'* is the proportionality constant.

The physical characteristics of a DTA signal can distinguish between a physical and chemical transition and decomposition in a specimen, as illustrated in Figure 2.3. A physical transition is indicated by a narrow peak (width or sharpness) whereas a chemical one will be wider. A decomposition trace will be indicated by the zig-zag-shaped curve. Melting of a solid represents a physical transformation, and a chemical transformation can be an allotropic change in a phase (for example, α-Fe$\rightarrow\gamma$-Fe). Decomposition is associated with vaporisation of the specimen upon melting. It is also noteworthy to mention here that the area under the curve depends on the mass of the reactive sample, its thermal conductivity, shape and form of sample as well as the reaction enthalpy.

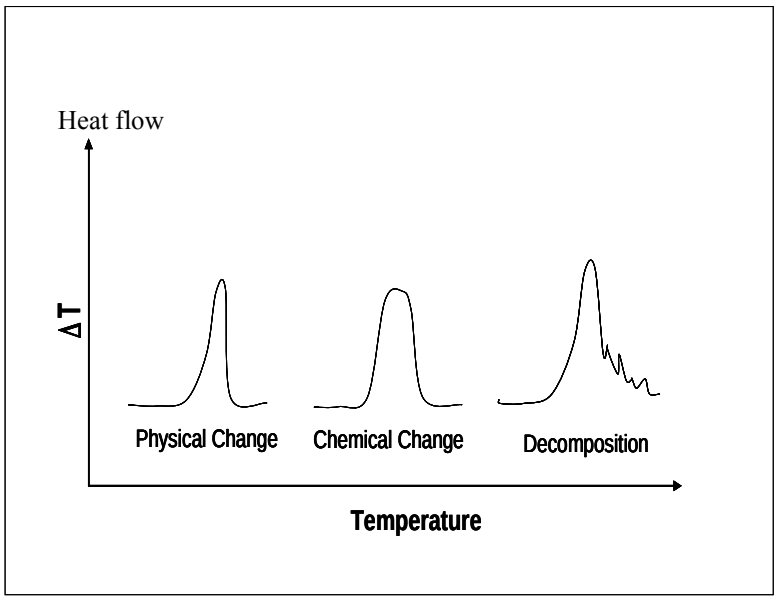

Figure 2.3 Characteristics of DTA signal after Schwendt (1997)

The use of DTA method for determining the liquidus temperatures has its shortfalls such as solid segregation developments, sluggish solid-state diffusion and undercooling problems that may contribute to inaccurate liquidus temperature measurement (Wu and Perepezko 2000). Undercooling is a phenomenon by which solidification takes place at temperatures below the liquidus temperatures. To prevent the occurrence of these effects the measurements for the liquidus temperatures are recorded on the heating cycles. Even with careful calibration, compositional segregation associated with the complex solidification and non-equilibrium microstructural constituents is likely to take place in ascast alloys. To eliminate this effect a method called "interrupted DTA" in which an isothermal period is introduced to allow for equilibrium between the phases has been suggested (Wu and Perepezko 2000). Wu and Perepezko (2000) examined extensively the applications of the DTA and detailed the shortfalls

associated with it. Their work introduced a concept called "interrupted DTA" which is a method of determining a phase boundary in a multicomponent system.

However, when compared to other methods such as electromagnetic levitation (EML) where pyrometry is used, the DTA technique has a better resolution. In EML technique the error in the measured liquidus temperatures is higher than when DTA is used. For instance, in the work by Bamberger (2002) EML method was used to measure the melting temperature of a copper rich Cu-2Co-2Fe (in wt.%) system. Their results differed by 100 °C for the same alloy composition measured by Maddocks (1936) who used the TA technique and reported the melting temperature to be 1100 °C. This difference in the measurements is a factor of the thermometry. In the DTA, or ordinary TA the thermocouples are in contact with the sample carriers whereas in the EML method the measurement is by radiation relying in the emissivity of the specimen.

2.4.3 High temperature laser scanning confocal microscopy

High temperature laser scanning confocal microscopy (HLSCM) is a technique employing a hot-stage on which a specimen can be heated and observed in-situ and the phase transformation temperatures recorded (Dippenaar and Phelan 2003; Phelan *et al.* 2005). The importance of temperature calibration for this technique is critical especially that the technique is susceptible to fluctuations caused by vapours from the decomposing alloys affecting the efficiency of the infrared heating and the measured temperature offset (Dippenaar and Reid 2004). This method is similar to annealing and quenching techniques and the only difference is that it does not depend on the matters of interpretation arising from phase transformation occurring during quenching. The details of how this technique is utilised in the current study is presented in Chapter 3 and the observations reported in Chapter 4.

The determination of phase transformation temperatures by DTA is comparatively more reliable than by HLSCM because of the positioning of thermocouples. In DTA the temperature sensors are placed underneath the sample and reference crucibles, whereas in the HLSCM the thermocouple is attached to the crucible holder placing it away from the localised infrared heating resulting in offset temperature readings (Dippenaar and Reid 2004).

These experimental methods in combination with quench equilibrium experiments and mathematical concepts described in the following sections contribute to the construction of phase diagrams and description of phase equilibria.

2.5 Phase Equilibria in the Fe-Co-Cu-Si System

The phase equilibria in the quaternary system Fe-Co-Cu-Si can be studied by reviewing phase equilibria studies published for the binary and ternary subsystems. The temperatures and concentrations published by various workers fall outside the regimes of the smelting conditions of copper slags. This renders it necessary to investigate phase equilibria at higher temperatures as defined in the current study.

2.5.1 Considerations on Phase equilibria

The determination of phase equilibria in materials has difficulties and problems associated with the experiments (Macchesney and Rosenberg 1970). Noteworthy issues and the solutions suggested are described in this section.

Accurate proportioning of the starting materials and their homogenisation is normally the first step. By using smaller amounts of starting materials, generally a few milligrams equilibrium can be attained under defined conditions. The other principal source of difficulty is that of accurate temperature measurements. The choice of thermocouples for the appropriate temperature regime is important as their sensitivity will vary with the type of thermocouple wire. These thermocouples must be calibrated periodically to assure accuracy. When it comes to rapid drop and quenching, the specimen can be suspended from heavy supporting wires.

Determination and verification of equilibrium can be judged by observing any of the following. (Macchesney and Rosenberg 1970).

a) General consistency of the data in a case where quality of data is sufficient
b) Microscopy on polished sections should show uniformity
c) Variation in time allowed for equilibrium.

The last method is not reliable due to possible existence of metastable phases (due to metastable equilibrium) that may not be detectable even at prolonged equilibration time. A preferred method to (c) is to approach equilibrium from both sides. To verify that this is the equilibrium phase assemblage, two specimens would be prepared. One quenched from temperatures above liquidus temperature and the other of the same composition annealed at sub solidus temperatures. These

two specimens would then be equilibrated at a temperature and they should yield identical phase assemblage.

2.5.2 Past Work on Phase Equilibria of Fe-Co-Cu-Si system

Literature on the physicochemical properties and thermochemistry of the ferrocobalt produced from the smelting of the waste copper slags is scarce. The literature reviewed is focussed on the phase equilibria studies conducted on the constituent binary and ternary subsystems of the Fe-Co-Cu-Si system. It is summarised based on the liquidus temperatures, liquidus profiles (in the case of binary systems) or surfaces (in the case of ternary systems), energies of transformation, phase equilibria and the assessed thermodynamic parameters. The phase equilibria for the binary and the ternary systems for specific compositions and temperature regimes have been published.

2.5.2.1 The Co-Cu System

This system has a peritectic type phase diagram and limited solid solubility of components in each other. The typical characteristic feature of the phase diagram of the Co-Cu system is the appearance of the liquidus curve which is nearly flat in the composition range 25 to 75% Cu at 1400 °C. This type of liquidus curve is indicative of the system having a tendency of liquid immiscibility depending on the composition and extent of supercooling (Munitz and Abbaschian 1996). In the review by Hansen and Anderko (1958), it is reported that Hashimoto *et al.* (1937) did not observe any liquid miscibility gap in the liquid phase. The phases present in this system are the liquid phase, the α-Co (0 to 20.9 wt.% Cu), and copper (93 to 100 wt.% Cu). The peritectic reaction occurs at 1112 °C.

The most recently assessed phase diagram shown in Figure 2.4 is by Nishizawa and Ishida (1984). The discrepancy in the retrograde solidus between the two studies (Hansen and Anderko (1958) and Nishizawa and Ishida (1984)) is an indication in the uncertainty that exist between calculated and experimentally determined phase diagrams. This was mentioned by Hasebe and Nishizawa (1980) in their thermodynamic studies of the Co-Cu system. The solidus and solubility curves are the main areas of concern in the cobalt rich side. The solidus retrograde can be estimated by relating the melting temperatures of the pure components and the interaction parameters in the solid and liquid phases. There is a dependence of the solidus curve on the difference in magnitude of the melting points of the components and the values of the interaction parameters in the solid phase (Hasebe and Nishizawa 1980).

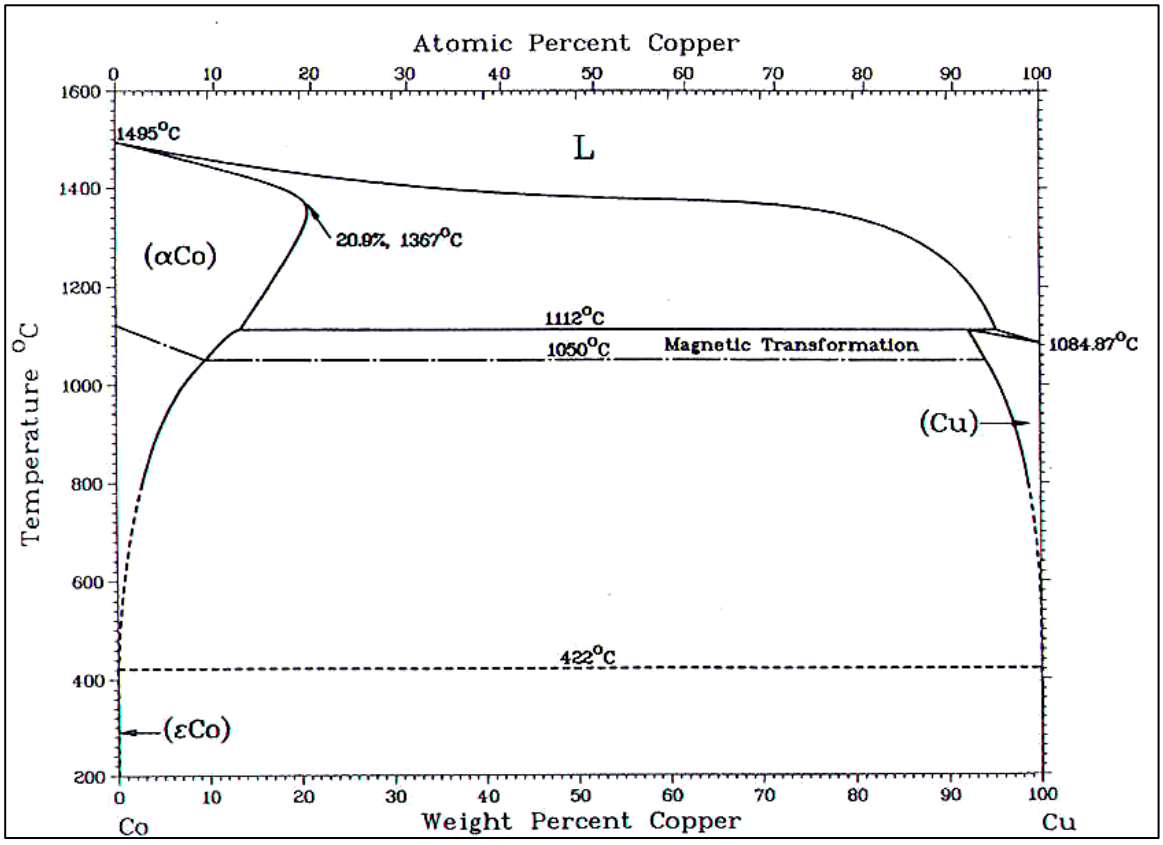

Figure 2.4 The Co-Cu binary phase diagram Nishizawa and Ishida (1984) publiblished by Massalski (2001)

Solution thermodynamics of this system show a positive deviation of the component activities towards the Raoult's law which is also a recipe for liquid immiscibility. The system exhibits a positive enthalpy of formation too (Cao *et al*. 2002; Kubišta and Vrešťál 2000; Nikolaenko and Turchanin 1997).

2.5.2.2 The Fe-Cu System

The liquidus temperature of the binary Fe-Cu system is characterised by a flat portion and has no intermediate compositional phases. There are five equilibrium phases in the Fe-Cu system. An iron-rich high-temperature bcc solid solution (δ-Fe), in the composition range 0 to 7 wt.% Cu, an iron-rich intermediate-temperature fcc solid solution (γ-Fe) at 0 to 13 wt.% Cu, a low-temperature bcc solid solution (α-Fe) in the composition 0 to 2.2 wt.% Cu, the fcc Cu-rich solution (Cu) from 96.7 to 100 wt.% Cu and the liquid phase L. There are two peritectic reactions in the system. The formation of γ-Fe at 1485 °C by the reaction δ-Fe + L = γ-Fe (7, 13, and 8 wt.% Cu), and another one at 1096 °C (8.2, 96.7 and 95.9 wt% Cu) by the reaction γ-Fe +

L = Cu takes place. The Fe-Cu phase diagram in Figure 2.5 shows the phases and the composition limits.

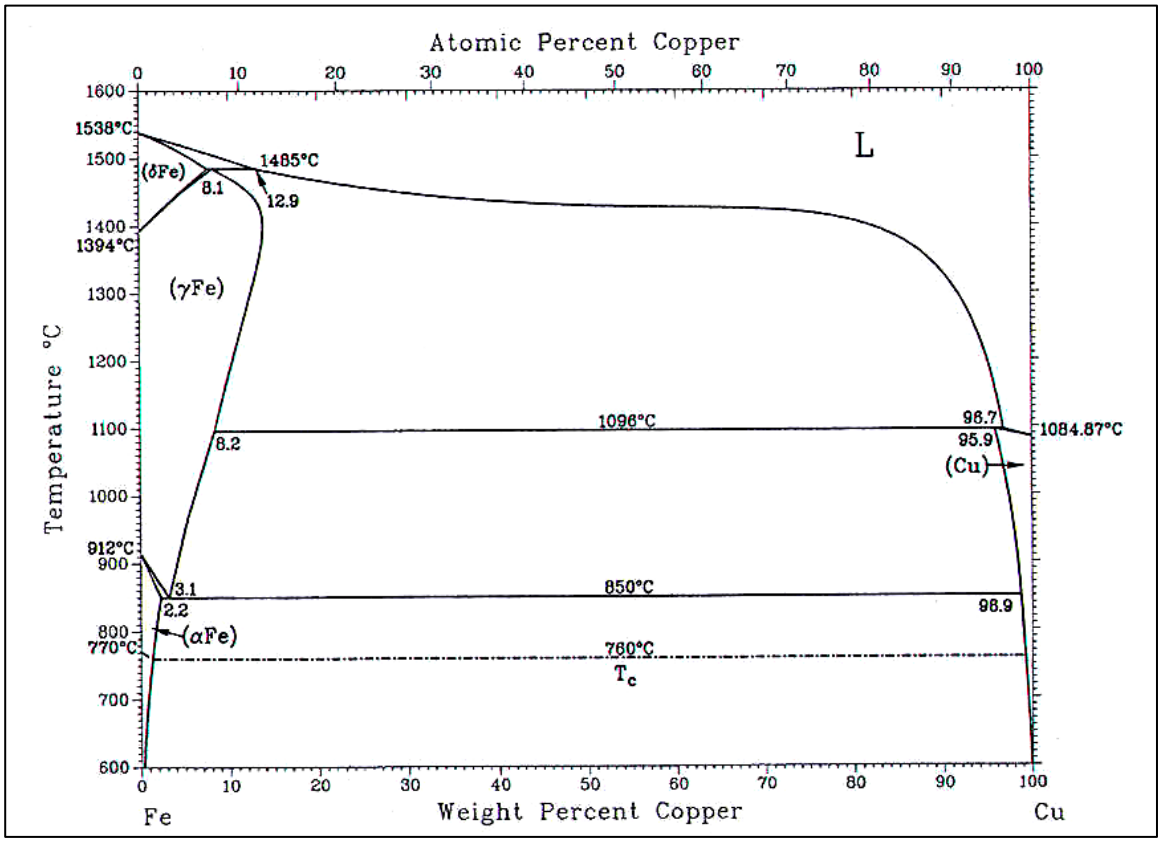

Figure 2.5 The Fe-Cu binary phase diagram after Swartzendruber (1990) publiblished by Massalski (2001)

Hansen and Anderko (1958), did not report the existence of a miscibility gap in the liquid phase. Instead, they reported a liquid segregation caused by contamination with silicon (in a 50 wt.% Cu alloy) and a carbon contamination higher than 0.02 to 0.03 % caused layering in the system. In 1980 Hasebe and Nishizawa (1980) recalculated the binary Fe-Cu system using data generated from examination of the phase boundaries and thermodynamic properties. They reported the existing discrepancies between the experimental data and the calculated ones on the solid solubility of copper in the iron rich side. Copper (Cu) exhibits a retrograde solubility in γ-Fe with a maximum of 14 wt.% Cu at about 1410 °C. The bcc α-Fe phase dissolves 2.2 wt.% Cu at the eutectoid temperature 850 °C and copper dissolves up to 4.1 wt% Fe at the peritectic temperature 1096 °C. Addition of copper to iron tends to stabilise the γ-Fe (fcc) structure and to lower the melting temperature.

As in the Co-Cu system the Fe-Cu system also has a positive enthalpy of formation and is more positive than it is between cobalt and copper (Nikolaenko and Turchanin 1997). Several

researchers have reported the positive deviation of thermodynamic quantities from Raoult's law in the Fe-Cu system albeit with a wide variations with respect to the maximum values and the concentration dependence of the thermodynamic quantities (Turchanin *et al*. 2003). All the evaluations reviewed by Turchanin *et al.* (2003) lack the consistence in accurately reproducing the parameters of phase equilibria and the thermodynamic quantities of the phases, particularly at high temperatures of the phase diagram. The reason given for this discrepancy is the assumption of a zero excess heat capacity of the phases. The majority of the phase transformations in this system occur over a wide range of temperature and composition and thus Turchanin et al. (2003) could not support a zero excess heat capacity.

2.5.2.3 The Fe-Co System

The Fe-Co system shown in Figure 2.6, has a very narrow solidification interval of 2 to 3 °C in the composition range 0 to 70 at.% Fe and a minimum in the liquidus temperature between 30 and 40 at.% Fe at about 1477 °C (Hansen and Anderko 1958). In the solid solution of this system, the α(fcc)-cobalt has continuous solubility with γ-iron over a wide range of temperatures. The α-Fe to γ-Fe (bcc) transformation covers a wide range of composition of cobalt and induces a maximum temperature for this transformation of 985 °C at 46 wt.% Co.

The melting point of the iron and cobalt differ only by 43 °C and the liquid solution is nearly ideal. The activity of cobalt in iron has a very slight deviation from the ideal solution behaviour. The enthalpy of mixing in the Fe-Co system has a negative deviation from ideal (Kongoli and Pelton 1999). From the perspective of the thermodynamic implications of enthalpy of mixing in solution and compound formation, the negative deviation is an indication of the tendency to form ordered compounds and a positive enthalpy of formation indicates the tendency of phase separation. This behaviour is evident in the Fe-Co system which has been shown to form an ordered solid solution (α – α') in the equi-atomic compositions region at about 730 °C.

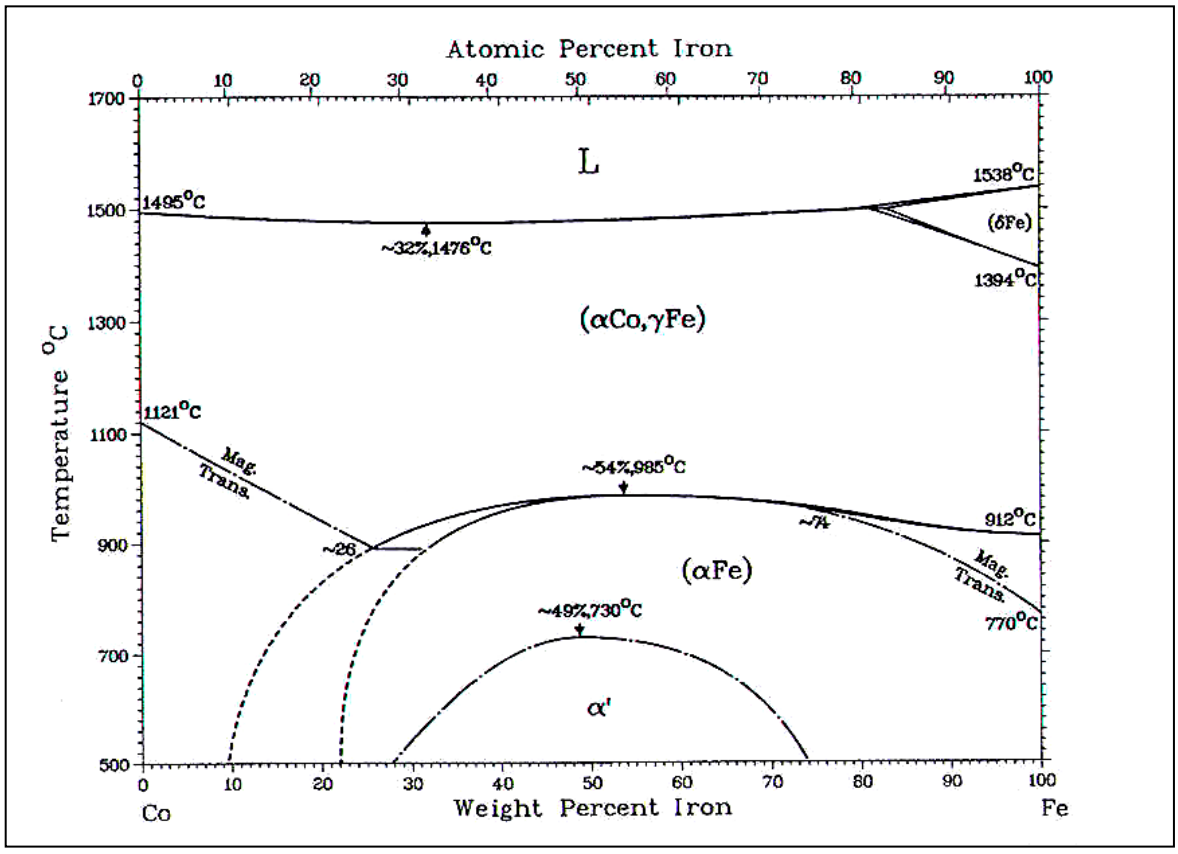

Figure 2.6 The Co-Fe phase diagram after Nishizawa and Ishida (1984) publiblished by Massalski (2001)

2.5.2.4 The Co-Si System

The Co-Si binary system in Figure 2.7 contains five intermediate phases Co_3Si (24.11 wt. % Si), αCo_2Si, βCo_2Si (19.24 wt. % Si), CoSi (32.28 wt. % Si), and $CoSi_2$ (48.8 wt. % Si) (Hansen and Anderko 1958). The melting temperatures of Co_3Si, Co_2Si, CoSi, and $CoSi_2$ reviewed by Hansen and Anderko (1958) are Co_2Si (1327 °C), and CoSi (1395 °C), whereas $CoSi_2$ is reported to form peritectically at 1277 °C. The existence of the phases and the reported transformation temperature were re-investigated by Haschimoto (1937) who studied the partial system CoSi-Si by thermal and microscopic methods from which it was found that $CoSi_2$ melts congruently at 1326 °C and is not formed peritectically at 1277 °C. In the investigation of the Co-CoSi partial system, Vogel and Rosenthal (1934) reported the existence of the Co_3Si at 13.71 wt. % Si.

Despite the discrepancies reported in the phase equilibria the system has been reported as established. Ishida and Nishizawa assessed the data of Vogel and Rosenthal (1934), Haschimoto

(1937), Koster *et al.* (1973), and Enoki *et al.* (1990) to produce the phase diagram in Figure 2.7 for the Co-Si binary system.

The thermodynamics of the liquid Co-Si binary system is not different from the other transition metals (iron, nickel, and manganese) except for copper and chromium where the entropy of mixing with silicon is slightly positive. The Co-Si system is characterised by a large negative enthalpy value and negative entropy of mixing (Witusiewicz 1994). The activity values show a negative deviation from ideal solution and thus the two elements chemically interact strongly in the alloy melts.

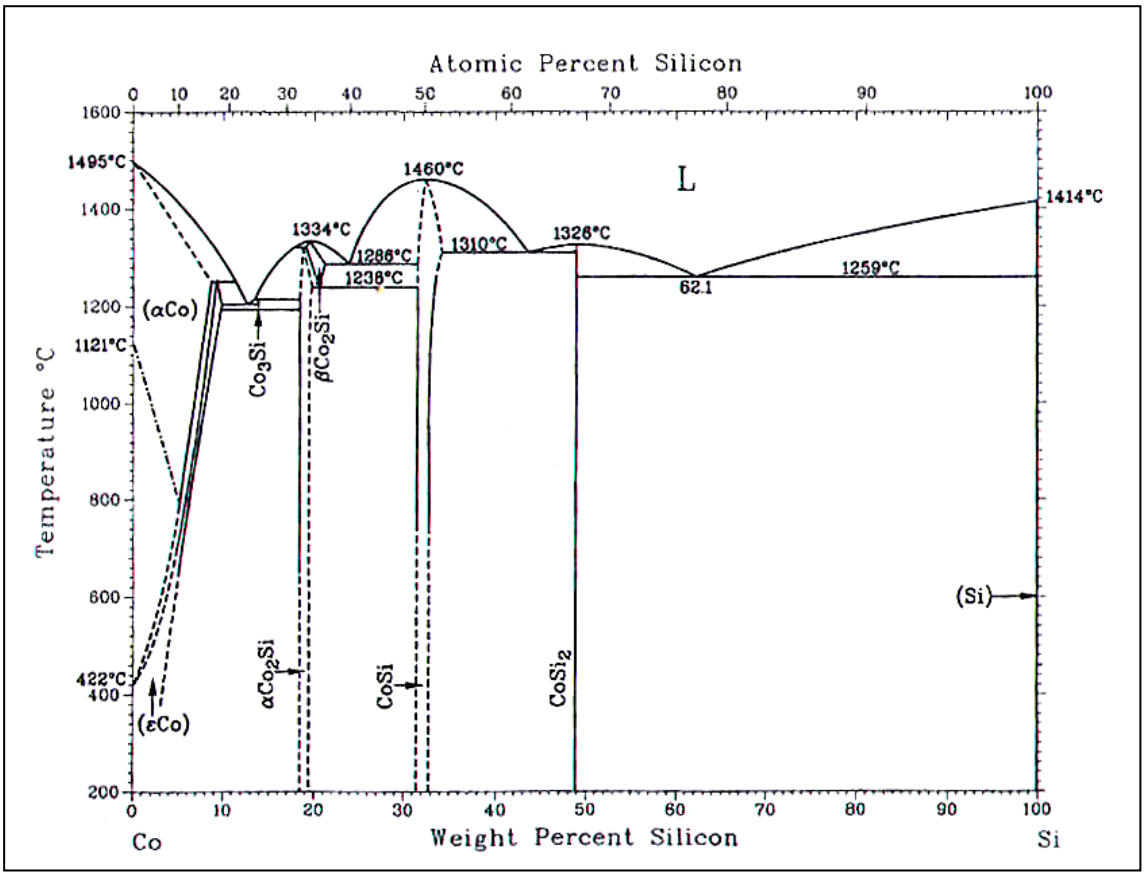

Figure 2.7 The Co-Si system after Ishida and Nishizawa (1990) publiblished by Massalski (2001)

2.5.2.5 The Fe-Si System

The Fe-Si system in Figure 2.8 has been reviewed by Kubaschweski (1982), who reported that the iron solid solution is restricted by a γ-Fe loop between 910 °C and 1381 °C with maximum silicon composition at 2.2 wt.%. The bcc phase α-Fe is stable over a wide range of composition having a maximum at approximately 15 wt. % Si at 1250 °C (Hansen and Anderko 1958). There is an intermediate phase FeSi that forms congruently at 1410 °C at about 33 wt.% Si, with a

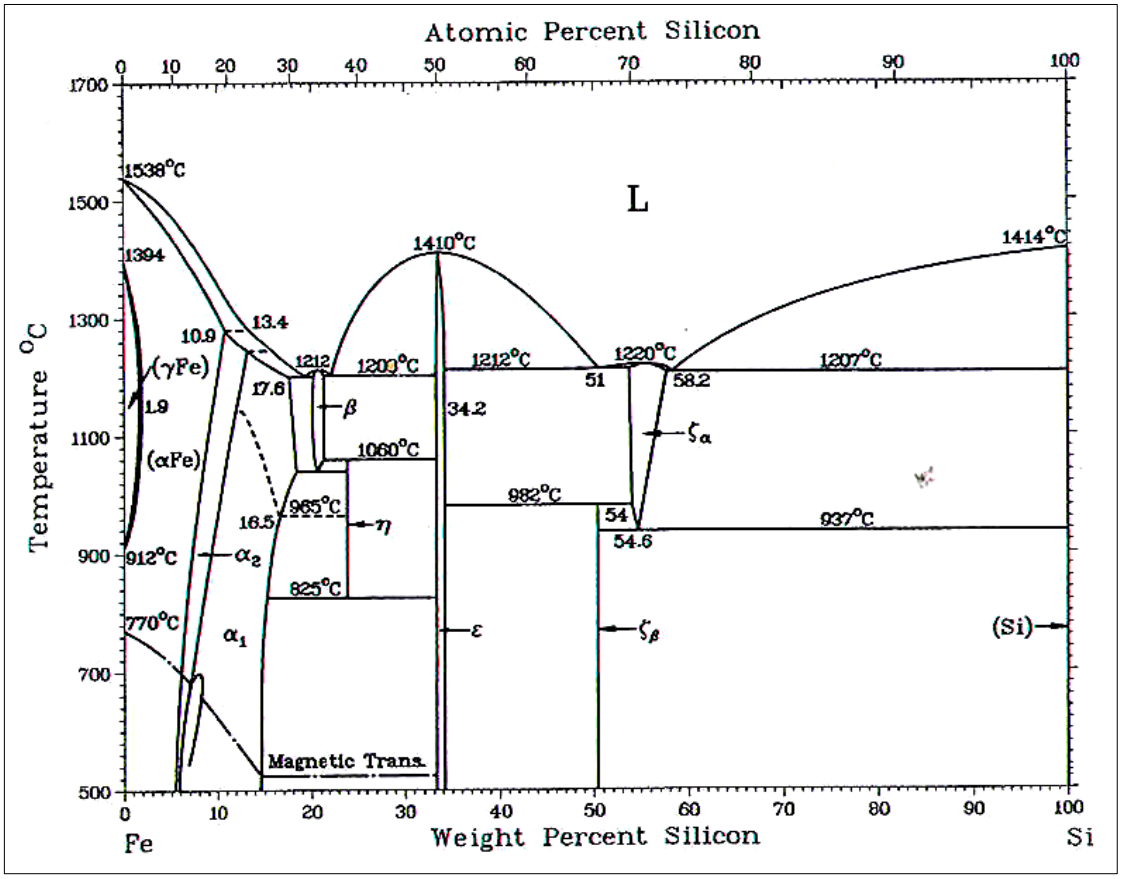

Figure 2.8 The Fe-Si System after Kubaschweski (1982) publiblished by Massalski (2001)

narrow range of homogeneity . Other reported intermediate phases are Fe_2Si, Fe_5Si_3, and $FeSi_2$. The solubility of iron in solid silicon is negligible. The eutectic and peritectic reactions take place at silicon concentrations higher than 2.2 wt.% Si.

2.5.2.6 The Cu-Si system

The most recent work on this system is a review paper by Okamoto (2002) which includes the work by Yan and Chang (2000). The phase equilibria of the Cu-Si are complex with eight intermetallic compounds and numerous invariant reactions in the composition regime of 10 to 15 at.% Si. A eutectic reaction at 802 °C yields Cu_2Si and Si. Several intermediate phases in the Cu-

rich side are stable below 900 °C. In the assessment of the Cu-Si system by Olensiki and Abbaschian (1986) it is reported that the terminal solid solution dissolves only small amounts of copper (Figure 2.9). The liquidus temperature on the silicon side drops from 1414 °C to 802 °C.

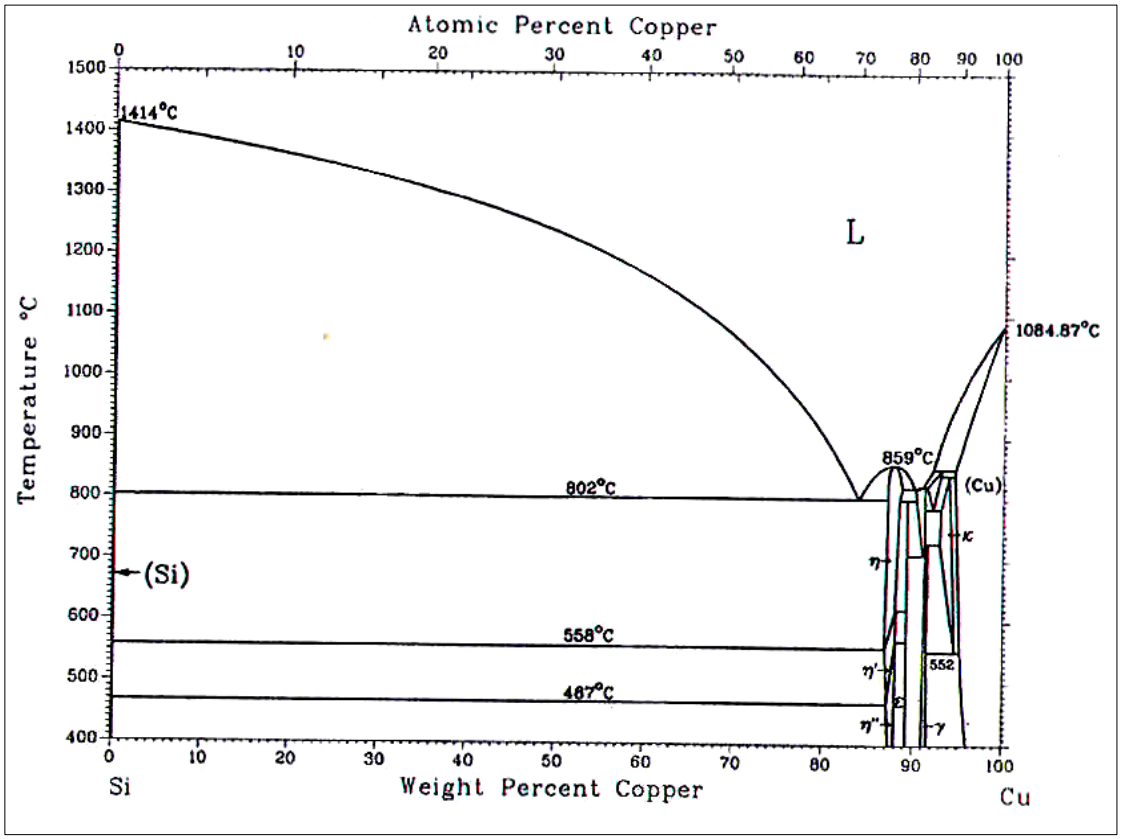

Figure 2.9 The Cu-Si system after Olesinski and Abbaschian (1986) publiblisheb by Massalski (2001)

2.5.2.7 The Fe-Co-Cu system

The literature on the ternary system Fe-Co-Cu can be categorised in two schools. There is a school that reports no liquid immiscibility (Maddocks and Clausen 1936) and the one that reports the presence of the liquid immiscibility in the ternary system (Raghavan 2002a). What bring about this apparent difference are the objectives of the study and the methods considered in the study of the system Fe-Co-Cu.

For instance, the review work by Raghavan (Raghavan 2002a) is based on the research carried out to investigate the metastable liquid phase separation (MLPS) in undercooled liquid specimen (Cao *et al*. 2002; Kim and Abbaschian 2000; Kubišta and Vrešťál 2000; Mingjun *et al*. 1999; Munitz and Abbaschian 1996).

Kim and Abbaschian (2000) determined the metastable liquid gaps in the Fe-Co-Cu system by a melting and solidification method using high frequency electromagnetic levitation technique. The microstructures resulting from the quenched specimen consisted of two liquids one rich in iron and cobalt and the other rich in copper. The separation temperatures of the two liquids were determined as well as the liquidus and solidus temperatures.

Wang *et al.* (2002) determined the phase equilibria in Fe-Co-Cu system in the high temperature region by equilibrating model alloys of Fe-Cu-X (X: Co, Si, V, Cr) in sealed quartz capsules for 336 to 1680 hrs and then quenched in ice water. They calculated isothermal sections at 1000, 1127 and 1300 °C based on experimental data determined earlier by Jellinghaus (1936), Maddocks and Clausen (1936), and Raghavan (1992).

The early work on the Fe-Co-Cu system reported no liquid immiscibility (Maddocks and Clausen 1936). The thermal analysis and metallography techniques were used for the study. Their work sought to answer questions of the existence of liquid immiscibility in particular and the extent of copper on the liquidus surface from the Fe-Co side of the ternary to the pure copper corner. They examined five lines of alloy compositions along the lines listed below and of which, lines 1 to 3 have been extended in this study.

- Line 1. Constant Cu/Co ratio = 1/1 from 80 to 100% iron
- Line 2. Constant Fe/Co ratio = 3/1 from 4 to 8% copper
- Line 3. Constant Fe/Co ratio = 1/1 from 0 to 100% copper
- Line 4. Constant Fe/Co ratio = 1/3 from 5 to 7% copper
- Line 5. Constant copper content = 50% copper.

The thermochemical properties of the Fe-Co-Cu system are not available in literature. Several experimental data on this system are thermodynamic assessments appropriate for phase diagram points. Palumbo *et al.* (2006) have shown this in the analysis of the thermodynamics of the stable and metastable phase diagrams of the Co-Cu and Fe-Co-Cu systems using the CALPHAD approach by Thermocalc. In this work it is observed that in all the related studies (Bamberger *et al*. 2002; Cao *et al*. 2002; Kim and Abbaschian 2000; Maddocks and Clausen 1936b) the miscibility gap was found to be metastable.

2.5.2.8 The Fe-Cu-Si System

Wang et al. (2002) who extended the work by Othani et al. (1997) present the experimental data in the higher temperature regimes of the Fe-Cu-Si system. They performed detailed experimental studies by equilibrating the model alloys of Fe-Cu-X (where X is Co, Si, V, or Cr) in sealed quartz capsules for 336 to 1680 hrs and then quenched in ice water to determine phase equilibria data for isothermal sections at 1250, 1350 and 1450 °C. Shown in Figure 2.10 is the isothermal section at 1450 °C. They observed that in the iron-rich side the solubility of copper increased with increasing silicon content. Hanson and West (1934) in earlier studies investigated the copper-rich corner of the Fe-Cu-Si system and reported the decrease in solubility of iron in the presence of silicon.

Ohtani *et al.* (1997) on the other hand studied the effect of silicon among other elements, on the solubility of copper in iron at 1100 °C. They equilibrated liquid Cu-X alloys (X: V, Cr, Co, Mn, Ni, Al, Si, Sn) with solid iron. A small increase of copper in iron was observed in the range of 3% Si but beyond this concentration a remarkable decrease in solubility of copper in iron was observed. This was due to the transformation of the crystal structure (α to γ) of the solid iron equilibrated with the liquid copper.

Despite having several workers reporting and confirming the existence of a miscibility gap in the Fe-Cu-Si system, there are inconsistencies in the data and phase diagrams. For instance, Raghavan (2002b) and Ohtani *et al.* (1997) reported a miscibility gap in the temperature range 1350 °C and 1450 °C whereas Wang (2002) reported that the miscibility gap is in touch with the Fe-Cu side and not the (γ + L_1) at 1450 °C. The discrepancy is because Raghavan (2002b) combined new experimental data and old thermodynamic data to draw the isothermal sections and ternary liquidus diagrams.

The liquid immiscibility or segregation due to silicon and carbon contamination alluded to by Hansen and Anderko (1958) in the binary Fe-Cu system exists in the Fe-Cu-Si ternary system. The presence of silicon stabilises the liquid phase separation between the iron rich and copper rich liquid phases through the invariant reactions in the temperature range 1350 to 1250 °C as follows:

a) Between 1450 and 1350 °C the miscibility gap is in contact with γ + L_1 to generate tie triangle γ + L_1 + L_2.

b) Between 1350 and 1250 °C U-type four phase invariant reaction occurs: $\gamma + L_1 \Leftrightarrow \alpha + L_2$ yielding the tie triangles $\gamma + \alpha + L_2$ and $\alpha + L_1 + L_2$.

c) Also the miscibility gap makes contact with the $FeSi + L_2$ two-phase field to generate the tie triangle $FeSi + L_1 + L_2$

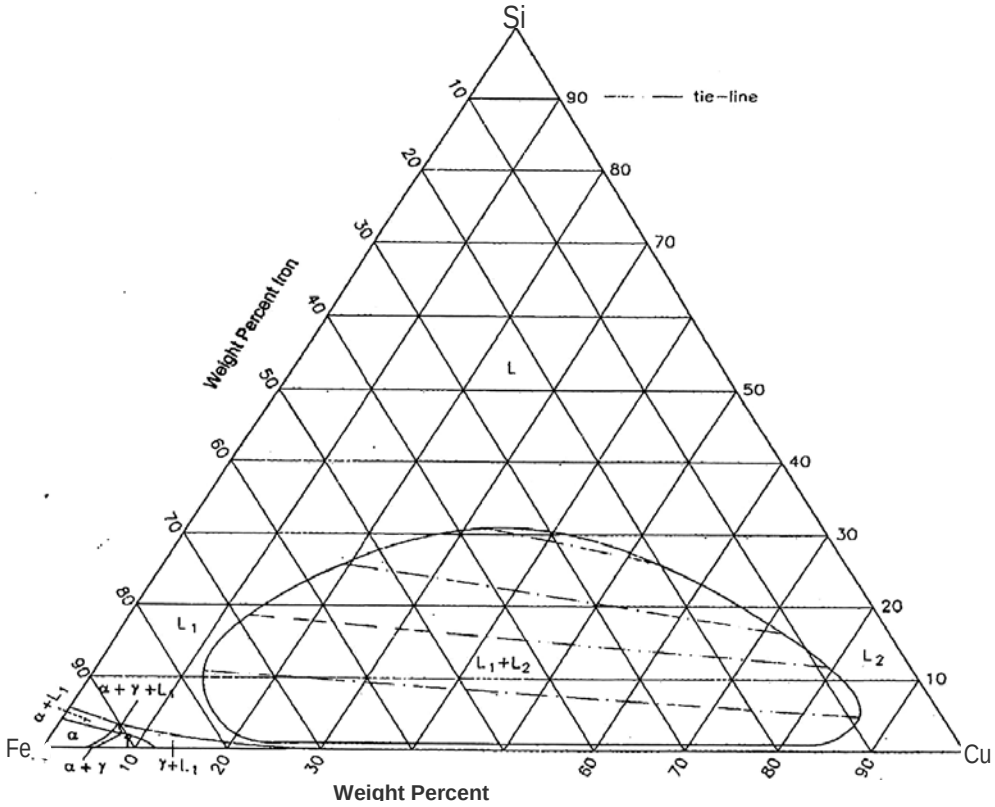

Figure 2.10 Cu-Fe-Si isothermal section at 1450 °C after Hino (1999)

2.5.2.9 The Co-Cu-Si System

There is not much information for the Co-Cu-Si system other than that reported by Revina *et al.* (1975) who studied the isothermal sections at 700, 900 and 1000 ^{o}C for the concentration range 95 to 100 wt.% Cu. The phase equilibria of the ternary Co-Cu-Si system is illustrated by Gronostajski (1968) in the vertical sections shown in Figure 2.11. However the vertical section is drawn at 1 wt.% Co in a copper rich corner at the temperature range 200 to 1000 °C. The section is pseudo binary with the influence of the Cu-Si binary system. This influence can be seen from the invariant reaction (Cu + L) for the formation of the liquid phase taking place at about 1000 °C and 10 at. % Si in Figure 2.9 and Figure 2.11.

There is a need for more experimental work to cover the wider concentration and higher temperature range to generate data that can be used in the thermodynamic assessment of the Co-

Cu-Si ternary system pertinent phase equilibria relevant to the production of Ferrocobalt from slag cleaning.

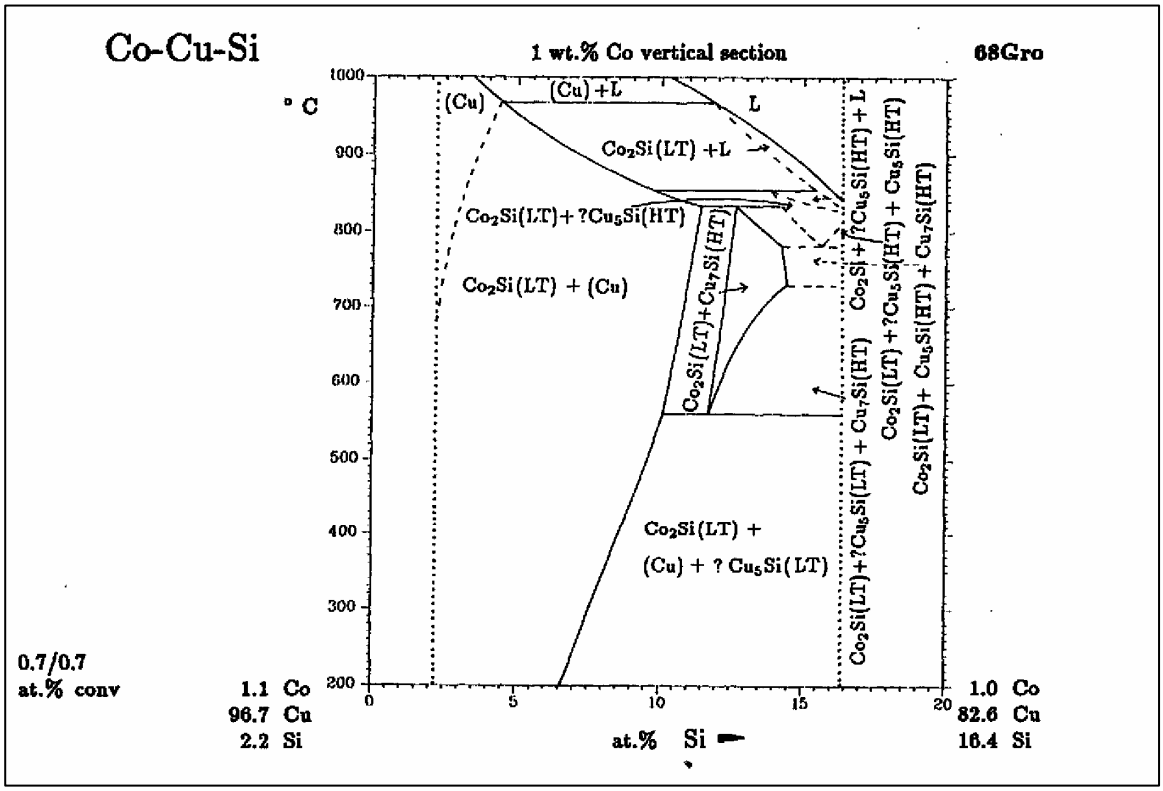

Figure 2.11 Vertical section of Cu-Co-Si alloy at constant cobalt content of 1 wt. % and 2.5 wt.% after Gronostajski (1968) published by Villars *et al.* (1991)

2.5.2.10 The Fe-Co-Si System

Vogel and Rosenthal studied and published the phase diagram for the alloy system Co-Fe-Si in 1935. Their original work (Vogel and Rosenthal 1935) is published in German language. The phase diagram is published in the AMS Handbook of Ternary Alloy Phase Diagram by Villars *et al.* (1991). Among the vertical and partial liquidus phase diagrams that have been published, the pseudo binary phase diagram shown in Figure 2.12 falls within the composition range pertinent to the study of the quaternary Fe-Co-Cu-Si with respect to ferrocobalt. It is clear from Figure 2.12 that an increase in silicon content lowers the liquidus temperature in the ternary Fe-Co-Si and there is no compound formation below 10 at.% Si. Therefore, compound formation between silicon and iron or cobalt at 5 at.% Si or lower should not be expected within the composition range studied in the Fe-Co-Cu-Si system.

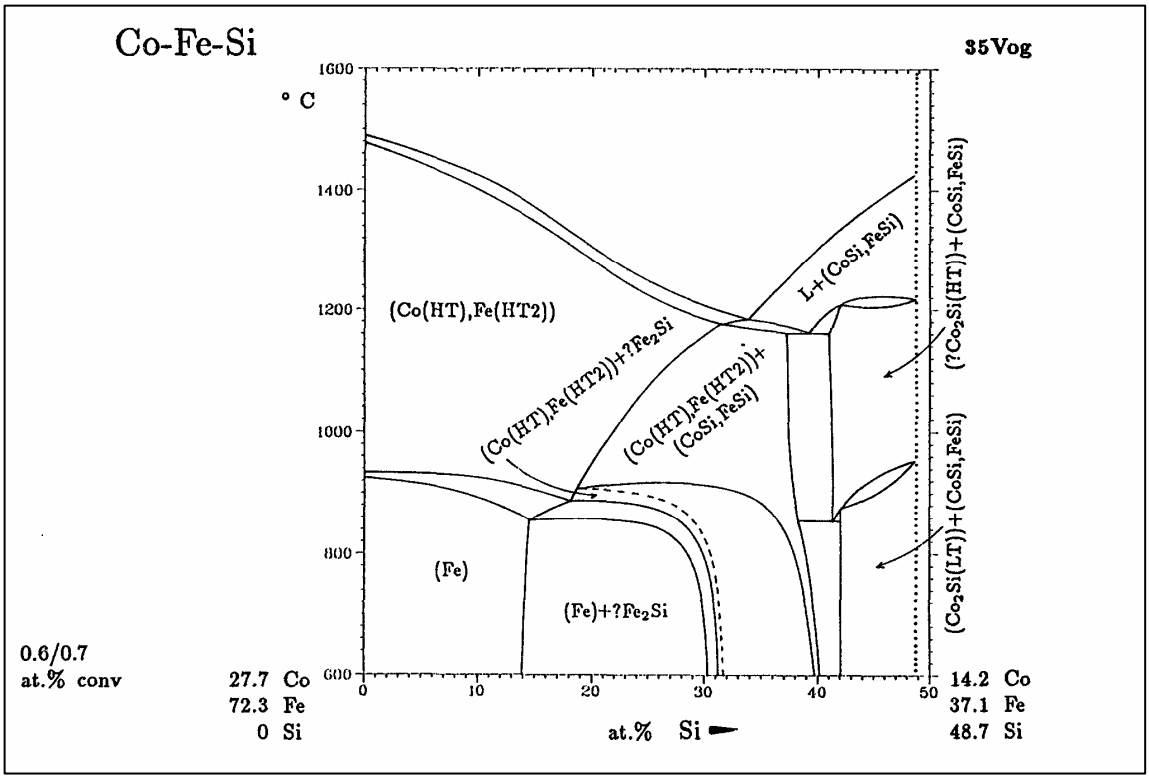

Figure 2.12 Co-Fe-Si vertical section at 27.7 at.% Co and 72.3 at.% Fe after Vogel and Rosenthal (1935) published by Villars *et al.* (1991)

2.5.3 Summary of literature in the Fe-Co-Cu-Si system

It is evident from the published literature of the four ternary subsystems of the Fe-Co-Cu-Si that only the three namely, Fe-Co-Cu, Fe-Cu-Si and Co-Cu-Si ternary systems influence the physicochemical properties of the Fe-Co-Cu-Si quaternary system. It is observed that a wide range of solid solution formation in the Fe-Co-Cu, Fe-Cu-Si and Co-Cu-Si ternary subsystems is a result of distribution of cobalt and silicon between α- or γ-iron and copper or liquid phases when added in certain amounts to the Fe-Cu alloy system (Wang *et al*. 2002). In particular, the solubility of copper in iron (and iron in copper) in the presence of either silicon and/or cobalt characterises the transformation temperatures and any liquid or solid miscibility gaps in the Fe-Co-Cu-Si system.

This behaviour is also evident in the theory of solution thermodynamics, particularly the enthalpies of formation, entropy of mixing, and the activities of components in the liquid alloys, discussed in the following paragraphs.

Witusiewicz (1994) determined the thermodynamics of the transition group metals (cobalt, copper and Nickel) in solution with metalloids by investigating the binaries Tr-Fe and Tr-Si (Tr: Co, Cu, Ni). The Tr-Si exhibited large negative enthalpy values and entropies of mixing. It was found that copper exhibits a higher interaction with silicon than cobalt, nickel or iron does. The general characteristic of the thermodynamic activity of the transition metals and silicon binary systems (Tr-Si) is a large negative deviation from Raoult's law indicative of the strong chemical interaction between the components in the liquid alloys. Kubaschweski (1982) has studied the thermodynamic activity of the Fe-Si system. Hasebe and Nishizawa (1980) on the other hand investigated the activities in the Fe-Cu and Co-Cu binary system.

The enthalpies of formation of liquid binary between the components copper and iron, copper and cobalt, and copper and nickel (Cu+Fe, Co, and Ni) alloy systems are positive (endothermic) with the excess thermodynamic functions decreasing from Cu-Fe, Cu-Co and Cu-Ni (Nikolaenko and Turchanin 1997). They (Nikolaenko and Turchanin 1997) used the direct reaction calorimetry (high-temperature isoperibolic calorimetry) technique to study the enthalpies of formation in the whole range of compositions at 1600, 1550, and 1480 ^{o}C.

Therefore, the investigations on the subsystems of the ferrocobalt form a basis for understanding the solution thermodynamics that may lead to understanding the reaction mechanism associated with smelting of copper slags. Also the energy balance of the furnace can be enhanced by incorporating the enthalpies of mixing as illustrated by Schlesinger and Xiang (2001) in their studies on the enthalpy of mixing of Fe-C-Si melts.

In the current study the activity of silicon in liquid Fe-Co-Cu-Si was determined by equilibrating the liquid binary systems with silica under controlled oxygen partial pressure. The subject on the equilibration of condensed phases with gas phases at high temperatures is widely used to study the thermodynamic activities and distribution of components between phases. The focus of literature for the present study was the equilibration of gases for the creation of the desired oxygen potential and is described in Appendix IV.

2.6 Thermodynamic Considerations

The computation of phase equilibria takes into consideration the Gibbs free energies of all the phases comprising the system. The knowledge of temperature and concentration dependence of

the Gibbs energies of the individual phases is critical to the calculation of the phase diagrams or thermodynamic quantity. The mathematical equalisation of the partial molar free energies of the adjoining phases at the equilibrium conditions yields a set of equations that require numerical methods to solve for the coefficients (thermochemical parameters). Several computational methods and application have been developed based on the computer program initially written by Kaufman and Bernstein (1970) to calculate the phase diagrams of binary and ternary systems. A summary of steps generally followed for calculating phase diagrams is illustrated in Figure 2.13 (Kuo *et al*. 1990).

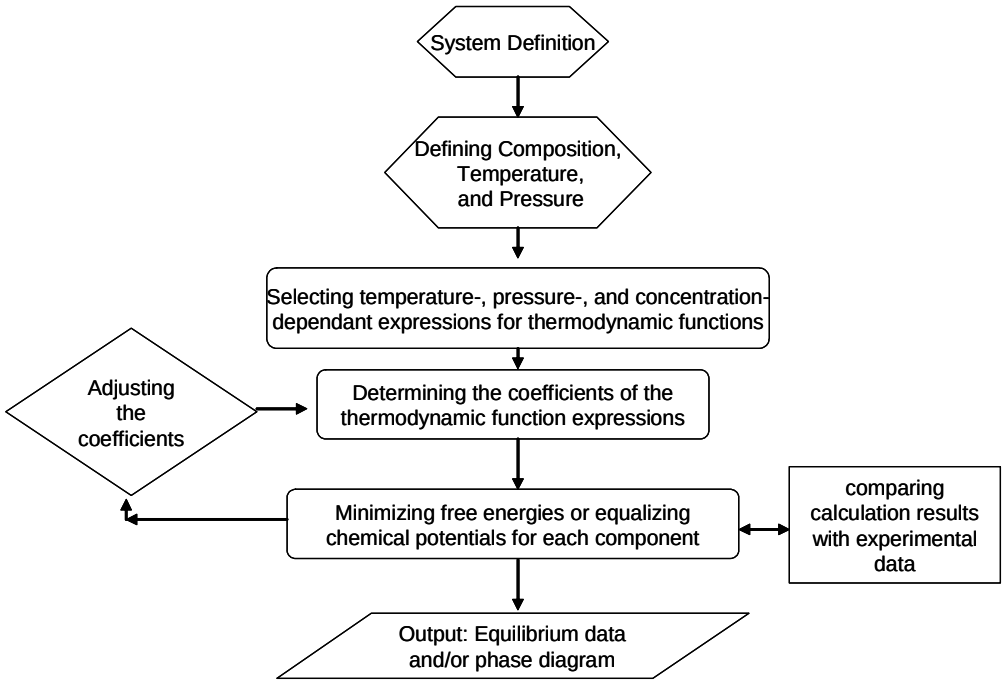

Figure 2.13 Steps of phase diagram calculation (Kuo *et al*. 1990)

Despite the advancement made in computational thermochemistry there are problems associated with calculation of phase diagrams. For instance, the collection of thermodynamic data from experimental data is particularly a challenge. Conventional metallographic methods rather than thermodynamic measurement have often been used to determine phase limits due to the difficulty in experimental measurements of the thermodynamic properties of metallic solutions. As a result, the number of systems for which phase diagrams have been determined is much greater than that for which thermochemical properties of phases are known (Lee and Lee 1985).

The basic thermodynamics applicable to calculating phase equilibria and phase diagram is summarised in the work by Kattner (1997) on the thermodynamic modeling of multicomponent

systems. The mathematical representation of equilibrium of two phases is the equalisation of the partial molar free energies of the adjoining phases.

2.6.1 Parameter estimation of thermodynamic solution models

The interaction parameters for various solution phases are normally calculated using binary phase diagram data. However, it is recognised that even a slight variation of the input phase boundary data gives rise to substantial fluctuations in the calculated thermodynamic values. This is evident in the discrepancies of the published data discussed in the following sections.

2.6.1.1 Binary boundary systems

The thermodynamic assessments of the binary and ternary systems Co-Cu, Fe-Cu, Fe-Co, Fe-Si, Co-Si, and Cu-Si have been conducted by several researchers described in section 2.4.2. The assessed interaction parameters in the binary systems are listed in Table 2.1.

2.6.1.2 Ternary system

The interaction parameters for the ternary systems Fe-Cu-Si and Fe-Co-Cu have been calculated by several workers (Ohtani *et al*. 1997; Palumbo *et al*. 2006; Wang *et al*. 2002). The values, listed in Table 2.1 were determined by detailed solid-liquid (Ohtani *et al*. 1997) and solid-solid (Wang *et al*. 2002) equilibrium experiments. On the other hand Palumbo (Palumbo *et al*. 2006) re-evaluated the experimental data for the binary Co-Cu and ternary Fe-Co-Cu to generate new parameters. The thermodynamic parameters have only been determined at 1300 °C or lower.

The solution models used to describe the Gibbs free energy of the liquid, the solid fcc (γ) and bcc (α) phases of the ternary systems Fe-Co-Cu and Fe-Cu-Si are the regular solution model (Ohtani *et al*. 1997); the subregular solution model (Wang *et al*. 2002); the conventional Maggianu polynomial (Palumbo *et al*. 2006). The Muggianu interpolation method is used for including binary terms in the Gibbs energy expressions of higher-order systems, similar to solution-type (Polynomial Kohler/Toop). Details of the solution models and the estimation of interaction parameters (ω^i) listed in Table 2.1 are discussed in Appendix V. Solution models are used to describe the non-ideal behaviour of species; the dependence of the activity coefficients of species on the melt composition and temperature.

Table 2.1 Thermodynamic interaction parameters for binary and ternary systems

System	Phase	Parameter values (J/mol)			Reference
		ω^0	ω^1	ω^2	
Fe-Cu	α	33984	$3.97T$	$(4480 - 9.104T)\ (x_{Fe} - x_{Cu})$	(Ohtani *et al*. 1997)
	γ	49293	$-10.08T$	$(-8274 + 4.352T)\ (x_{Fe} - x_{Cu})$	(Ohtani *et al*. 1997)
	L	44865	$-7.9939T$	$(6355 - 4.062T) - (x_{Fe} - x_{Cu})$	(Ohtani *et al*. 1997)
Fe-Co	α	-23669	$103.9627T$	$-12.7886T\ln T$	(Ohtani *et al*. 1997)
	γ	-8471		$(-1181 + 1.6544T)(x_{Fe} - x_{Co})$	(Ohtani *et al*. 1997)
	L	-9312		$1752(x_{Fe} - x_{Co})$	(Ohtani *et al*. 1997)
Cu-Co	α	2000			(Ohtani *et al*. 1997)
	γ	49400	$-13.26T$	$(3675-1.03T)(x_{Cu} - x_{Co})$	(Ohtani *et al*. 1997)
	L	$38810 - 6.782T$	$(-3183 + 3.355T)(x_{Fe} - x_{Co})$	$(17100 - 9.66T)(x_{Fe} - x_{Co})^2$	(Ohtani *et al*. 1997)
Fe-Si	α	$-27809 + 11.62T$	$-115449(x_{Fe} - x_{Si})$	$3890(x_{Fe} - x_{Si})^2$	(Ohtani *et al*. 1997)
	γ	$-125248 + 41.116T$	$-142708(x_{Fe} - x_{Si})$	$899907(x_{Fe} - x_{Si})^2$	(Ohtani *et al*. 1997)
	L	$-164435 + 41.977T$	$-21.523T(x_{Fe} - x_{Si})$	$(-18821 + 22.07T)\ (x_{Fe} - x_{Si})^2 + 9696(x_{Fe} - x_{Si})^3$	(Ohtani *et al*. 1997)
Cu-Si	α	0	0	0	(Ohtani *et al*. 1997)
	γ	$-38089.5-0.4916T$			(Ohtani *et al*. 1997)
	L	$-36249.8 + 12.1983T$	$(-58931.9 + 37.1222T)\ (x_{Cu} - x_{Si})$		(Ohtani *et al*. 1997)
Fe-Co-Cu	Liquid	5760	-42000	13400	(Palumbo *et al*. 2006)
		22000	-32000	-1500	(Wang *et al*. 2002)
				-30000	(Ohtani *et al*. 1997)
	fcc (γ)	$-47900 + 20T$	$-47900 + 20T$	$-47900 + 20T$	(Palumbo *et al*. 2006)
		$-35327.7 + 8T$	$-87000 + 58T$	$-93000 + 50T$	(Wang *et al*. 2002)
				$-93650 + 50T$	(Ohtani *et al*. 1997)
	bcc (α)	$-114000 + 50T$	$-114000 + 50T$	$-114000 + 50T$	(Palumbo *et al*. 2006)
		$-155000 + 75T$	$-155000 + 75T$	$-155000 + 75T$	(Wang *et al*. 2002)
		0	0	0	(Ohtani *et al*. 1997)
Fe-Cu-Si	Liquid	0	0	0	(Ohtani *et al*. 1997)
		$23000 - 19.5T$	$50000 - 19.5T$	$23000 - 19.5T$	(Wang *et al*. 2002)
		$19000 - 22.5T$	$19000 - 22.5T$	$19000 - 22.5T$	(Hino *et al*. 1999)
				$(50000 - 50T)x_{Cu} + (90000 - 50T)x_{Fe} + (110000 - 50T)x_{Co}$	(Miettinen 2003)
	fcc			$-200000 + 100T$	(Miettinen 2003)
		$-187300 + 100T$	$-187300 + 100T$	$-187300 + 100T$	(Hino *et al*. 1999)
		$-231494.5 + 130T$	$-231494.5 + 130T$	$-231494.5 + 130T$	(Wang *et al*. 2002)
	bcc	$-237300 + 100T$	$-237300 + 100T$	$-237300 + 100T$	(Wang *et al*. 2002)
				$-200\ 000 + 100T$	(Miettinen 2003)
		$-158642.5 + 50T$	$-182105.5 + 70T$	$-158642.5 + 50T$	(Wang *et al*. 2002)

2.6.1.3 Quaternary system

The work by Balitchev *et al.* (2003) is a good illustration of the expansion of a database to include descriptions of ternary phases to model the quaternary systems. They re-evaluated experimental data from literature resources and carried a thermodynamic optimisation using the

CALPHAD method. Even though the quaternary Al-Fe-Mn-Si is irrelevant to the ferrocobalt system the approach can be adapted to describe the solution phases of the ferrocobalt system. Similarly, the work by Bratberg and Frisk (2004) in which the substitutional solution model has been used to describe phases of the quaternary Fe-Cr-V-C system.

There is no thermodynamic or thermochemical information in literature that describes solution phases of the Fe-Co-Cu-Si system.

CHAPTER 3

EXPERIMENTAL TECHNIQUES AND PROCEDURES

A combination of thermal analysis, melt-and-quench, and metallography was used to study the liquidus and phase equilibria in the Fe-Co-Cu-Si quaternary system. The first sections of the chapter describe the procedures and techniques of preparation and classification of the model alloys. The detailed experimental procedures employed to address the objectives of the study are outlined in the subsequent sections.

3.1 Model alloy design and equipment set up

The model alloys used in the experiments were prepared by mixing metal powders of purity 99.99+ % in required proportions and induction-melted in recrystallised alumina crucibles placed in a graphite crucible as illustrated in Figure 3.1. Induction melting is based on the principle by which an induced electrical current in the material causes it to heat up to melting temperatures. Model alloys were prepared in this manner. The purpose of graphite crucible was twofold; primarily it served as an oxygen receptor to prevent oxidation of the alloy and secondly, graphite is a good conductor and during induction-heating it heats up to high temperatures releasing heat energy that aided in melting the metal in the non-conducting alumina crucible by conduction and radiation. Argon gas was purged over the sample crucible to create an inert atmosphere in the heated chamber.

After cycles of melting and cooling, the alloys were cut in sections for metallographic examination to test for homogeneity and the other sections reserved for thermal and quench experiments as described later in the chapter. The alloy sample size was 16 mm diameter and 0.38 mm thick.

The proportions used for the compositions of the Fe-Co-Cu-Si quaternary system are listed in Table 3.1 and were formulated such that the ratio of cobalt to iron was 0.2 and not exceeding 1.0 and that of cobalt to copper was 0.5 and no more than 2.0. The basis on which the Fe-Co-Cu-Si system is constituted was discussed in section 2.3. The subsystems were constituted in a similar manner so as to remain in the vicinity of the composition pertinent to slag cleaning.

Table 3.1 Typical composition range of the metal system as analysed from DC arc operations

Element	Si	Co	Cu	Fe	Co/Fe	Co/Cu
Composition range, wt%	0 – 5%	10 – 30%	10 – 20%	50 – 80%	0.2 – 1	0.5 – 2

3.1.1 Induction furnace setup

An illustration of the induction furnace set-up is shown in Figure 3.1. The sample crucible was placed in a graphite crucible with the bubble alumina placed around it to fill the space between the sample crucible and the graphite crucible wall to improve thermal coupling between the induction coil and the crucible assembly; close coupling increases the flow of eddy currents and therefore increasing the amount of heat produced in the workpiece. Other than that, the graphite crucible acted as the susceptor of any electromagnetic interference from the induction heating on the thermal EMF in the thermocouple. The melting of alloys was conducted in an inert atmosphere that was induced by purging argon gas (ultra high purity grade) over the sample crucible.

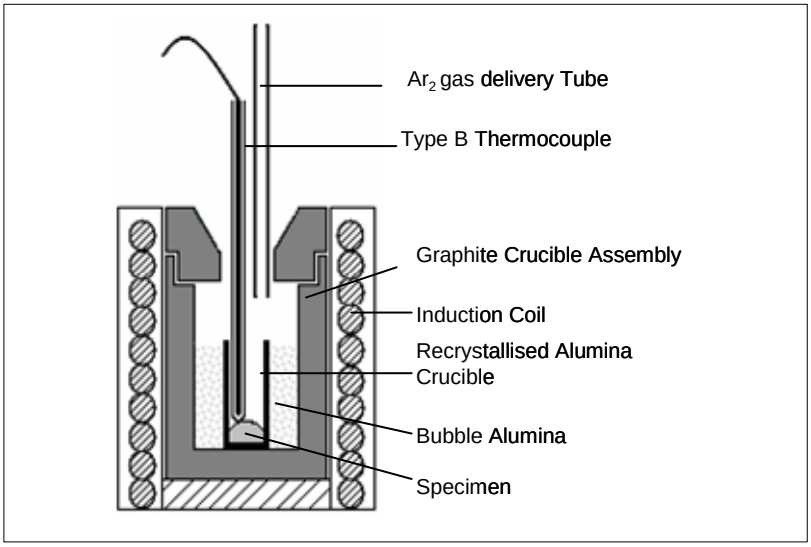

Figure 3.1 An illustration of the induction melting of alloy in the graphite-alumina crucible assembly

A type B thermocouple connected to a Eurotherm 2132 temperature reader was inserted into the crucible through the holes provided in the graphite crucible assembly. An alternate temperature reader a Hewllet Packard 3466A digital multimeter reading temperature in mV and converted to degrees Celsius using the type B emf to ^{o}C conversion tables. All melting procedures were conducted at 176 V, 1.5 kW and 8.4 kHz settings of the furnace maximum rating; 440 V, 15 kW and 10 kHz respectively.

3.1.2 Temperature measurements

Pure iron, copper and cobalt metals were used to validate thermocouple sensitivity. The criterion was to observe the incidence of melting of the metal in an induction furnace at a selected power input. The calibration was verified for both high and low melting temperatures. Pure iron and cobalt metals served as high melting temperature specimen and copper as a low melting

specimen. To prevent contamination of the alloys a thermocouple was used for each metal and all temperature measurements were recorded from room temperature. The tip of the thermocouple sheath was kept in contact with the metal through out the measurement duration. The time required to achieve complete melt at a predetermined power output of the induction furnace was established to be within 10 minutes. For all subsequent alloy melting these conditions were maintained.

The temperature readings obtained were consistent with the melting temperatures of the pure metals. In Figure 3.2, the heating of copper is plotted on a time-temperature chart and the observed change in slope was at about 1080 °C. This value is close to 1084 °C .the theoretical melting temperature of copper and therefore, the time and temperature for complete melting of the samples was validated in this manner.

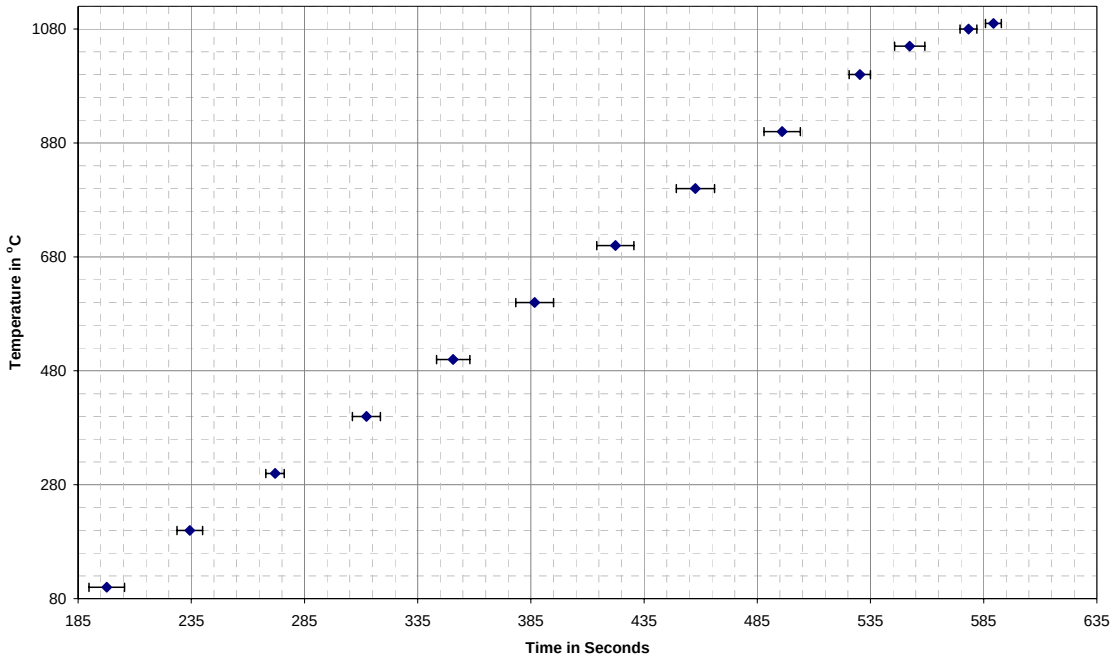

Figure 3.2 A plot of time of heating copper to liquidus temperature in an induction furnace set at 40% of furnace rating

3.1.3 Materials and procedures

The metals used in the experiments of the study were pure grade 99.99+ %. Alloys were prepared from iron, cobalt, copper and silicon powder. The mass of each alloy was about 5g constituted from composition ranges described earlier in Table 3.1. The compositions of the alloys prepared for the experiment are listed in Table 3.2. Among the model alloys a composition

described by Bamberger *et al.* (2002) was included and designated alloy as T. A quaternary Fe-Co-Cu-Si alloy system was prepared by adding silicon powder to the alloy C mixture in proportions to attain a 1 to 5wt.% Si and melted and re-melted so as to attain homogeneity. Because silicon is a metalloid it is usually difficult to melt it by induction heating. However, it was not the case in this study since the silicon concentrations relative to the other elements was very low and it most likely melted by dissolution in the melted metal rather than melting in its pure form.

Table 3.2 Bulk Composition of alloys used in the experiments

	Nominal Compositions, wt%					
Alloy	Fe	Co	Cu	Si	Co/Fe	Co/Cu
Binary alloys						
U	70.0	30.0			0.43	
V	80.0		20			
W	95.0			5.0		
X		60.0	40.0			
Y		95.0		5.0		
Z			95.0	5.0		
Ternary alloys						
A	80.0	10.0	10.0		0.13	1.00
B	70.0	15.0	15.0		0.21	1.00
C	60.0	20.0	20.0		0.33	1.00
D	55.0	25.0	20.0		0.46	1.25
E	50.0	30.0	20.0		0.60	1.50
F	65.0	15.0	20.0		0.23	0.75
T	42.0	20.0	38.0		0.48	0.53
*PQR#2	74.5		19.6	5.89		
Quaternary alloys						
C#01	56.7	18.9	18.9	5.5	0.33	1.00
C#02	57.0	19.0	19.0	5.0	0.33	1.00
C#03	57.6	19.2	19.2	4.0	0.33	1.00
C#04	57.2	19.4	19.4	3.0	0.33	1.00
C#05	58.5	19.5	19.5	2.5	0.33	1.00
C#06	58.8	19.6	19.6	2.0	0.33	1.00
C#07	59.1	19.7	19.7	1.5	0.33	1.00
C#08	59.4	19.8	19.8	1.0	0.33	1.00
*VWXY#1	76.0	9.5	9.5	5.0	0.125	1.00
*VWXY#2	77.6	9.7	9.7	3.0	0.125	1.00

** Alloys prepared by arc melting* [3]

The procedure referred to as homogeneity test (Yakowitz *et al*. 1972) was adopted to test the alloys prepared in the induction furnace. From the alloy button, transverse sections were cut and examined using the light microscope and the scanning electron microscope (SEM) with energy-

[3] Arc-melted alloys were prepared for validation of composition of the alloys produced from the silica-alloy-gas experiments described in section 3.4. They also served as Fe-rich specimen to expand the Fe-Co-Cu-Si composition field.

dispersive spectroscopy (EDS) in backscattered electron (BSE) beam imaging mode. The phases in the sample were classified in colour shades as dark, grey, and light. At least sixteen areas were examined and individual readings for each element in the specimen recorded.

The coefficient of variance (CV) represented by Equation (3.1), was used to indicate homogeneity (distribution of elements) by checking the precision of replicates. By definition, if CV is low then the precision of the replicates is good, and poor if it is high.

$$CV = \frac{100\sigma}{N}(\%) \tag{3.1}$$

Where σ is standard deviation, in counts, of a particular data array (iron, cobalt, or ccpper) and N is the average number of counts for each element in a transverse section. The precision of replicates was found to be

- between 1.5 % and 7.5 % for Fe in all phases,
- 2.8 % for cobalt in grey and 11.6 % for cobalt in white phases, and
- 0.6 % for copper in white and 7.3 % copper grey phases respectively.

3.2 Determination of transformation temperatures

The methods of determining thermal properties such as liquidus and solidus temperatures of materials are based on the principle of measuring temperature changes versus time as energy is supplied to the material. By so doing one can observe and deduce the temperatures where thermal activity is taking place during the heating process. As explained in Chapter 2, this thermal activity will appear in the form of either an endotherm or exotherm peak depending on whether a melting or solidification process is underway respectively. The solidus temperature is indicated by the onset of melting and the peak on the heating trace indicates the liquidus temperature. Other energies of transformation such as enthalpies and heat capacities of materials can be measured in a similar way, depending on the configuration of the thermal measurement.

A differential thermocouple arrangement shown in Figure 3.3 measures the temperature difference between a symmetrically placed reference crucible and a sample crucible in the furnace exposed to the same heating rate.

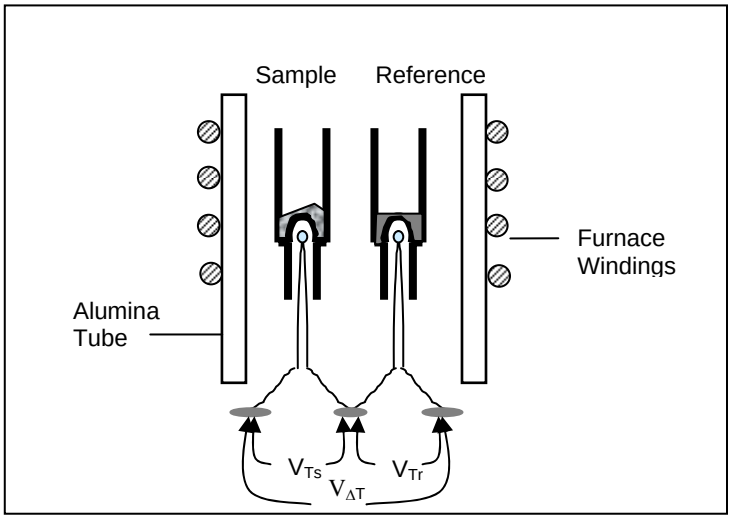

Figure 3.3 Schematic drawing of the differential thermal analyser and arrangement of differential thermocouples

3.2.1 Differential thermal analysis: equipment and calibration

3.2.1.1 Equipment description

The equipment used in the study of transformation temperatures is a NETZSCH STA (simultaneous thermal analyser) 409C. The temperature range on DTA mode and type S thermocouple is 20 to 1650 ^{o}C. The reference and sample crucibles were slip-on types held on a pedestal that in turn is supported on a balance for thermogravemetric analysis (TGA) if required. Underneath the sample and reference crucibles are two thermocouples arranged on a differential configuration measuring temperature of the sample and reference material through a heating cycle. The furnace can be operated under vacuum, inert, reducing, or oxidising conditions depending on the experiment requirements. Measurement data is stored and processed with thermal analyser software (Proteus) with which transformation temperatures and related thermal properties can be calculated.

For all the measurements conducted in this study, an empty reference crucible was used while the sample crucible contained the specimen of particular mass which ranged from 20 mg to about 180 mg.

3.2.1.2 Sensitivity and temperature calibration

Stein *et al.* (2002) has discussed the shortcomings of the DTA to measure quantitative energies by noting the discrepancies in the measured values of different specimens obtained from the

same alloy sample. To minimise this uncertainty, sensitivity and temperature calibration procedures were followed through for this study. Also, when measuring the peak areas the limits of the peak were carefully terminated relative to the point where the first derivative plot of the heating trace was constant (or parallel to the horizontal axis) as illustrated in Figure 3.4.

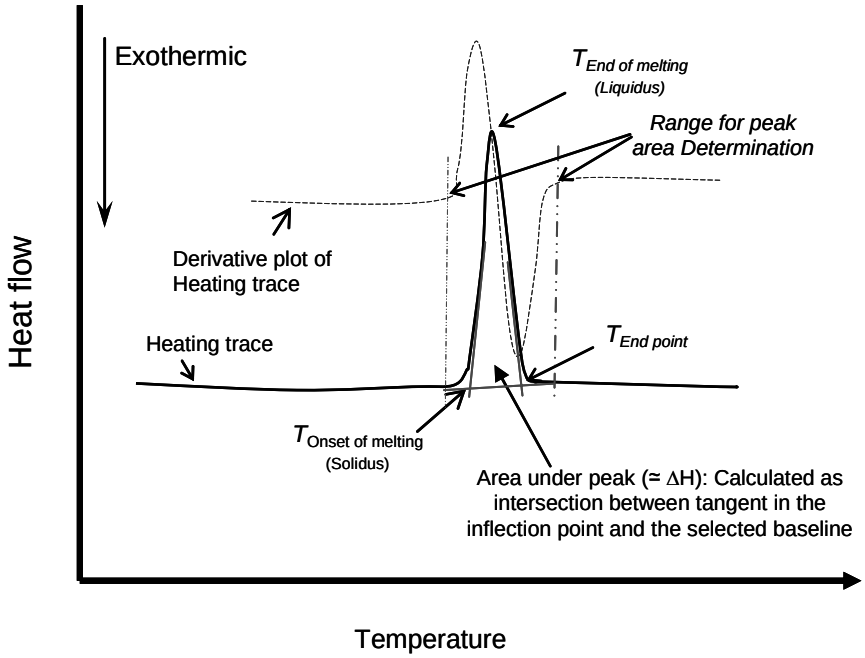

Figure 3.4 A DTA heating trace and its derivative plot. Note the illustration of the range selection for peak area calculation, where the solidus, liquidus and end point lie on the heating trace

Standard calibrating metals as stipulated in the manufacturer's manuals were employed to set sensitivity and temperature recalibration charts for the Netzsch STA 409C analyser. The readings from four melting and cooling cycles for each pure metal were recorded and the mean for each specimen was used, together with the literature melting values, for the temperature and sensitivity calibration.

Other than using the standard pure metals for calibration check, the melting temperatures of pure nickel and cobalt metal were determined at 1450 and 1495 °C, respectively. The peritectic reaction temperature of Co-Cu was measured to be 1111.7 °C which is consistent with the peritectic temperature 1112 °C reported in literature for this system. The melting temperatures of nickel and cobalt provided a calibration for higher temperatures.

The correction equations and the calibration coefficients calculated with NETZSCH-Proteus thermal analysis software are listed Equations 3.3 to 3.6. The expression for calculating the calibration factor is *y* and *T* is the temperature of transformation.

$$y = (p_2 + p_3 \cdot z + p_4 \cdot z^2 + p_5 \cdot z^3) \cdot Exp(-z^2) \quad (3.3)$$

where

$$z = (T - p_0) / p_1 \quad (3.4)$$

p_0 to p_5 are calibration coefficients with values calculated as

$p_0 = 661.299\text{K}; p_1 = 1041.2895\text{K}; p_2 = 0.2902; p_3 = -0.02237; p_5 = p_4 = 0$

Therefore,

$$y = (0.29023 - 0.02237 \cdot z) \cdot \exp(-z^2) \quad (3.5)$$

$$z = \frac{(T - 661.299)}{1041.292} \quad (3.6)$$

This means that the calculated area under the peak is equivalent to the transformation enthalpy multiplied by a factor *y* at the transformation temperature *T* of the alloy.

The calculated coefficients from calibration procedures are utilised in the temperature correction (Equation 3.7). The significance of the expression is that for the measured thermal activities, the correction factor at the particular temperature constitutes the error of measurement. In the temperature range of the transformation temperatures measured, a correction of less than 2 °C on average was required.

$$Correction, {}^{o}C = b_0 \cdot 10^{-3} + b_1 \cdot 10^{-5} \cdot T_{\exp t} + b_2 \cdot 10^{-8} \cdot T_{\exp t}^2 \quad (3.7)$$

where the coefficients values are

$$b_0 = -5258.8; b_1 = 793.6; b_2 = -216.6 \quad (3.8)$$

therefore, placement in equation (4.5) yields

$${}^{o}C = -5.2588 + 7.936 \times 10^{-3} T_{\exp t} - 2.166 \cdot 10^{-6} T_{\exp t}^2 \quad (3.9)$$

The charts in Figure 3.5 and Figure 3.6 are graphical representation of the sensitivity and the temperature calibration results respectively.

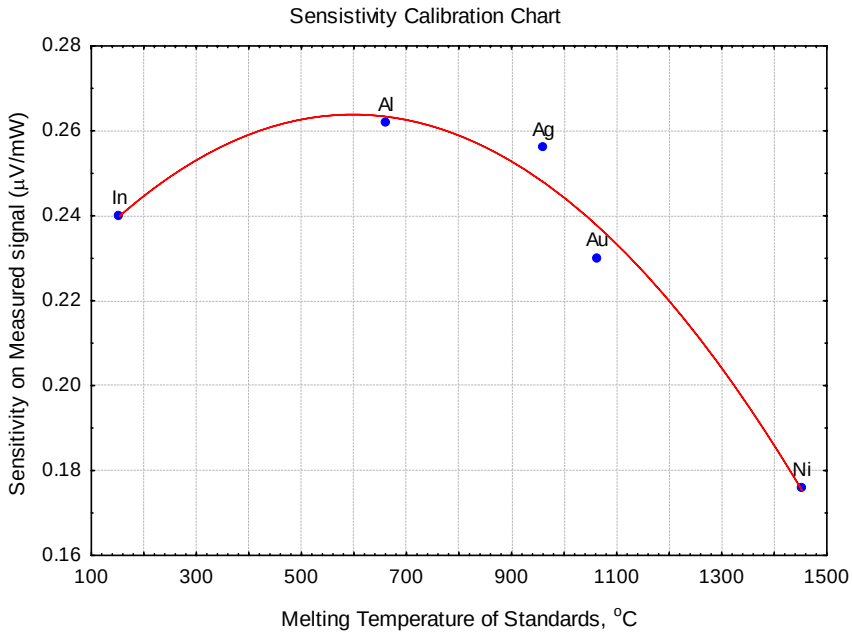

Figure 3.5 Sensitivity calibration curve fitted as a polynomial on measured enthalpies of the standard specimens. The coefficients of the polynomial are expressed in equation 3.3

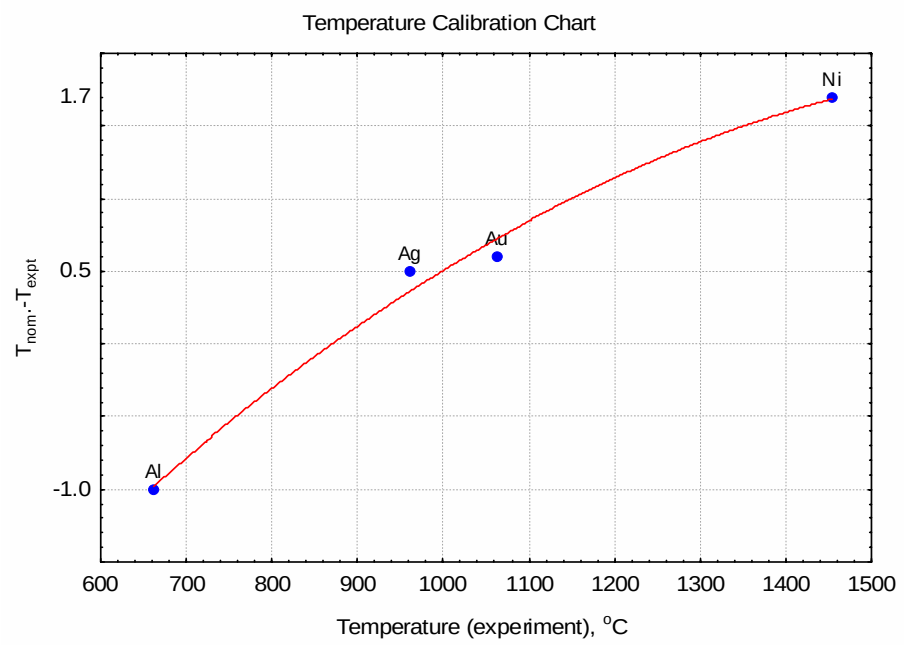

Figure 3.6 Temperature calibration curve fitted with expression described by equation 3.7

3.2.2 Measurement procedure

The specimens were cut from alloys prepared as described in section 3.1. Masses of both reference and sample crucibles were recorded and used to set up the measurement scheme on the

computer attached to the STA. An empty reference crucible and the crucible containing the specimen were inserted in the furnace.

The furnace was evacuated to a vacuum lower than 10^{-4} Pa and filled with instrument grade argon gas to create an inert test environment. The gas flow rate of 60 ml/min was controlled by mass flow controllers (MFC). The MFC are calibrated at 21 °C, atmospheric pressure and laminar flow of nitrogen gas. A conversion factor for argon (1.784) was applied to achieve a flow rate of 60 ml/min. The reading on the flow controller indicates the flow of nitrogen gas and so to obtain the actual flow rate of argon gas the conversion is applied according to the manufacturers instructions: $Q_{Ar} = K \square Q_{N_2}$ (Q_{Ar}: Argon gas flow rate, K: calibration factor, Q_{N2}: Nitrogen flow rate indicated on flow meter reader). All measurements were set to begin recording at 1000 ^{o}C and measurements terminated at 1510 ^{o}C. Heating curves for the binary and ternary subsystems were generated followed by another set of composition of the quaternary Fe-Co-Cu-Si system containing silicon up to 5 wt.%.

Prior to sample measurements, a "blank" run was conducted with empty reference and sample crucibles, to create a baseline at exactly the same conditions as for the measurement for which actual measurements were conducted.

3.2.2.1 Heating rate for DTA

The heating rate effect was determined by performing a series of analyses at different heating schemes. Figure 3.7 shows the DTA traces of alloy C, at four heating schemes labelled 1 to 4 on the curves.

The heating trace labelled (1) was the fastest scheme at 25 °C/min followed by number (2) at 15 °C/min and then the slowest (3) at 2 °C/min. Not all schemes yield useful traces due to seemingly premature terminating temperature set for a 1450 °C as final measurement temperature. On the other hand, a heating rate of 15 °C/min resulted in a definite peak above 1400 °C compared to either a 25 °C/min or a 2^{o}C/min heating rate. This effect has to do with the response rate of the differential signal to thermal activity as can be seen in the drift in the indicated transformation temperatures indicated on the traces. A discussion on this effect has been addressed in Chapter 2. For the measurements conducted in the study a heating rate of 10 °C/min was select and the terminating temperature of 1510 °C instead of 1450 °C was selected.

The resulting trace is labelled (4) in Figure 3.7 with distinctive transformation peaks and a completed liquidus transformation indicated by the return of the trace to the baseline.

Other information obtainable from thermal traces is the energy of transformation which is measured as the area under the peak. This signal is best measured when the differential scanning calorimetry (DSC) mode is used to measure the quantitative energies of transformation. DSC utilises the output signal measured as the difference of the addition of energy to a substance and a reference material. The area between the DSC curve and the selected baseline is proportional to the change in enthalpy and is related by Equation 3.2.

$$\Delta H = \frac{F}{m \cdot k} \tag{3.10}$$

where, H = enthalpy (J/g); F = peak area; K = calibration factor; m = sample mass (g). DSC mode was not used in the current study and all the energy measurements were conducted in DTA mode since the peaks produced were large enough for area analysis.

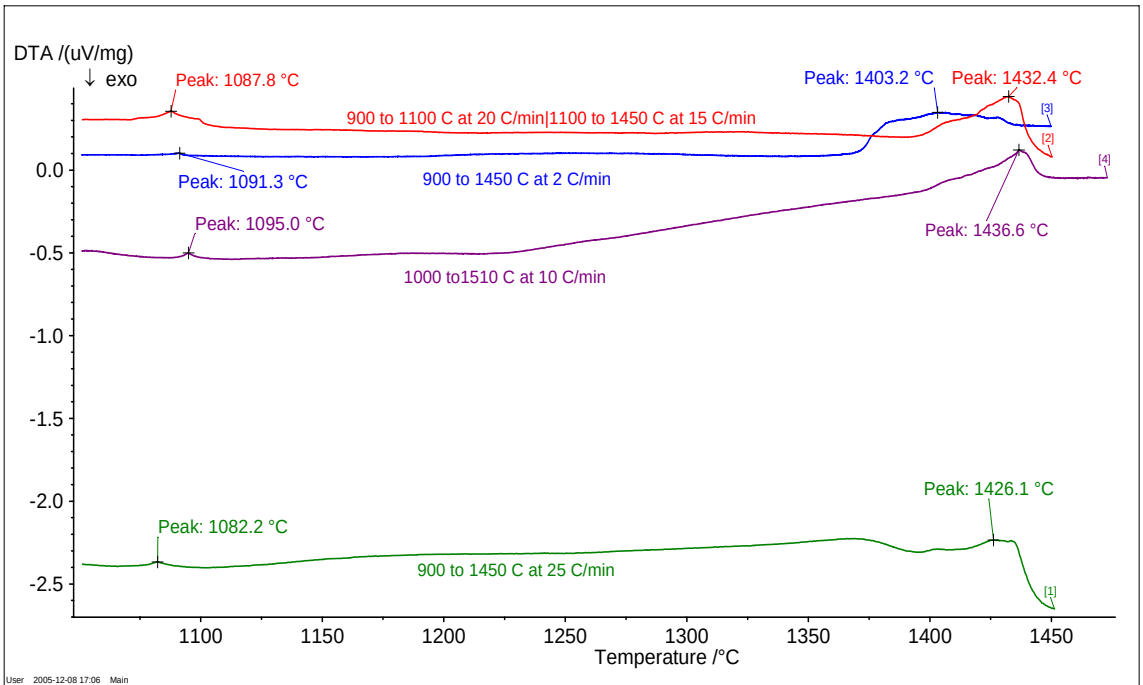

[#] Instrument	File	Identity	Sample	Date	Mass	Segment	Range	Atmosphere	Corr.
[1] NETZSCH STA 409 C/CD	1CFECOCU.SSS	#1C	FeCoCu Alloy	2003-03-04 16:44	11.200 mg	1-2/2	20/50.0(K/min)/900/25.0(K/min)/1450/	argon/50 / ---/--- / ---/---	---
[2] NETZSCH STA 409 C/CD	2CFECOCU.SSS	#2C	FeCoCu Alloy	2003-03-04 19:55	16.000 mg	1-4/4	20....1450/15.0....50.0K/min	argon/50 / ---/--- / ---/---	---
[3] NETZSCH STA 409 C/CD	3CFECOCU.SSS	#3C	FeCoCu Alloy	2003-03-05 15:21	18.500 mg	1-3/3	20....1450/2.0....50.0K/min	argon/50 / ---/--- / ---/---	---
[4] NETZSCH STA 409 C/CD	C000.DSS	C000	C000	2004-02-25 19:20	20.600 mg	1/1	1000/10.0(K/min)/1510	argon/60 / ---/--- / ---/---	020

Figure 3.7 DTA heating traces of alloy C at the indicated heating rates

3.2.3 High temperature confocal microscope: In-situ melting of alloys

The application of the high temperature laser scanning microscope (HLSCM) for phase transformation studies has been reported in the work by Dippenaar and Phelan (2003), and Phelan *et al*. (2005). Four alloys (A, C, D, and E) were submitted for analysis at the BHP steel institute.

Temperature readings are displayed on the cathode ray tube (CRT) together with the images which were simultaneously recorded on videotape at a rate of 30 frames per second. The clips of melting observations were reproduced as micrographs from the video recordings. The specimen holders consist of 5 mm and 10 mm diameter round holders or rectangular holders measuring 10 mm long, 5 mm wide and 3 mm thick, consisting of a polymeric end-piece, alumina 2-bore tube with an outer silica support tube and a platinum holder welded to the B type thermocouple wire (Dippenaar and Reid 2004). The thermocouple is welded on the outside of the specimen holder assembly rendering an offset temperature reading. This offset can be determined by melting pure metal of known melting temperature. The temperature melting displayed on the CRT can be compared to the known melting temperatures to determine the offset.

Samples were sectioned to fit into a 4 mm diameter alumina crucible with parallel faces 3 mm thick, with one face ground on 1200 grit grinding paper and followed by polishing with 6, 3, and 1 micron diamond pastes. The samples were then cleaned in ethanol and dried. All observations were made in an inert argon gas environment. The results from this analysis are presented and discussed in Chapter 4.

3.3 Phase equilibria experiments

Drop quench techniques when used in conjunction with metallographic methods facilitate the study of phase equilibria of the alloys at different temperatures. Solid to liquid phase transformations in alloys occur over a specific temperature range that are detectable by thermal analysis as described in the previous section. Information such as relative atomic fractions generated from scanning electron microscope (SEM) using energy dispersive spectroscopy (EDS) relates compositional information to a tie line on the phase diagram. The use of this technique to determine the liquidus surface of multicomponent slags was applied successfully by (Kongoli *et al*. 1998). By quenching the specimen between the liquidus and solidus, they

determined an exact liquidus point for an alloy with composition of the quenched liquid and of liquidus temperature equal to quench temperature.

The difficulties associated with studying phase equilibria by quenching techniques are described and discussed in Chapter 2. The fixed temperature profile of the furnace was determined to address the uncertainties in location of the constant hot zone in the furnace at experiment conditions. A type B thermocouple was utilised to validate the position of the constant hot zone of the furnace as well as establish the difference between the controller temperature and the furnace constant temperature zone.

3.3.1 Furnace Setup

A vertical tube furnace as illustrated in Figure 3.8 was set up for this experiment. The furnace consisted of an alumina tube and six lanthanum chromite elements arranged symmetrically around the tube. An eight segment programmable Eurotherm 2016C temperature controller was attached to the furnace alongside an over-temperature controller to arrest over-heating above the set point. Gas to the furnace was supplied through the bottom via a hydro-sorb and oxy-sorb system that are described later in this section. The samples were held in position by a platinum wire that was wound around slits in the crucibles. The arrangement was such that more than one crucible could be inserted in the furnace at a time.

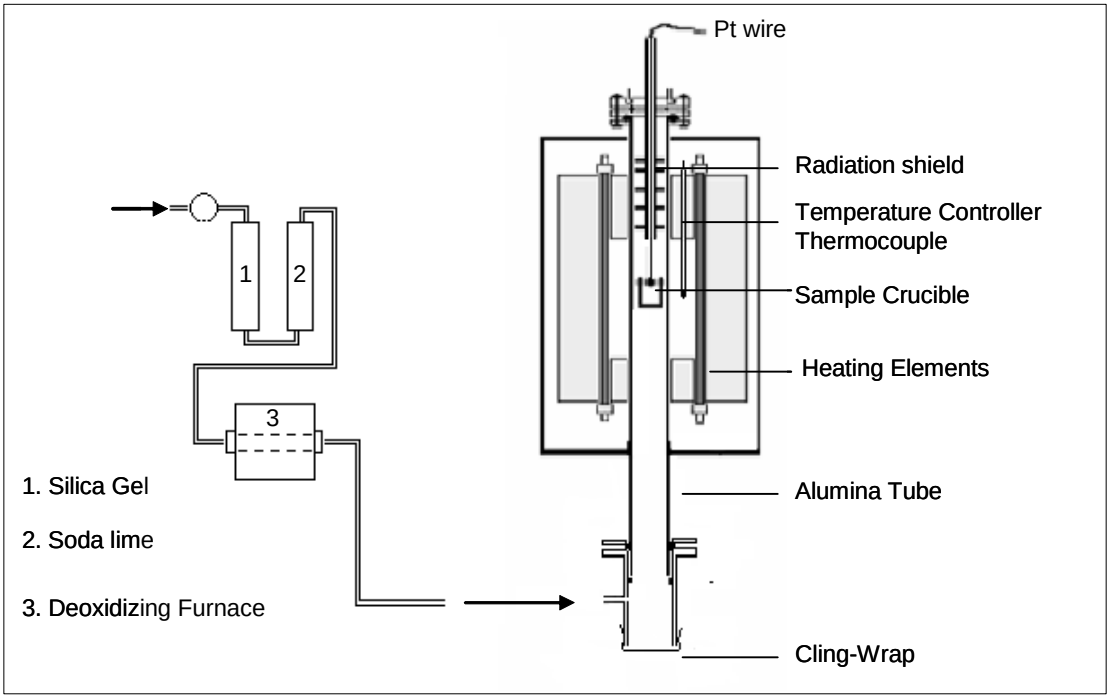

Figure 3.8. A schematic diagram of the furnace arrangement used in quench studies

The specimen holder was designed such that more than three crucibles could be quenched at a time. Sample crucibles were suspended on a alumina ring and secured to a platinum 6 % rhodium wire. The total length of supporting wire, including the crucible height was 490 mm, a length sufficient to place the specimen in the hot zone of the furnace.

The furnace reaction tube was sealed at both ends. At the bottom end, cling-wrap plastic was wrapped around the stainless steel extension piece that was immersed shallowly in water in the quench tank. At the top end two water-cooled stainless steel flanges were bolted together to cause a squeeze on the rubber seal, so sealing the furnace from the atmosphere and holding the flanges to the ceramic tube. Ice water mixture was used as the quenching medium. A leak-test was conducted on all the fasteners and on joints in the gas train.

3.3.1.1 Temperature Profile of Furnace

Prior to using the furnace for the quench experiments, a temperature profile was examined to establish the location of the hottest zone of in the furnace. This investigation was conducted with a meter long Type B thermocouple. Measurement of the profile was carried out at two temperatures, 1030 °C, and 1550 °C. The objective was twofold: to determine the temperature profile of the furnace and the temperature drift of the controller temperature from the thermocouple temperature reading inside the furnace.

Measurements of temperature were taken at 10 mm spacing from the top to the bottom of the tube at the selected temperatures. Figure 3.9 shows the temperature profile of the hot zone of the furnace plotted for the two temperatures. The hottest zone of the furnace was at 480 mm measured from the top end of the furnace, with a drop of about 1 °C to 2 °C for every 10 mm above or below this value. It was also observed that at the lower temperature, the difference between the furnace temperature controller and the thermocouple was 6 ^{o}C, and 15 ^{o}C at the higher temperature.

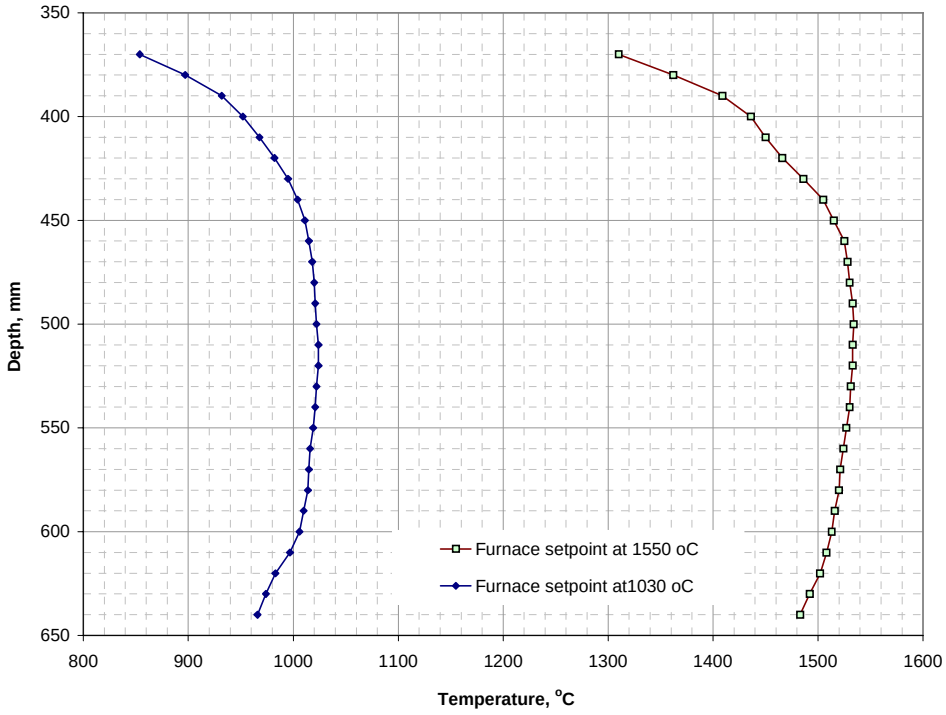

Figure 3.9 Temperature profiles of the tube furnace measured at 1030°C and 1550°C

3.3.1.2 Gas purification

Apart from temperature calibration, the reaction atmosphere was controlled and maintained at inert conditions. All the components in the gas purifier were fabricated in-house and consisted of two cylinders containing silica gel and soda lime and a horizontal tube furnace containing copper turnings. Ultra high purity (UHP) argon gas (99.999%) was cleaned by passing it over (i) silica gel to remove moisture, (ii) soda lime to remove CO_2 gas, and (iii) over hot copper turnings set at 500 °C to remove oxygen. A horizontal resistance tube furnace was adapted to heat the copper turnings. The flow rate of the gas was 2 *l*/min at room temperature and atmospheric pressure.

3.3.2 Experimental Procedure

The measured solidus and liquidus temperatures from DTA were used to set the temperature boundaries for quench experiments of each sample. Six quench temperatures for each composition range of the Fe-Co-Cu system were selected at intervals between the liquidus and solidus temperatures and above the liquidus and below the solidus temperatures too. Table 3.3 lists the temperature regimes for the quench experiments. The quench temperatures for the quaternary alloy (C#02) Fe-Co-Cu-Si system were selected in a similar way.

Table 3.3 Liquidus and solidus temperatures and corresponding quench temperatures for Fe-Co-Cu alloy system

	DTA T, °C		Quench Temperature, °C					
Sample ID	T_onset (solidus)	T_peak (liquidus)	T1	T2	T3	T4	T5	T6
A	1452.0±1.95	1470.1±1.99	1450	1455	1460	1465	1470	1475
B	1437.7±1.92	1456.7±1.96	1435	1440	1445	1450	1455	1460
C	1398.1±1.84	1436.0±1.92	1395	1405	1415	1425	1435	1445
D	1394.8±1.83	1434.4±1.91	1390	1400	1410	1420	1430	1440
E	1416.0±1.88	1429.4±1.90	1415	1420	1425	1430	1435	1440
F	1419.8±1.88	1435.6±1.92	1415	1420	1425	1430	1435	1440
T	1388.0±1.81	1399.8±1.84	1380	1385	1390	1395	1400	1405
C#02	1317.0±1.80	1367.0±1.88	1317	1328	1360	1369	-	-

The furnace was slowly heated to 350 °C (at 10 °C/min) prior to placing the specimen in the furnace. This was maintained as the minimum operating temperature of the furnace to prevent thermal shock on the alumina tube. The specimens were first heated at 50 °C/min to 1050 °C, a temperature near the peritectic transformation temperature, and isothermally heated for 30 minutes at 1050 °C. Then the specimens were heated at 10 °C/min to the desired quench temperature (see Table 3.3) at which the specimen was again isothermally heated for 2 hours. Since the equilibrium time for the specimen was not established for this experiment attention was paid to the heating rate on the assumption that a slower heating rate should allow for sufficient time for phases in the alloy to come into "equilibrium" because the supply of heat to the specimen would be slow and constant. In addition, smaller specimen masses ranging between 100 mg and 500 mg were used to minimise the equilibration time required (Hume-Rothery *et al*. 1952). Further more, reference was made to the work by Haworth and Hume-Rothery (1958-59) who kept their alloys system at the desired quenching temperatures for at least 7 minutes and yet found the microstructure satisfactory for the liquidus and solidus determination. In similar work on the platinum-chromium by Waterstrat (1973), the alloys were kept for 2 hours at the desired temperature before quenching. Therefore, the alloy systems studied for the Fe-Co-Cu-Si phase equilibria represent microstructures that are in chemical equilibrium.

3.4 Gas-Alloy-Silica Equilibrium Experiments

The objective of this experiment was to study the activity of silicon in the liquid Fe-Co-Cu-Si system was studied by chemical equilibration using a gas/silica/alloy technique at 1450 °C as well as at varying from 1400 to 1500 °C. The binary and ternary alloy subsystems of the quaternary Fe-Co-Cu-Si system were equilibrated in quartz (silica) crucibles at 10^{-13}, $10^{-14.1}$, and 10^{-15} atmospheres of oxygen partial pressures. The oxygen partial pressure was created from the C-H-O gas system. The Gibbs phase rule was satisfied by fixing the temperature, since only one

degree of freedom needed to be fixed (f = 2 Components + 2 – 3 Phases). The ratios of CO_2/H_2 required at a given temperature were determined from the tables by Deines *et al.* (1974).

3.4.1 Equipment Description

For this part of the experiments a vertical tube furnace with a 2.5 mm diameter working tube positioned inside a hollow, spiral-cut silicon carbide resistance element was used. A non-programmable Rex F4 temperature controller was fitted to the furnace. Both ends of the furnace tube were fitted with water-cooled brass flanges through which gas was supplied to and from the furnace, and samples were secured to a molybdenum wire and introduced from the top end of the furnace. A rubber stopper with a hole through which the Mo wire was secured was used to plug the top end and the wire was held in two positions by two clamps. The double clamp ensured that when the sample was released for quenching no air ingress into the furnace occurred. As in the previous experiments, the bottom end was sealed with cling-wrap plastic on which vacuum grease was smeared to prevent H_2 diffusion.

3.4.1.1 Gas Delivery System

Three gases, carbon dioxide (CO_2), hydrogen (H_2) and argon (Ar) were pre-cleaned and mixed before going to the furnace. Oxy-sorb and hydro-sorb cylinders were fitted along the gas trains to remove oxygen and moisture from the gas respectively. Mass flow controllers (MFC) were used to control the volumetric flow rates and proportions of gases to the furnace.

Gas mass flow controllers were calibrated on Nitrogen and flow rates validated on actual gas for experiment. A 1000 cm^3/min (STP) MFC was used for H_2 and a 20 cm^3/min (STP) for CO_2. The verification of the gas flow rates at room temperature and atmospheric pressure was attained by comparing U-tube manometer flow rates to the MFC set flow rates. The resulting charts are presented in Figures IV-1 and IV-2 in Appendix I.

3.4.1.2 Furnace Temperature Profile

The furnace temperature profile was determined by the method described in section 3.3.1(a). The hot zone was at 450 to 460 mm from the top and a temperature difference of 14.4 °C to 15 °C between the set value and the hot zone of the furnace was observed. An illustration of the furnace and the profile of the hot zone is shown in Figure 3.10

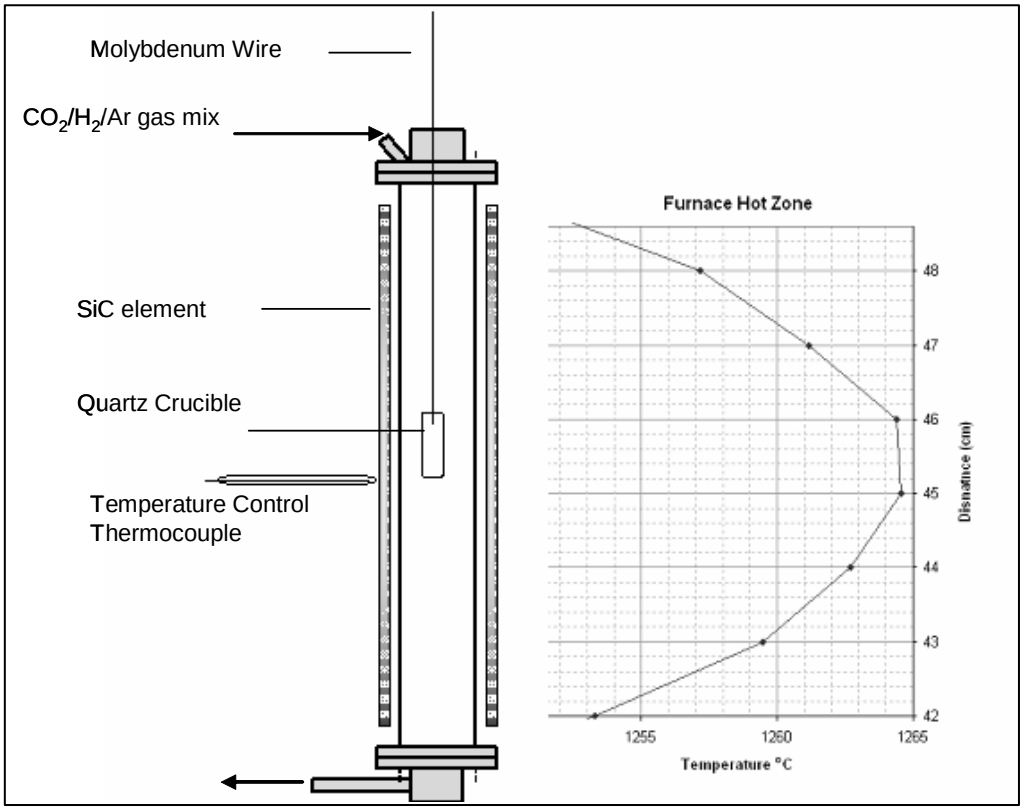

Figure 3.10 Schematic furnace setup and temperature profile determined at 1250 ^{o}C for the SiO_2– gas-alloy equilibration experiments

3.4.2 Determination of Equilibration Time

Initially an experiment was conducted to test the design of the experiment by equilibrating a quartz crucible with a Fe-Co-Cu alloy. Quartz crucibles were made from quartz tubes and measured 7 mm ID. Preliminary results from 15 hours equilibration of the Fe-Co-Cu alloy showed that about 5 wt.% silicon partitioned to the alloy at equilibration temperature of 1405 °C and log pO_2 = -15. Secondly, equilibration time was determined by carrying out experiments at time intervals of 4 hour, 8 hours, 16 hours, and 24 hours at a higher pO_2. Fifteen specimens consisting of Fe-Co-Cu and the limiting binaries (Fe-Cu and Co-Cu) were equilibrated with quartz crucibles under an oxygen potential equivalent to $1x10^{-13}$ at 1450 °C, above the liquidus temperatures of the alloys. The outcome of the experiments is shown in Figure 3.11 and it was

concluded that equilibration time was at about 8 hours since no increase in the concentration of silicon in the alloy took place at longer times with respect to the pO_2 set for the experiment.

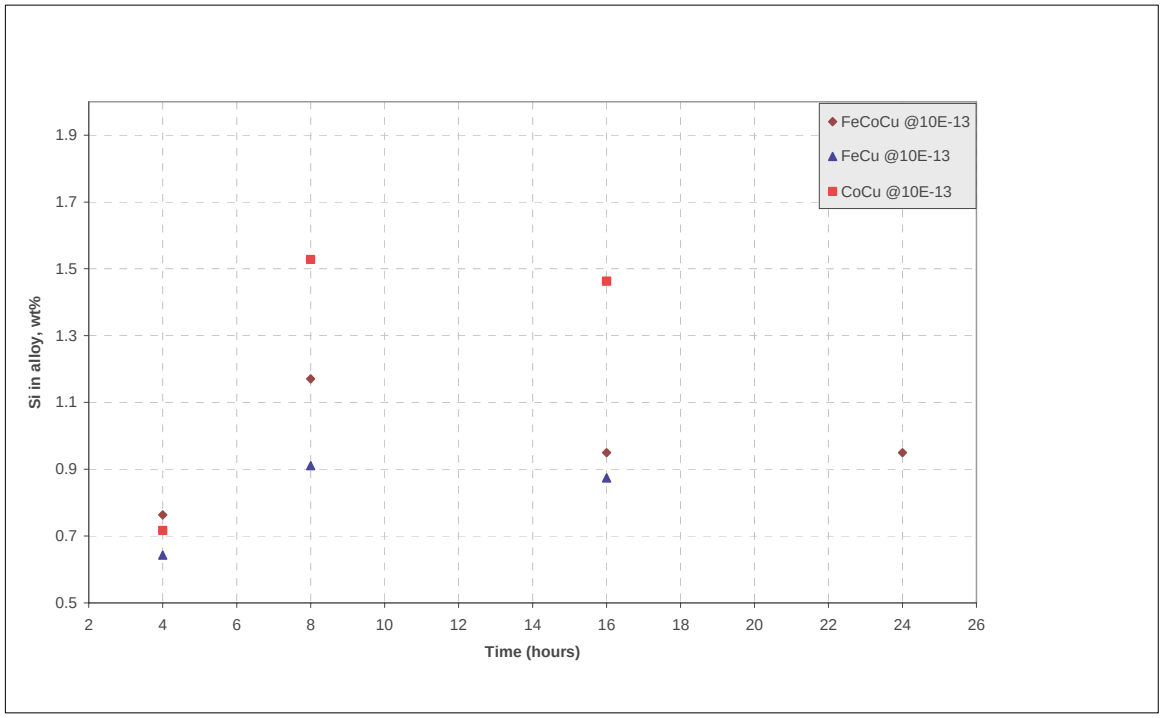

Figure 3.11 Equilibrium-time experiments for Fe-Co-Cu at log pO_2 = - 13 and T=1723K

3.4.2.2 Validation of Oxygen Partial Pressure

Verification of equilibrium was by a reverse-equilibrium-approach. Oxygen partial pressure was verified by observing the oxide formation of Cr_2O_3 from pure Cr at 1450 ^oC and log pO_2 ranging from -13.5 to -14.5. The oxygen potential diagram shows that the Cr_2O_3 can be reduced to Cr at log pO_2 = -14.0 at 1450 ^oC. The colour change from lustrous grey of pure Cr metal to green (Cr_2O_3) at log pO_2 = 13.5 and the reversal of it at log pO_2 = 14.5 was used as an indicator for correctness of pO_2 in the system.

3.4.3 Procedure

A pure quartz (SiO_2) crucible, Fe-Co-Cu alloy, and the premixed CO_2/H_2 gas in ratios listed in Table 3.4 were equilibrated for about 8 hours at temperatures above the liquidus of the alloy determined by DTA in section 3.2, quenched in cold water and prepared for SEM/EDS analysis.

Table 3.4 Gas ratios used in the experiment to obtain pO_2

log pO_2	CO_2 cc(STP)	H_2 cc(STP)	Total Vol. cc (STP)	CO_2/H_2	T, K
-14.1	1.119	510.516	511.635	2.193E-03	1723.15
-13.0	3.618	506.376	509.994	7.145E-03	1723.15
-15.0	0.760	985.987	986.747	7.704E-04	1723.15
-15.0	1.253	995.063	996.316	1.259E-03	1673.15

3.5 Analytical Techniques and Procedures

All the alloys were analysed by SEM in EDS mode. Mounted specimens were polished to a 1 micron finish, examined on light microscope for microstructure and the carbon coated for SEM/EDS to determine phase equilibrium compositions. Initial calibration of the equipment was conducted with pure iron, cobalt and copper metals prepared from the same powder as used for the alloys. Further details on the procedures are discussed in Appendix III.

CHAPTER 4

RESULTS AND DISCUSSION

This chapter presents the results generated from experiments described in Chapter 3 and the discussion thereof. The results of the preliminary experiments and validation procedures show that within the experimental errors the data obtained in this study are valid. The first section (4.1) of the chapter contains measurements of liquidus and solidus temperatures, and other transformation temperatures. Phase equilibria in the quaternary system Fe-Co-Cu-Si and subsystem Fe-Co-Cu were determined at selected temperatures. The results are summarised in section 4.2. The activity and activity coefficient of silicon calculated from gas-alloy-silica chemical equilibrium experiments are tabulated and discussed in section 4.3. Thermodynamic descriptions of the liquid phase in the Fe-Co-Cu-Si system are discussed in section 4.4.

4.1 Transformation temperatures and invariant reactions in Fe-Co-Cu-Si

The results of the invariant reactions and the transition temperatures determined by DTA are discussed in the following sections. Where possible, the results are compared to the FactSage™ and/or MTData calculated values. The FactSage™ calculated results are based on the thermodynamic database FSstel where as the MTData calculations are based on the SGTE database, which are described in detail in section 4.4.

4.1.1 Binary systems

The results of the invariant reactions and the transition temperatures in the binary systems of the Fe-Co-Cu-Si are listed in Table 4.1. The measured values are in agreement with the calculated values from FactSage™ and published phase diagrams discussed earlier in section 2.4.2. The liquidus temperatures and the accompanying energy of transformation are listed in Table 4.2. The energies of transformation were calculated by integrating the area under the curve as described in section 3.2.1.1 (see equation 3.9)

A typical output of a DTA measurement is illustrated in Figure 4.1 The peak at the end of the trace indicates the measured liquidus temperature and the solidus temperature is indicated as the onset of melting on this peak. The enthalpy of transformation is calculated as the area under the final peak in J/g. Similarly, other transition temperatures such as the peritectic reactions were determined. The DTA measured transformation temperatures of the alloys Fe-20wt% Cu and Fe-

40wt% Cu show a good agreement with the published phase diagram data (Chen and Jin 2005; Hasebe and Nishizawa 1980; Turchanin *et al*. 2003). Figure 4.2 is a phase diagram for the binary Fe-Cu calculated with the FactSage™ software. Shown in the figure are the measured transformation temperatures at the indicated compositions.

Table 4.1 Transition temperatures determined by DTA method in the binary systems

Alloy	Code #	Nominal Composition, wt. %				Invariant Reaction	Temp. °C	Source
		Fe	Cu	Co	Si			
Fe-Cu	1	80	20			L + γ-Fe⇔Cu	1093	This work
	3	60	40				1098	This work
							1094	(Hasebe and Nishizawa 1980)
							1096	(Chen and Jin 2005)
		80	20				1096	Calculated
		60	20				1096	Calculated
Fe-Co	1	80		20		α-Fe ⇔ γ-Fe	954	This work
	3	60		40			993	This work
	4	50		50			996	This work
		54		46			985	(Hansen and Anderko 1958)
		80		20			947	Calculated
		60		40			975	Calculated
Co-Cu	1		50	50		L + α-Co ⇔ Cu	1117	This work
	3		40	60			1116	This work
							1112	(Hasebe and Nishizawa 1980)
			40	60			1111	Calculated
Co-Si	1			90	10	hcp +Co_2Si ⇔ hcp	1197	This work
				90	10		1191	Calculated
	1			90	10	hcp ⇔ hcp + L	1207	This work
				90	10		1213	Calculated
				90	10	hcp + L ⇔ fcc + L	1238	This work
				90	10		1254	Calculated

The results for the Fe-Co system are consistent with the published data for both the transformation temperature of α to γ and the liquidus and solidus temperatures. Figure 4.3 shows the measured transformation temperature plotted on a calculated phase diagram.

Table 4.2 Transformation temperatures and energy of transformation

System	Specimen#	Nominal Composition, wt. %				Transition Temperature, ^{o}C		Transformation Energy, (Area under melting peak) J/g	Source
		Fe	Cu	Co	Si	Liquidus	Solidus		
Fe-Cu	1	80	20			1456	1484	150	This work
	3	60	40			1431	1485	144	This work
Fe-Co	1	80		20		1501	1487	122	This work
	3	60		40		1492	1430	115	This work
	4	50		50		1492	1415	155	This work
Co-Cu	1		50	50		1384	1363	70	This work
	3		40	60		1393	1378	131	This work
Co-Si	1			98	2	1481	1451	102	This work
				98	2	1460			Calculated
	2			90	10	1285	1234	87	This work
				90	10	1306			Calculated

The temperatures of transformation for Co-Cu were measured at compositions pertinent to the composition of the quaternary system of the ferrocobalt. Again good agreement was obtained between the measured and calculated values for this system as indicated on the phase diagrams in Figure 4.4.

The measured transition temperatures for Co-Si binary are in agreement with the calculated phase diagrams as listed in Table 4.2 and Table 4.3. These data points are shown in Table 4.3. However, this system shows a slight deviation of the data points at high temperatures. This deviation can be attributed to the loss of material from the crucible during heating of the specimen. According to the characteristics of the DTA traces, described in section 2.3.2, the peaks at 1207 and 1238 °C in Figure 4.6 are physical transformations of the solid in which the solid phases are in equilibrium with a liquid phase formed at 1207 °C by the invariant reaction indicated in Table 4.1. This liquid solution is in equilibrium with the solid over a relatively wide temperature that during the measurement loss in the metal content may change affecting the composition of the alloy and thus liquidus temperature. It would follow then that the actual composition of the alloy could have been lower than the nominal alloy composition of 90 wt. % Co-10 wt. % Si.

The measured phase diagram data for the binary systems and the calculated phase diagrams compare fairly well within the experimental errors. It is shown from these results that the optimised database for these binary systems provides a platform to perform the phase equilibria calculations in the binary systems Fe-Co, Fe-Cu, Co-Cu, Cu-Si and Co-Si. So apart from the results in this section serving as the validation for the experimental setup and techniques, they also show that the databases used in the calculations for the binary phase diagrams are extensively assessed. Therefore these phase diagrams can be used to describe terminal binary systems for the ternary systems of the quaternary Fe-Co-Cu-Si.

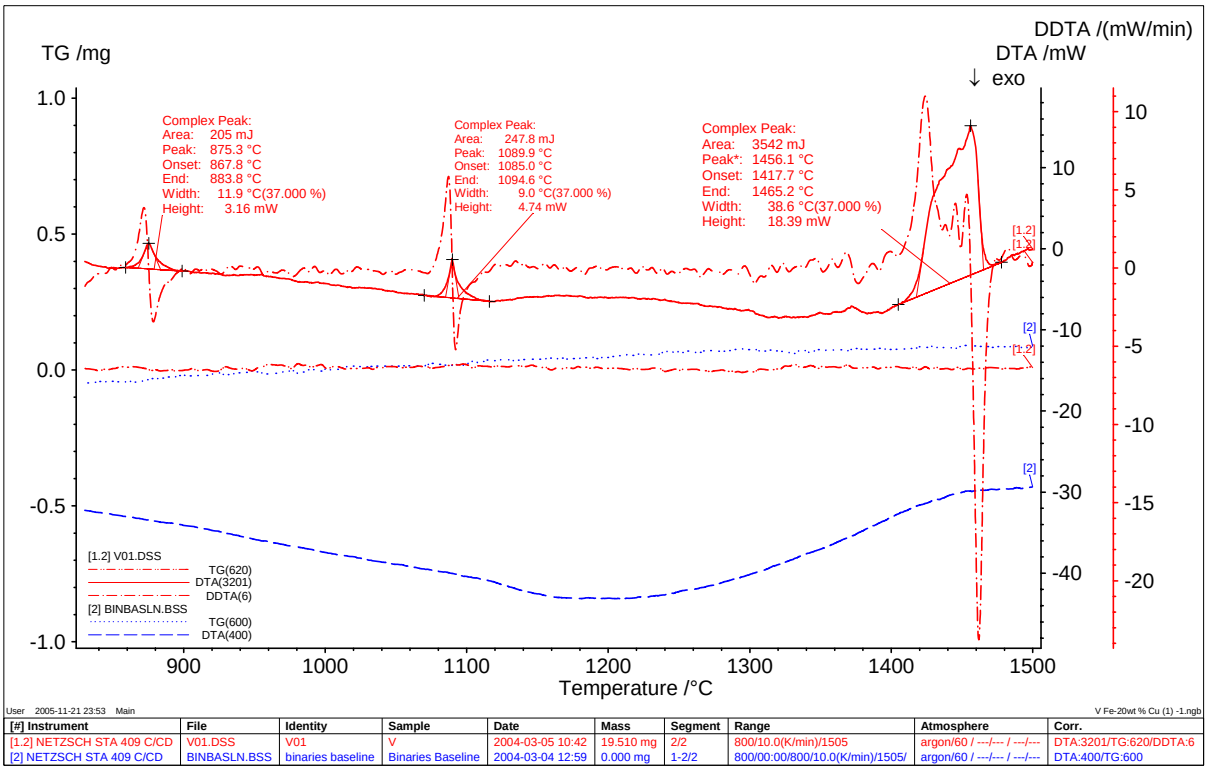

[#] Instrument	File	Identity	Sample	Date	Mass	Segment	Range	Atmosphere	Corr.
[1.2] NETZSCH STA 409 C/CD	V01.DSS	V01	V	2004-03-05 10:42	19.510 mg	2/2	800/10.0(K/min)/1505	argon/60 / ---/--- / ---/---	DTA:3201/TG:620/DDTA:6
[2] NETZSCH STA 409 C/CD	BINBASLN.BSS	binaries baseline	Binaries Baseline	2004-03-04 12:59	0.000 mg	1-2/2	800/00:00/800/10.0(K/min)/1505/	argon/60 / ---/--- / ---/---	DTA:400/TG:600

Figure 4.1 A typical DTA output file indicating calculated values for Fe-20 wt% Cu alloy

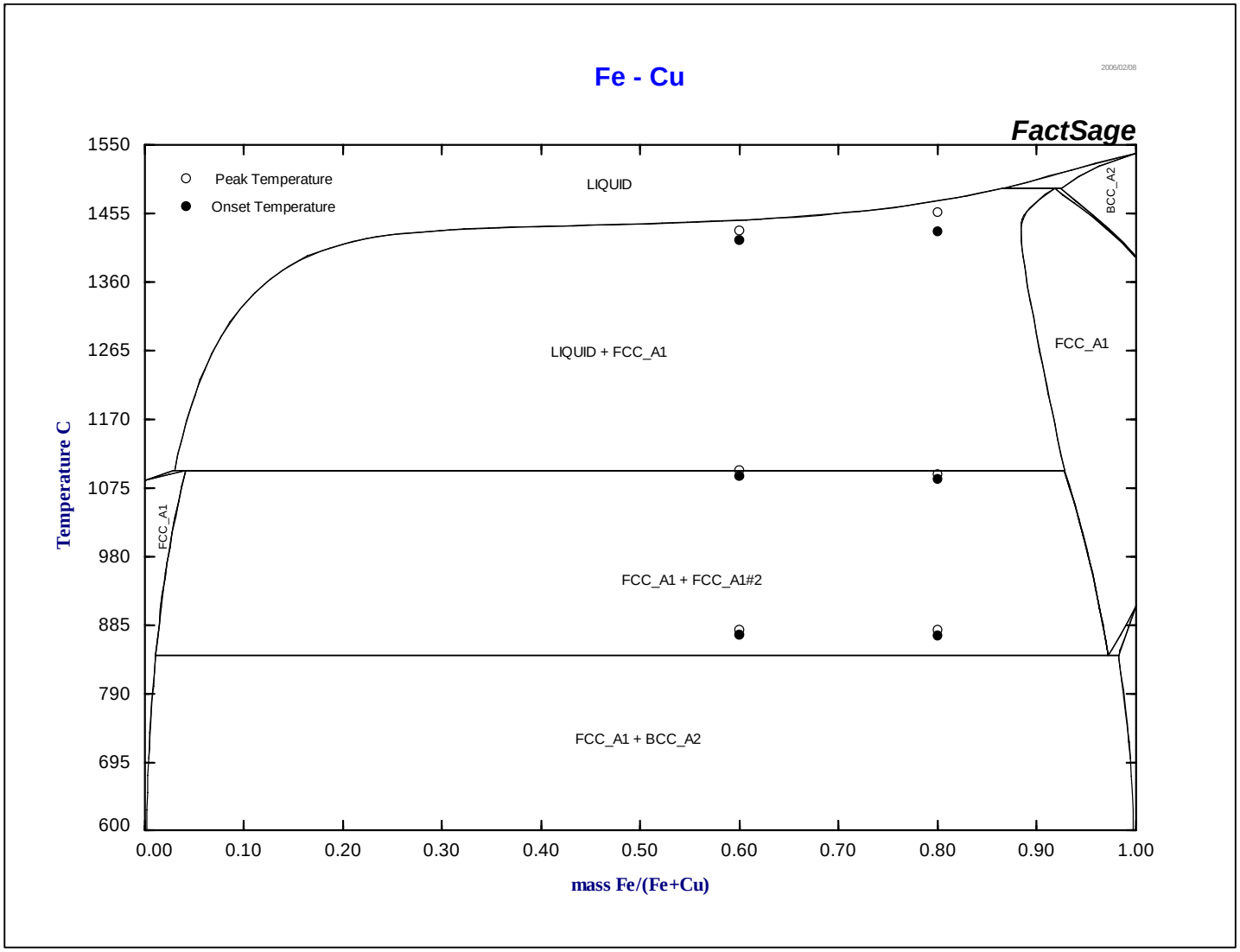

Figure 4.2 The Fe-Cu binary phase diagram calculated and drawn with FactSage™ showing DTA measured transformation temperatures at selected compositions

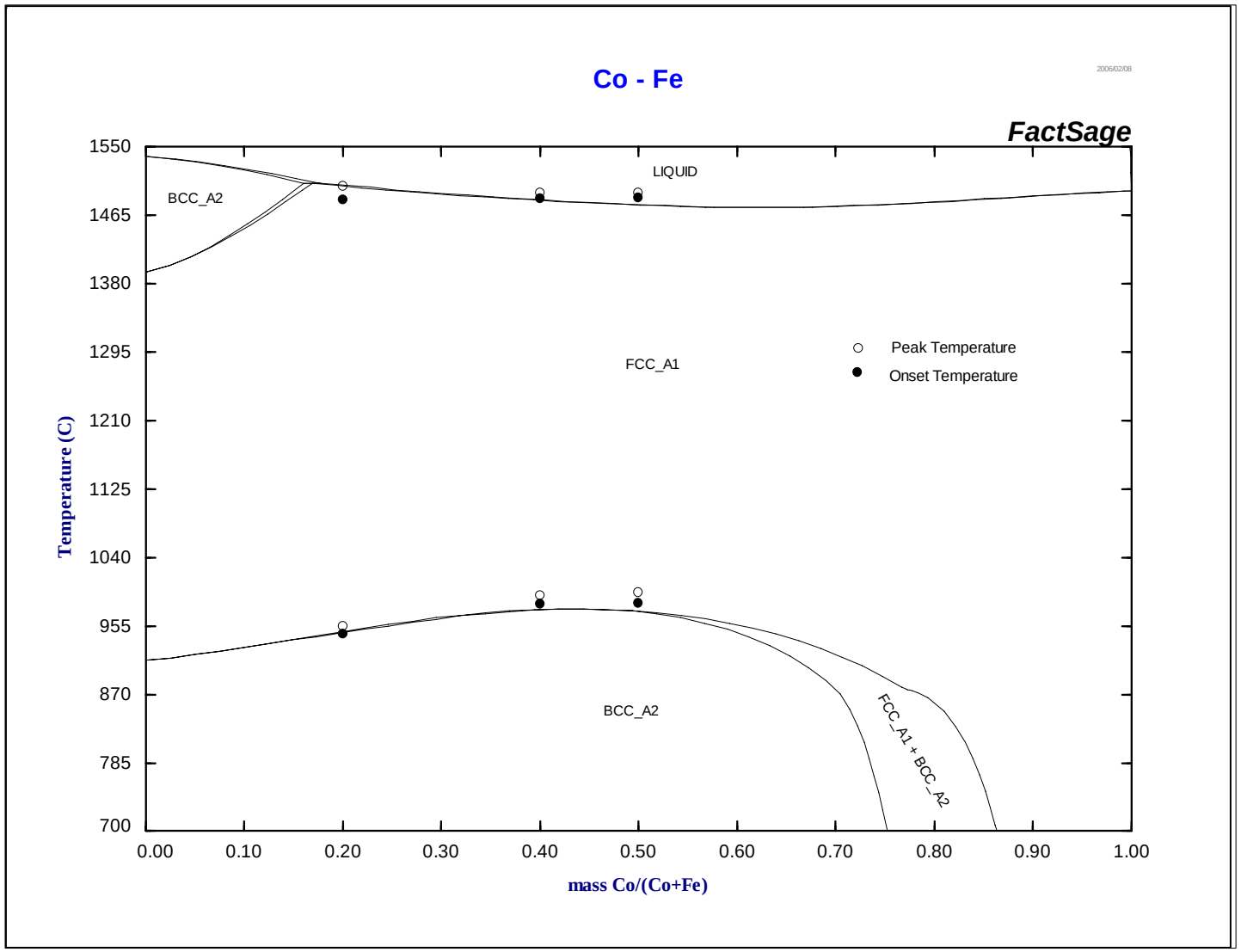

Figure 4.3 The Fe-Co binary phase diagram calculated and drawn with FactSage™ showing DTA measured transformation temperatures at selected compositions

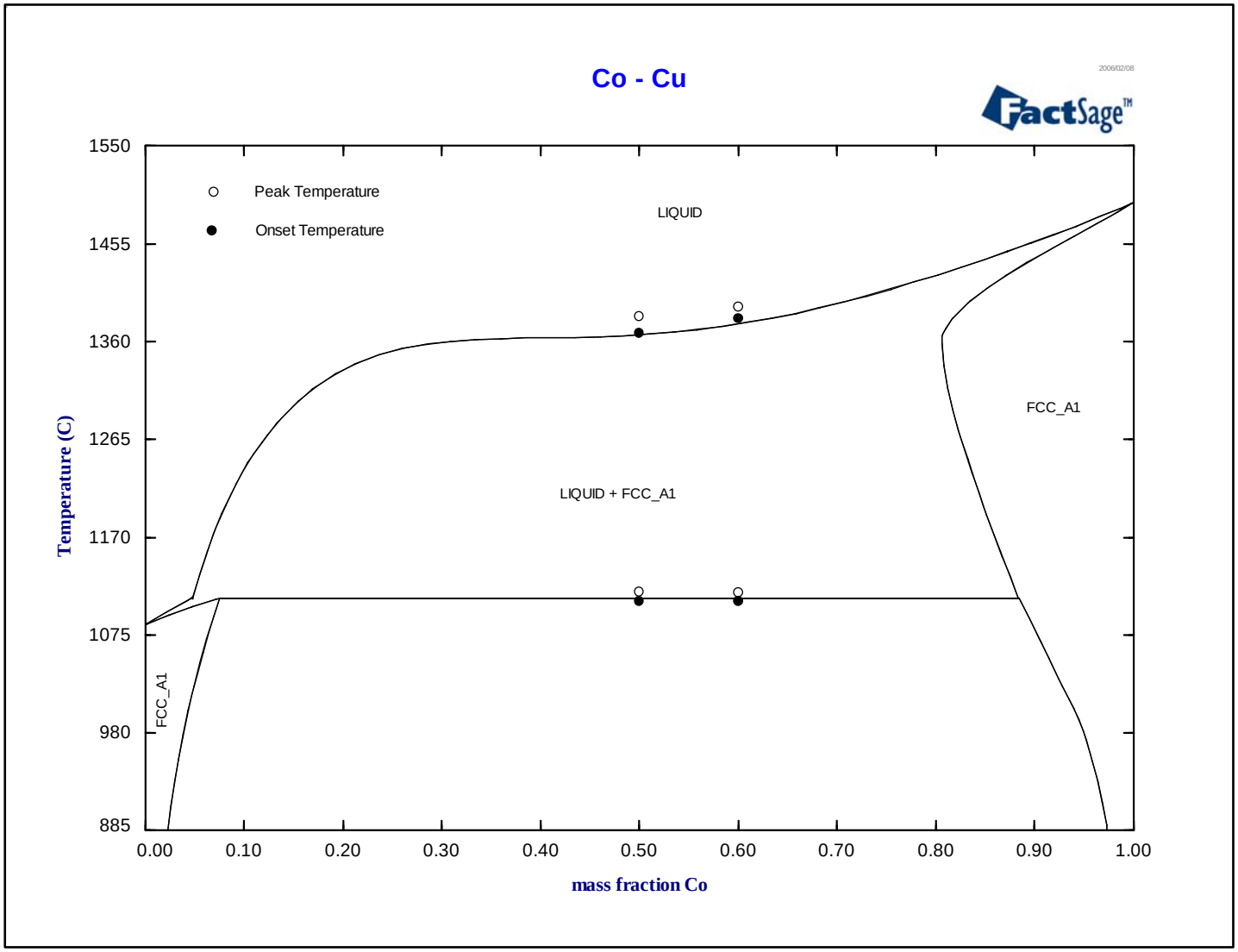

Figure 4.4 The Co-Cu binary phase diagram calculated and drawn with FactSage™ showing DTA measured transformation temperatures at selected

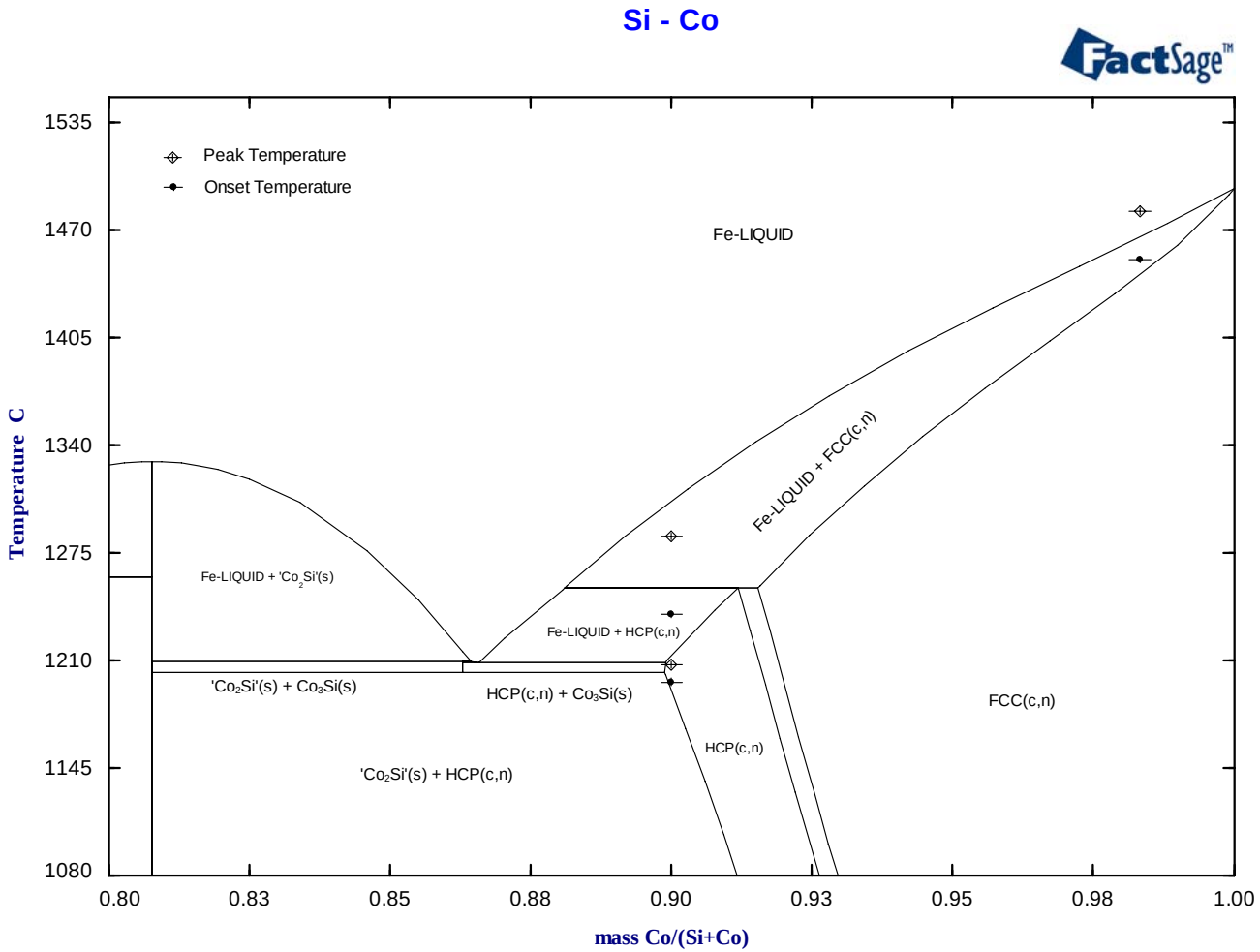

Figure 4.5 The Co-Si diagram calculated and drawn with FactSage™ showing DTA measured transformation temperatures at selected compositions

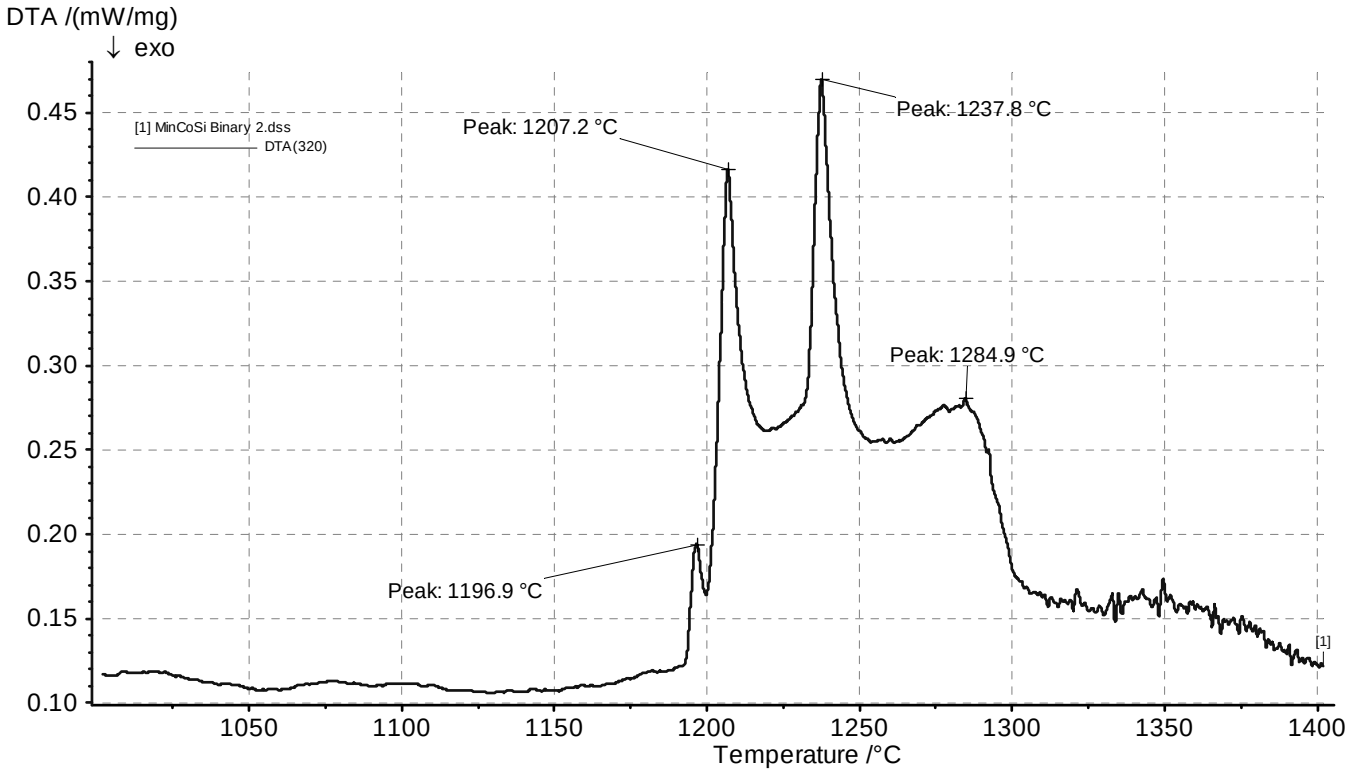

Figure 4.6 The DTA heating trace of the Co-10wt. %Si showing the temperatures of the invariant transformations and liquidus

4.1.2 Ternary Systems

The results of the DTA measured invariant reaction temperatures and the liquidus temperatures of the ternary systems are discussed in this section. The literature data is listed in the tables where available.

4.1.2.1 Fe-Co-Cu

The ternary Fe-Co-Cu system has peritectic type invariant reactions between 1090 °C and 1100 °C as listed in Table 4.4 and is characteristic of the terminal binary systems Fe-Cu and Co-Cu. Because of this behaviour Maddocks and Clausen (1936) described the Fe-Co-Cu ternary as a θ-Cu quasibinary where, θ represented the Fe-Co side.

Table 4.3 The invariant reaction temperatures in Fe-Co-Cu system

Alloy	Composition, wt. %			Invariant Reaction	Temp. °C
	Fe	Cu	Co		
A	79.12	10.60	10.53	none	
B	68.54	16.20	15.16	L + fcc ⇔ Cu	1092
C	63.40	23.24	17.45		1095
D	54.32	27.18	18.17		1094
E	50.49	31.05	18.89		1096
F	64.77	15.23	20.36		1095
T	40.31	20.89	38.07		1097

The general behaviour of the ternary alloy with respect to the liquidus temperatures is characterised by the ratio of iron to copper, Table 4.5. It has been observed in this work that the liquidus temperature is more strongly dependent on the copper content than the cobalt content. This is in agreement with the findings by Maddocks and Clausen (1936). The copper-rich liquid associated with the peritectic reaction is larger in proportion to the solid phase at higher copper content and acts as a buffer to the dissolution of iron and cobalt from the solid phase. This is also evident from the solid/liquid equilibria studies by Ohtani *et al.* (1997). Therefore, the presence of cobalt in the alloy does not change the solubility of copper in solid iron. Moreover, cobalt exhibits complete solid solubility in iron in the composition range studied.

Table 4.4 Transformation temperatures and energy of transformation in the ternary Fe-Co-Cu system

Alloy	Composition in wt%			Ratio			Transition Temperatures °C		Area : Lquidus Peak J/g	Source
	Fe	Co	Cu	Co/Cu	Fe/Cu	Fe/Co	Liquidus	Solidus		This work
A	79.12	10.60	10.53	1.0	7.5	7.5	1470	1452	141.3	This work
B	68.54	16.20	15.16	1.1	4.5	4.2	1456	1438	104.6	This work
C	60.79	20.48	18.74	1.3	3.6	2.7	1436	1398	148.3	This work
D	54.32	27.18	18.17	1.5	3.0	2.0	1434	1395	166.1	This work
E	50.49	31.05	18.89	1.6	2.7	1.6	1429	1416	139.9	This work
F	64.77	15.23	20.36	0.7	3.2	4.3	1435	1420	136.7	This work
T	40.31	20.89	38.07	0.5	1.1	1.9	1400	1388	139.4	This work
T	*42.00*	*20.00*	*38.00*				*1300*			*(Bumberger et al. 2002)*
T	*40.00*	*20.00*	*40.00*				*1392*			*(Kim and Abbaschian 2000)*

A ternary composition of Cu-38 wt.%Fe-20wt.%Co, as reported by Bamberger *et al.* (2002) was included in the DTA experiments to reproduce their results. The onset temperature of melting (solidus) for this alloy (designated alloy T in Table 4.6) was determined to be 1388 °C and the peak temperature was 1400 °C. The outcome of the analyses differ remarkably from that reported by Bamberger *et al.* (2002) who reported 1300 °C as the melting temperature. On the other hand, the liquidus temperature measured by Kim and Abbaschian (2000) for this alloy composition was 1392 °C, fairly close to the DTA value reported here. As mentioned in section 2.3.2 this difference is mainly due to the different techniques used.

The experimental results are in fair agreement with the published phase diagram data (Bamberger *et al*. 2002; Kim and Abbaschian 2000; Maddocks and Clausen 1936b; Palumbo *et al*. 2006; Wang *et al*. 2002). The experimental data from literature is shown in Figure 4.7(a) to which a surface was fitted by a polynomial, Figure 4.7(b).

The polynomial of the surface fit was used to regress the liquidus temperature data. The regression model can describe about 88 % (Figure 4.8) of the data using the prediction equation (4.1):

$$\begin{aligned} T_{liquidus} = {} & 15.29 \cdot Y_{Fe} + 15.28 \cdot Y_{Co} + 10.74 \cdot Y_{Cu} - 0.037 \cdot Y_{Fe} \cdot Y_{Co} + 0.0402 \cdot Y_{Fe} \cdot Y_{Cu} \\ & + 0.0521 \cdot Y_{Co} \cdot Y_{Cu} + 0.5 \times 10^{-3} \cdot Y_{Fe} \cdot Y_{Co} \cdot (Y_{Fe} - Y_{Co}) \\ & - 0.825 \times 10^{-3} Y_{Fe} \cdot Y_{Cu} \cdot (Y_{Fe} - Y_{Cu}) - 0.199 \times 10^{-3} Y_{Co} \cdot Y_{Cu} \cdot (Y_{Co} - Y_{Cu}) \\ & - 0.001 \cdot Y_{Fe} \cdot Y_{Co} \cdot Y_{Cu} \end{aligned} \quad (4.1)$$

Y_i is the mass fraction of component *i* the alloy.

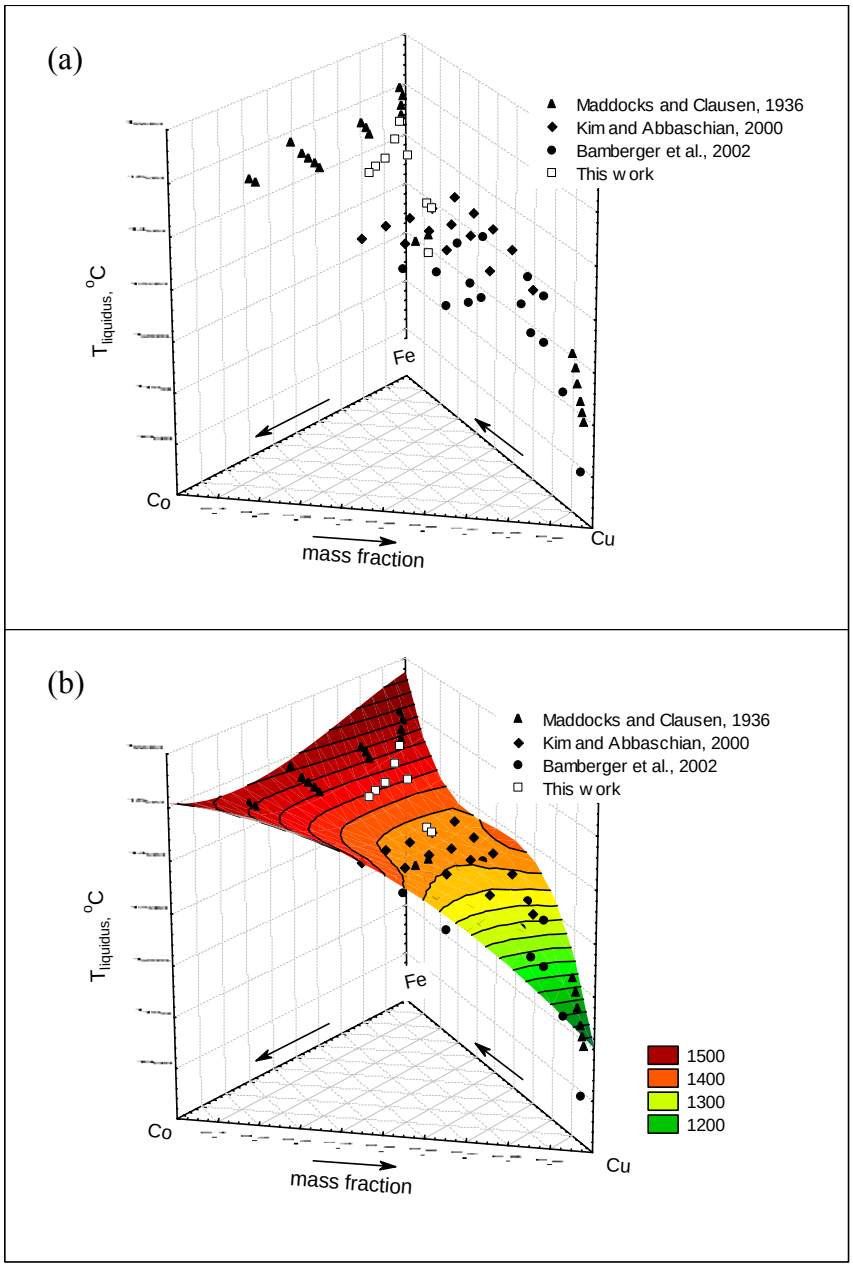

Figure 4.7 A 3-D scatter plot of (a) experimentally determined liquidus temperatures and (b) a surface fitted by a full cubic polynomial

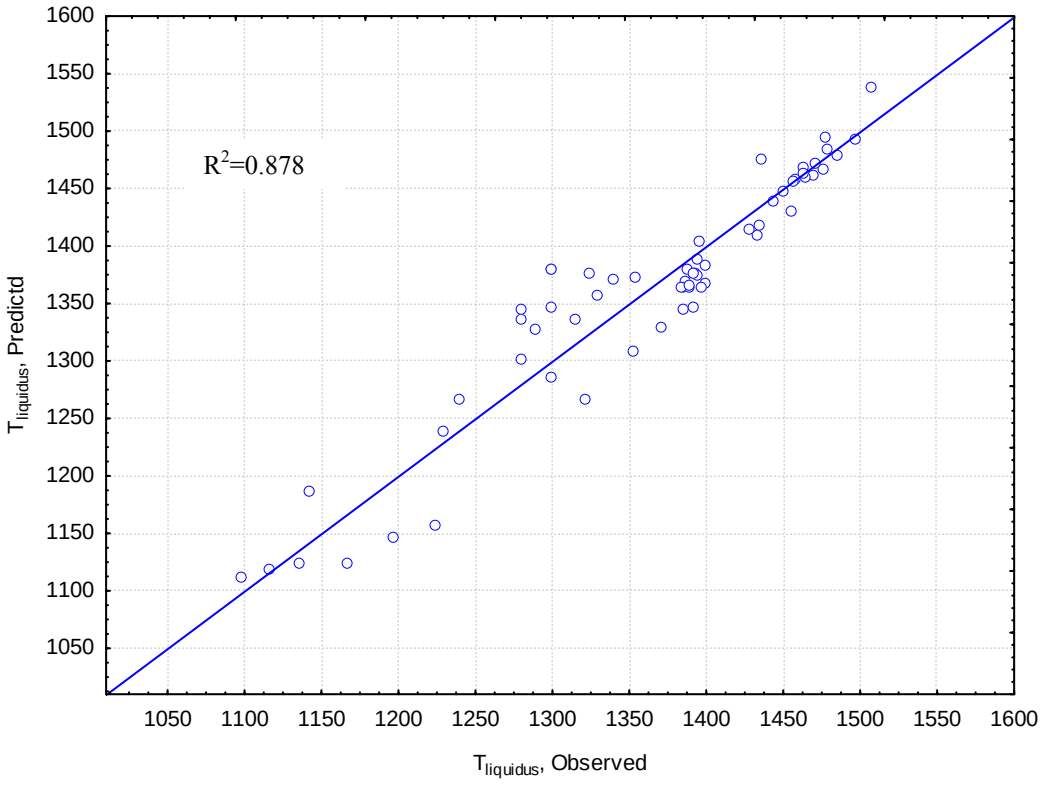

Figure 4.8 The predicted liquidus temperatures in the ternary Fe-Co-Cu

The liquidus temperatures were calculated with the FactSage™ and the MTData thermodynamic software as well. The comparison between the experimental liquidus temperature data and the calculated values is shown in Table 4.5. There is a notable discrepancy between liquidus temperatures between the measured and the calculated. This difference is an indication of the uncertainty that exist in the purported optimised data bases. For example, in the FSstel database, the data used in the optimisation for the Fe-Co-Cu (and Fe-Cu-Si) system is that by Ohtani *et al.* (1997) whose interaction parameters differ from the latter work by Wang *et al.* (2002) and Palumbo *et al.* (2006) (see Table 2.1 in Chapter 2). The database is recommended for the iron-rich alloys, which is the reason the liquidus temperature for alloy A compares well with the calculated one.

No metastable phase transformation temperatures were observed in the heating traces generated for the composition confirming that the miscibility gap reported in the ternary Fe-Co-Cu (Raghavan 2002a; Wang *et al*. 2002) were induced by undercooling effects and so are purely metastable. It can be confirmed in this study that the liquid phase separation takes place during solidification of a liquid alloy on undercooling. The liquid phase separation was observed during the in-situ solidification sequence studies of the Fe-Co-Cu alloy system conducted on the laser

scanning confocal microscope (LSCM). Selected alloys were subjected to LSCM analyses in addition to DTA determined liquidus temperatures.

Table 4.5 Comparison of measured and calculated Liquidus temperatures

Alloyn	Liquidus Temperatures			Temperature Deviations	
	Calculated		DTA	Factsage	MTdata
	FactSage	MTdata	Measured		
A	1470.1	1462.6	1470.1	0	7.5
C	1409.9	1434.1	1436.0	26.1	1.9
D	1390.0	1427.2	1434.4	44.4	7.2
E	1379.1	1419.7	1429.4	50.3	9.7
T	1322.7	1412.2	1399.8	77.1	-12.4

Alloy C (Fe-20.5wt.%Co-18.7wt.%Cu) exhibited a liquid separation when it was cooled at an undercooling of about 60 °C below its liquidus temperature. The images in Figure 4.9, Figure 4.10, Figure 4.11, and Figure 4.12 are solidification sequence of alloy C (Fe-20wt.%Co-19wt.%Cu) captured from the in-situ solidification video clips. Figure 4.9 shows a liquid alloy C at temperature below the liquidus at the inception of undercooling which is followed by a metastable liquid separation in Figure 4.10. The indicated temperatures on the images are higher in Figure 4.11 and Figure 4.12 than the preceding images. This is because liquid phase separation is an exothermic transformation and the energy released counter the undercooling rate resulting in apparent rise in temperature reading. This MLPS observation is comparable to the reported liquid separation measured by Kim and Abbaschian (2000) at steep undercooling.

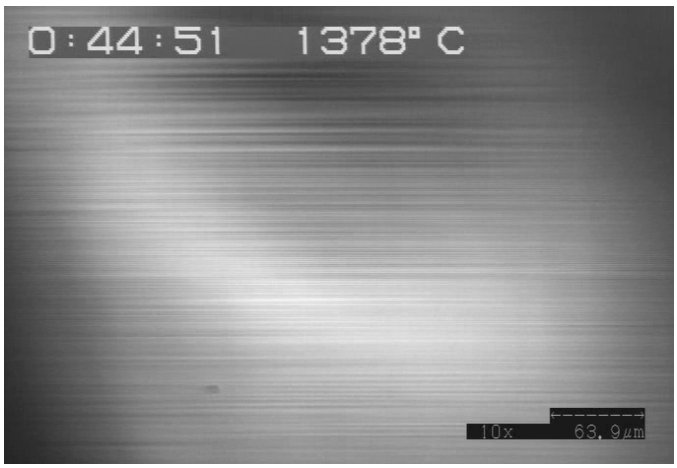

Figure 4.9 Liquid alloy Fe-20wt.%Co-20wt.%Cu (C) before an undercooling event

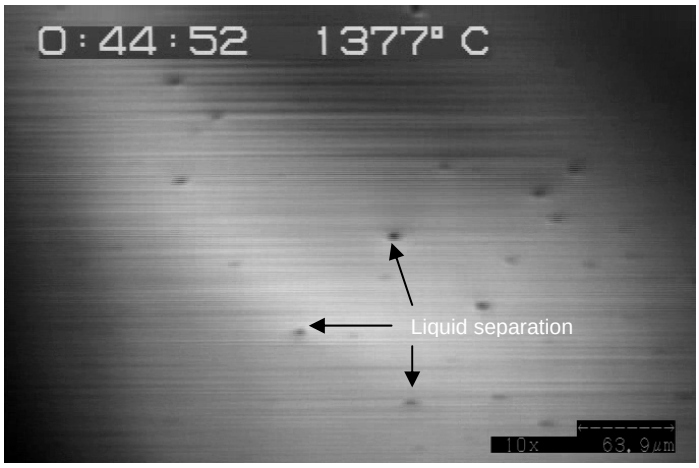

Figure 4.10 Commencement of liquid separation on undercooling of liquid alloy Fe-20wt.%Co-20wt.%Cu (C)

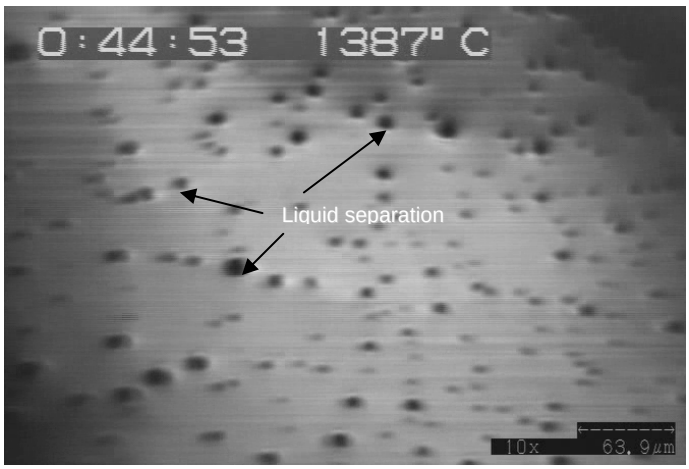

Figure 4.11 Progression of liquid separation on further undercooling of liquid alloy Fe-20wt.%Co-20wt.%Cu (C)

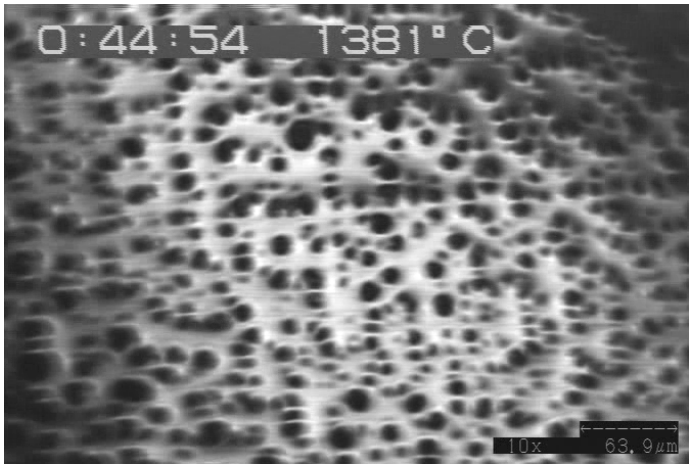

Figure 4.12 Metastable liquid separation in alloy Fe-20wt.%Co-20wt.%Cu (C) on further undercooling

The images in Figure 4.13, Figure 4.14, Figure 4.15, and Figure 4.16 are on the other hand melting sequence images of alloy A (Fe-10wt.%Co-10wt.%Cu) captured from video recording. During melting no liquid separation was observed. An interesting melting phenomena was observed during the melting of alloy A. The alloy underwent an inter-granular melting resulting in free-floating grains shown in Figure 4.15 and Figure 4.16.

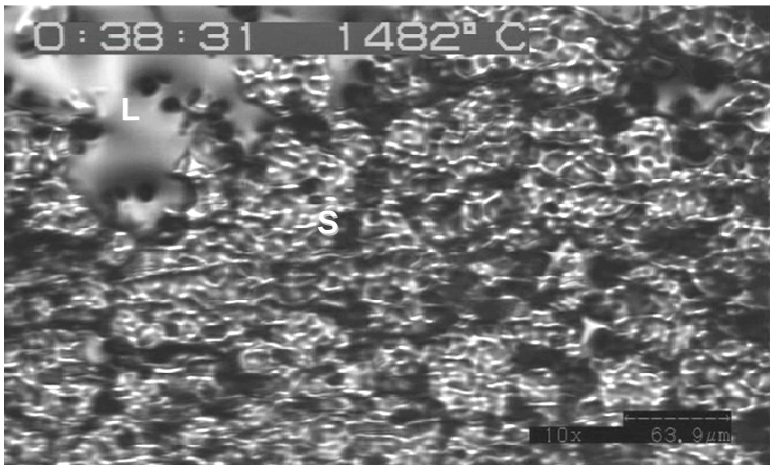

Figure 4.13 Melting of alloy Fe-10wt.%Co-10wt. %Cu (A001) as observed on LSCM. Indicated on the image are the observed liquid (L) phase and solid (S) phase

Figure 4.14 Melting of alloy Fe-10wt.%Co-10wt. %Cu (A001) as observed on LSCM. Indicated on the image are the observed liquid (L) phase and solid (S) phase

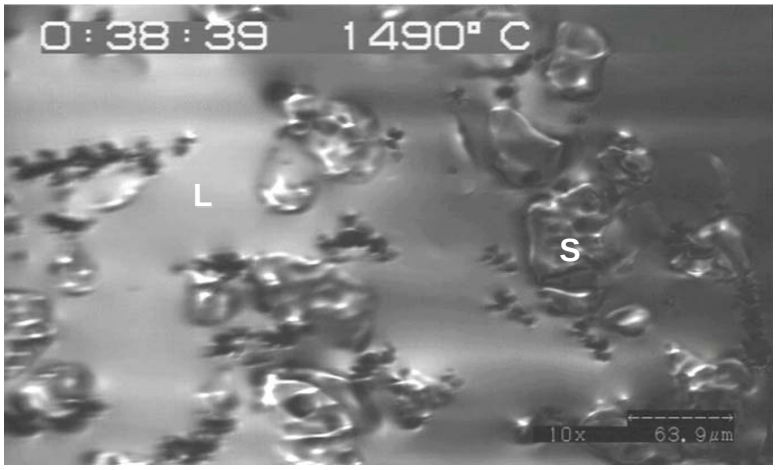

Figure 4.15 Melting of alloy Fe-10wt.%Co-10wt. %Cu (A001) as observed on LSCM. Indicated on the image are the observed liquid (L) phase and solid (S) phase

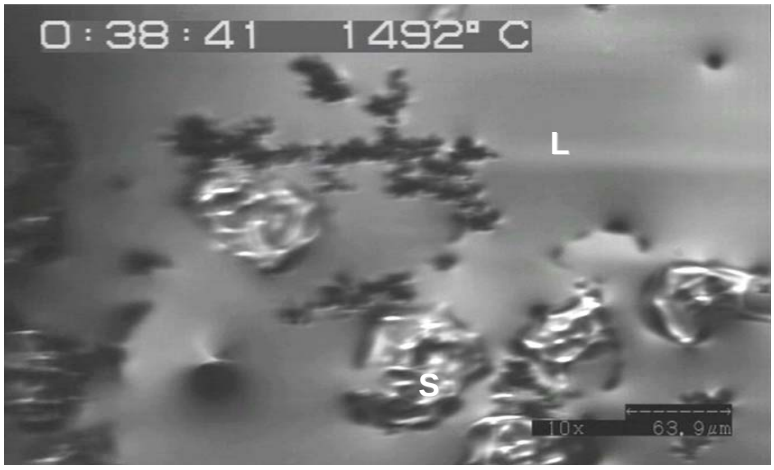

Figure 4.16 Melting of alloy Fe-10wt.%Co-10wt. %Cu (A001) as observed on LSCM. Indicated on the image are the observed liquid (L) phase and solid (S) phase

4.1.2.2 Fe-Cu-Si

The measured transformation temperatures at the selected compositions for the Fe-Cu-Si ternary system are listed in Table 4.2. The Fe-19.6wt.%Cu-5.9wt.%Si system exhibits a concurrent transformation at 1345 °C and 1374 °C indicated by the "double-peak" on the DTA traces in Figure 4.17. This according to DTA characterisation of the peaks, is an occurrence of a chemical transformation where change in composition of a phase transpires resulting in more than one phase present. The transformation preceding this stage is a physical (solid to liquid) transformation in the range 1073 °C to 1092 °C. As the silicon concentration is decreased the prominent "double-peak" region in the traces only appears as a shoulder on the main peak as shown in the traces in Figure 4.17. The liquidus temperature decreased with increased silicon concentration.

This transformation sequence is in fair consistence with the observation made by Hino *et al.* (1999) in this composition regime of the Fe-Cu-Si system. They observed that between 1450 and 1350 °C the miscibility gap is in contact with γ-Fe + L_1, to generate tie triangle γ-Fe + L_1 + L_2, between 1350 and 1250 °C a four phase invariant reaction occurs: γ-Fe + $L_1 \Leftrightarrow \alpha$-Fe + L_2 yielding the tie triangles γ-Fe + α-Fe + L_2 and α-Fe + L_1 + L_2. Also, the miscibility gap makes contact with the FeSi + L_2 two-phase field to generate the tie triangle FeSi + L_1 + L_2.

Table 4.6 The invariant reaction temperatures in Fe-Cu-Si system

Code #	Composition, wt. %			Invariant Reaction	Temp. °C	Source
	Fe	Cu	Si			
pqr#2	74.5	19.61	5.89	$\gamma\text{-Fe} + L_1 \Leftrightarrow \alpha\text{-Fe}$	1073	This work
	74.5	19.61	5.89	$\gamma\text{-Fe} + L_1 \Leftrightarrow \text{FeSi(s)}$	1062	calculated
	74.5	19.61	5.89	$\gamma\text{-Fe} + L_1 \Leftrightarrow \alpha\text{-Fe}$	1198	calculated
pqr#2	74.5	19.61	5.89	$\gamma\text{-Fe} + L_1 \Leftrightarrow \alpha\text{-Fe} + L_2$	1345	this work
	74.5	19.61	5.89	$\gamma\text{-Fe} + L_1 \Leftrightarrow \alpha\text{-Fe} + L_2$	1335	calculated
p1	76.3	20.09	2.58	$\gamma\text{-Fe} + L_1 \Leftrightarrow \alpha\text{-Fe}$	1091	this work
p1	76.3	20.09	2.58	$\gamma\text{-Fe} + L_1 \Leftrightarrow \alpha\text{-Fe}$	1090	calculated
	76.3	20.09	2.58	$\gamma\text{-Fe} + L_1 \Leftrightarrow \alpha\text{-Fe} + L_2$	1387	this work
*P	82.00	16.31	0.87	$\gamma\text{-Fe} + L_1 \Leftrightarrow \alpha\text{-Fe}$	1091	this work
	82.00	16.31	0.87	$\gamma\text{-Fe} + L_1 \Leftrightarrow \alpha\text{-Fe}$	1095	calculated
*P	82.00	16.31	0.87	$\gamma\text{-Fe} + L_1 \Leftrightarrow \alpha\text{-Fe} + L_2$	1438	this work

The results of the liquidus temperature and the corresponding energies of transformation are listed in Table 4.8. The energies of transformation were calculated for the parent peak because the double peaks could not be analysed further. The software used does not support the peak separation techniques that are necessary for such peak conditions. It should also be noted that because the parent peak in the traces comprise two invariant reactions the energies of these reactions may not necessarily be the total area under the parent peak.

Table 4.7 Transformation temperatures and energy of transformation in the ternary Fe-Cu-Si system

Specimen	Composition in wt%			Transition Temperatures °C		Area: Lquidus Peak Area J/g	Source
	Fe	Cu	Si	Liquidus	Solidus		This work
pqr#2	74.5	19.61	5.89	1374	1320	98.5	this work
*P	82.00	16.31	0.87	1452	1423	130.3	this work
*Pi	76.30	20.09	2.58	1445	1436	92.0	this work

* *Binary alloy silica equilibrated*

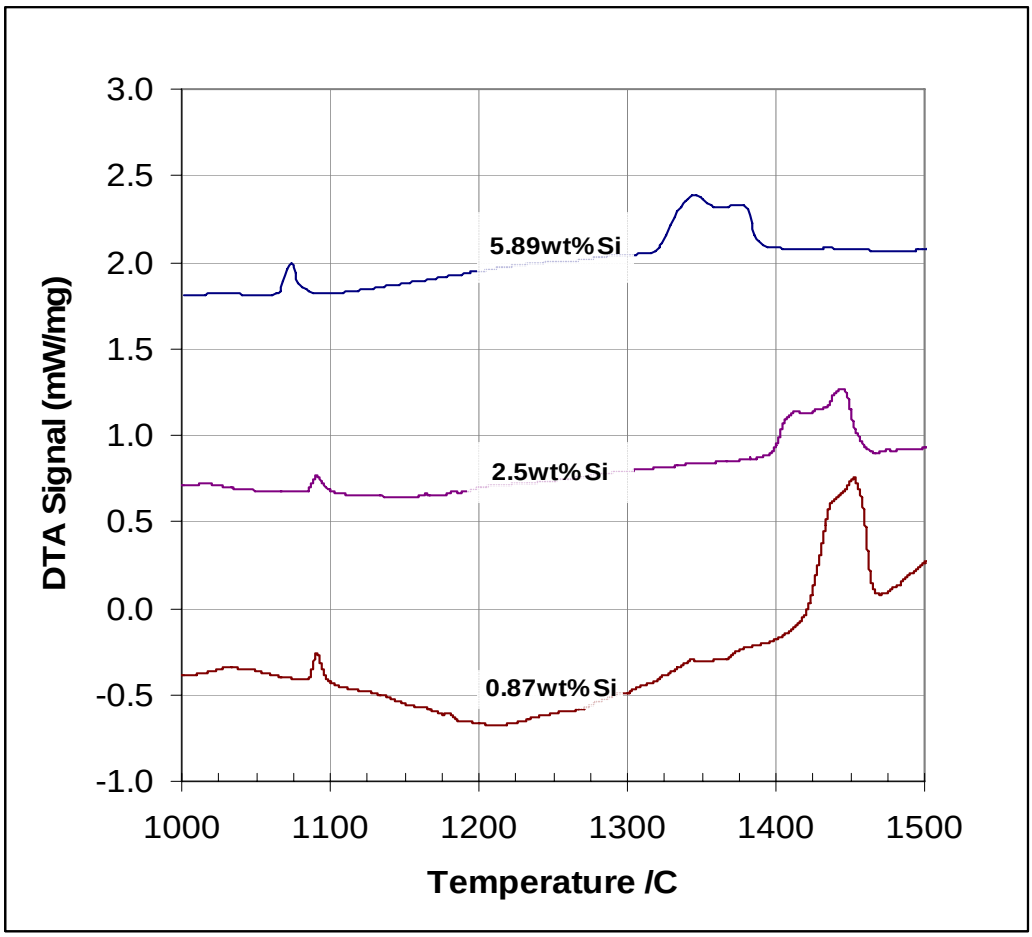

Figure 4.17 DTA heating traces of the ternary systems Fe-19.6wt %Cu-5.9wt. %Si (top), Fe-20.1wt %Cu-2.6wt. %Si (middle), and Fe-16.3wt%Cu-0.9wt.%Si (bottom). The "double-peak" region diminishes with decreasing silicon concentration

The ternary Fe-Cu-Si is peritectic system in which the dominant phases are copper-rich liquid phase that forms at about 1090 °C on heating and iron-rich phase (α-Fe or γ-Fe solid solutions). The liquid phases are reportedly metastable in the binary form and the addition of silicon stabilises the liquids rendering them to coexist (Hino *et al*. 1999). The locations of the "double-peaks" on the DTA heating traces in Figure 4.17 indicate the coexistence of the two liquids. The peaks diminishes with decreasing silicon content.

4.1.2.3 Co-Cu-Si

The liquidus and transition temperatures of the cobalt rich ternary system Co-Cu-Si at two compositions was determined by DTA and the results are listed in Table 4.9. Since information on experimental phase diagram data, particularly the liquidus temperatures of this system is lacking, the results obtained in the experiments are compared to the calculated values only. It is

worthy to point out that even though the underlying database (FSstel) used in calculations with the FactSage™ software does not contain optimised thermodynamic data for the ternary Co-Cu-Si. It is only the binary systems Co-Cu and the Cu-Si that are optimised in this database. The calculations of the phase diagram data can therefore not be acceptable unless evaluated or validated by experiments.

Table 4.8 The invariant reaction temperatures in Co-Cu-Si system

Alloy	Composition, wt. %			Invariant Reaction	Temp. °C	Source
	Cu	Co	Si			
Co-Cu-Si	84.82	15.87	1.46	$liquid_1+solid_1 \Leftrightarrow solid_2$	1110	this work
	82.58	14.50	4.95		1099	
	84.82	15.87	1.46	$liquid_1+solid_2 \Leftrightarrow liquid_2$	1361	
	82.58	14.50	4.95		1295	

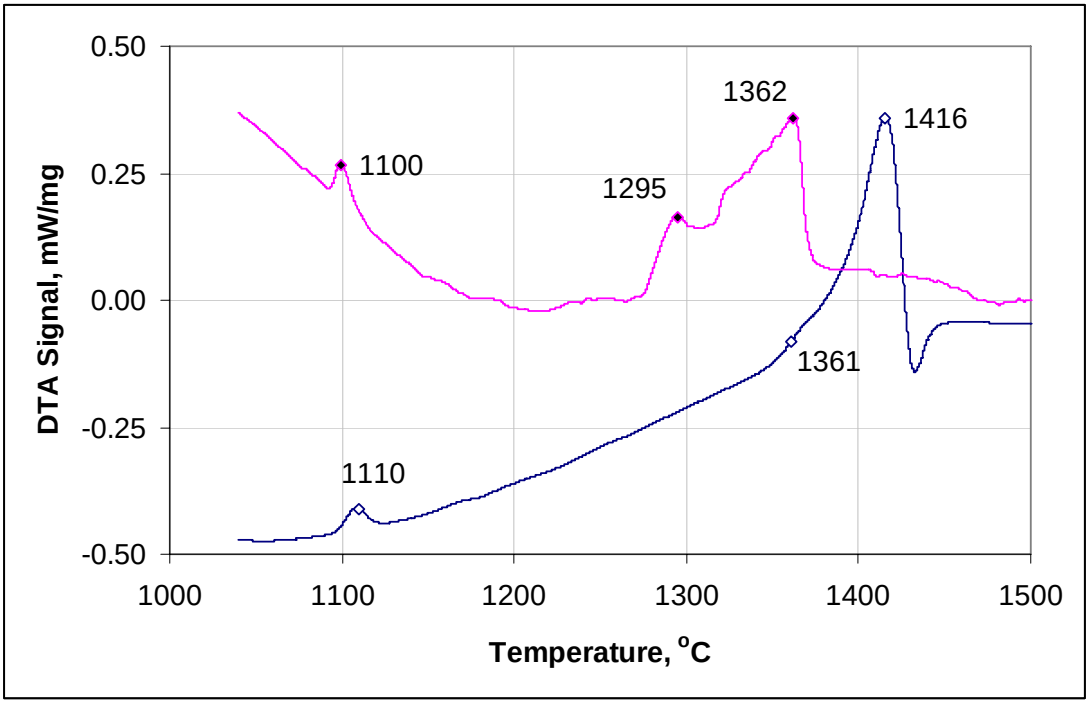

Figure 4.18 DTA heating traces of the ternary systems Co-16wt %Cu-4.9wt. %Si (top), Co-14.5wt %Cu-1.5wt. %Si (bottom). The transition temperatures in °C are indicated. The "double-peak" region diminishes with decreasing silicon concentration

Table 4.9 Measured liquidus temperatures of ternary systems of the Co-Cu-Si system

Specimen	Composition in wt%			Transition Temperatures °C		Area: Liquidus Peak J/g
	Co	Cu	Si	Liquidus	Solidus	
*R:Co-Cu-Si	84.82	15.87	1.46	1415	1399	104.1
*R:Co-Cu-Si	82.58	14.50	4.95	1362	1317	102.6

* *Binary alloy silica equilibrated*

4.1.2.4 Fe-Co-Si

Only one composition point was thermally analysed for this system. There is no literature experimental data in this Fe-17.6wt. % Co-6.7wt. % Si system to compare to the results obtained for the transition temperatures. On heating the alloy the invariant transformation at 1015 °C occurs. This transformation does not involve the formation of a liquid phase as shown in the phase diagrams of the Fe-Co-Si (Vogel and Rosenthal 1935). The liquidus temperature for the system at this composition is 1409 °C. Once more only two binary systems have been optimised in the database of FactSage™, namely Fe-Co and Fe-Si. The measured values are therefore used preferentially to describe the system Fe-Co-Si.

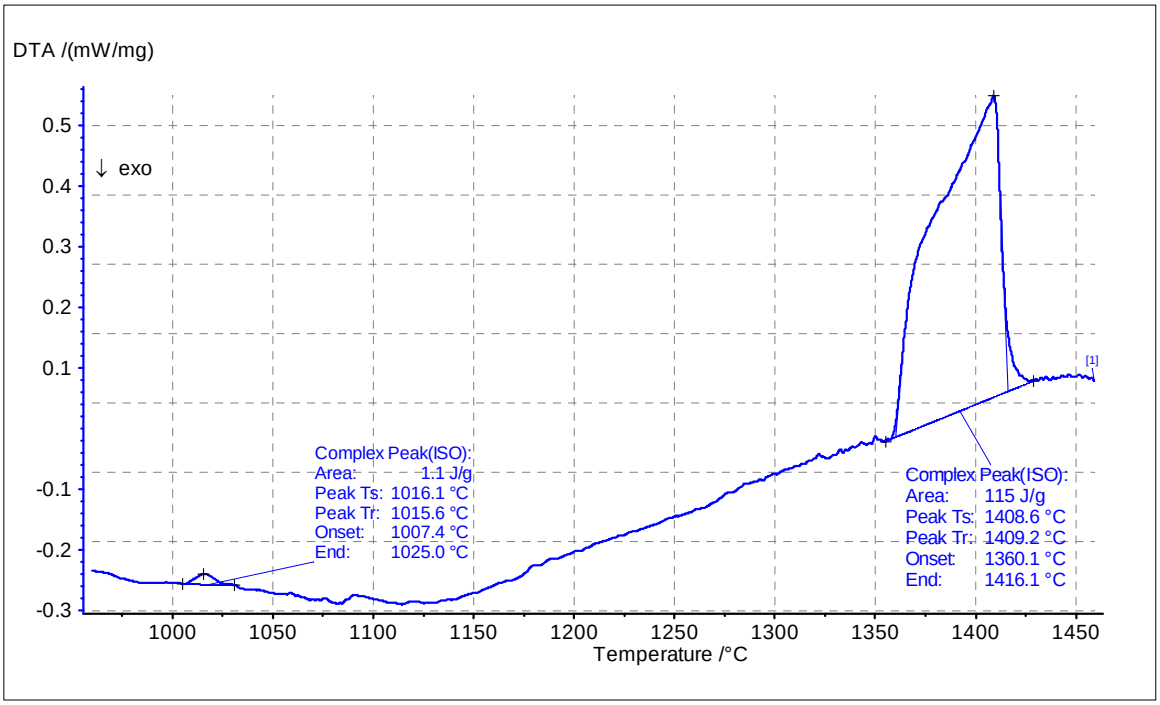

Figure 4.19 DTA heating traces of the ternary system Fe-17.6wt %Co-6.7wt. %Si (top), The transition temperatures are indicated

4.1.3 The quaternary Fe-Co-Cu-Si

The transformation temperatures in the quaternary Fe-Co-Cu-Si are listed in Table 4.11 The ternary system containing copper and cobalt at 20 wt. % and iron as balance (alloy C in Table 4.4) was the master alloy to which silicon was added. Silicon was added to the alloy such that the final alloy composition contained 1, 1.5, 2, 2.5, 3, 4, 5 and 5.5 silicon by mass percent. This composition range falls within the range describing the ferrocobalt defined and characterised in section 2.2. The model alloy labelled "VWXY" in Table 4.11 contained more iron to cater for the

higher iron concentration region. The quaternary alloys attained by equilibrating silica (quartz) with liquid ternary Fe-Co-Cu are prefixed "MExpt" and are listed in Table 4.11 too.

Table 4.10 Transformation temperatures and energy of transformation in the quaternary Fe-Co-Cu-Si system

Specimen	Composition in wt%				Transition temperatures °C				Ratio	Area: Liquidus Peak J/g
	Fe	Co	Cu	Si	peritectic	P_1	Liquidus (P_2)	Solidus	Fe/Cu	
C#01	56.7	18.9	18.9	5.5	1084	1329	1362	1305	3.0	153.8
C#02	57.0	19.0	19.0	5.0	1084	1330	1367	1317	3.0	94.26
C#03	57.6	19.2	19.2	4.0	1086	1355	1384	1327	3.0	155.4
C#04	57.2	19.4	19.4	3.0	1089	1373	1407	1358	2.9	155.6
C#05	58.5	19.5	19.5	2.5	1089	1384	1414	1370	3.0	112.5
C#06	58.8	19.6	19.6	2.0	1091	1394	1421	1378	3.0	142.3
C#07	59.1	19.7	19.7	1.5	1089	1414	1440	1419	3.0	156.3
C#08	59.4	19.8	19.8	1.0	1088	1408	1433	1391	3.0	117.2
MExpt#1-C	60.2	20.8	17.0	1.0	1096	1409	1438	1395	3.5	107.9
MExpt#1-C#7	59.3	20.0	17.4	1.0	1093	1408	1423	1388	3.4	107.4
MExpt#2:C	60.2	20.8	17.0	1.0	1096	1407	1436	1416	3.5	108.5
MExpt#8-C	54.1	23.0	18.5	2.7	1094	1371	1406	1353	2.9	115.2
MExpt#9-E	51.0	30.2	16.8	1.2	1094	1395	1421	1394	3.0	113.9
MExpt#9-C#05	61.1	19.6	14.7	2.6	1089	1374	1408	1362	4.2	136.2
MExpt#10-C	55.8	18.1	22.4	1.9	1094	1397	1424	1375	2.5	120.6
MExpt#11-D	51.3	23.4	22.5	1.5	1093	1393	1427	1376	2.3	100.4
MExpt#13-C	60.6	20.3	11.1	7.6	1080	1350	1389	1378	5.5	92.2
VWXY#1	76.0	9.5	9.5	5.0	1078	1370	1413	1347	8.0	98.3
VWXY#2	77.6	9.7	9.7	3.0	1085	1381	1446	1453	8.0	94.4

The significant characteristic of the melting sequence is the "double-peak" region, labelled P1 and P2 in Figure 4.20. The "double-peak" constitute the invariant reaction in the temperature regime 1329 to 1400 °C appearing initially as a peak in high silicon alloys and then as a shoulder in the lower silicon alloys. The peritectic type invariant transformation occurs in the range 1084 to 1093 °C within the compositions studied. The similarities between the profiles of the heating traces of the quaternary Fe-Co-Cu-Si and the ternary Fe-Cu-Si and Co-Cu-Si can be used to describe the phase transformations in the quaternary system.

The transformations in the alloys from the gas-alloy-silica experiments, prefixed "MExpt" are consistent with the one in the model alloys of similar compositions. For instance the measured liquidus temperatures of alloy C#08 and alloys MExpt#2-C and MExpt#1-C are comparable and the same can be said about alloys C#04 and MExpt#8-C. The difference in measured temperatures between the two alloy types can be attributed to the change in copper content expected in high temperature experiments. The alloys of the series "MExpt" were equilibrated in

quartz crucibles for over 8 hours prior to quenching in water at 1450 °C. The copper rich liquid, which forms predominantly by the invariant reaction (peritectic), has a lower liquidus temperature and so copper loss by vaporisation in this phase might occur due to over exposure at the relatively higher quench temperature.

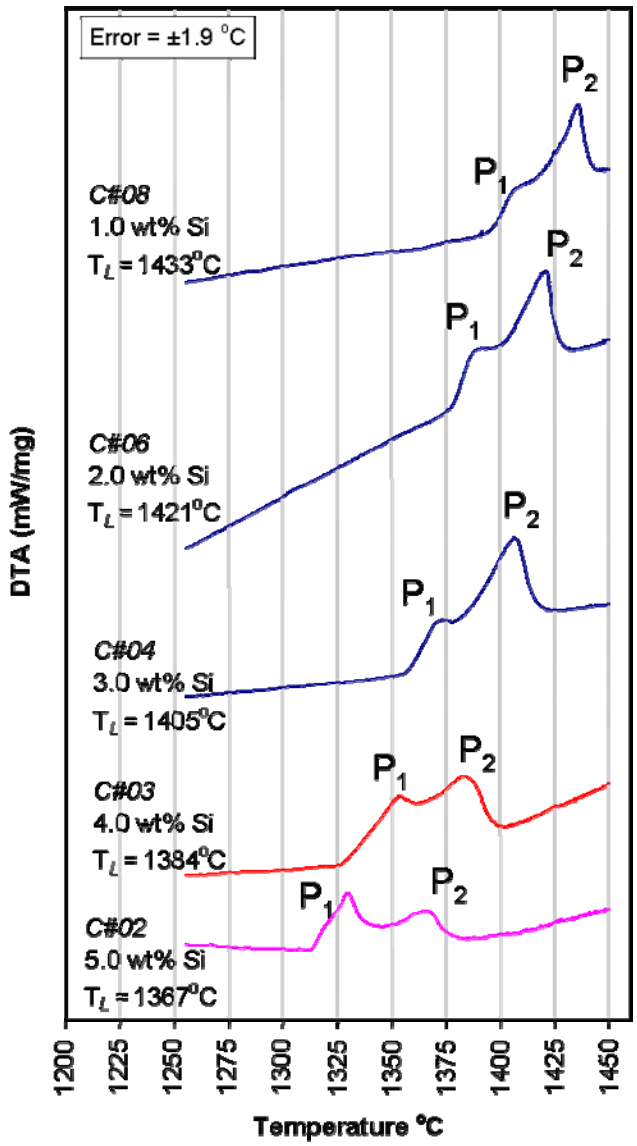

Figure 4.20 The heating traces of the quaternary Fe-Co-Cu-Si alloy. Note transitions P_1 and P_2 in relation to the concentration of silicon. T_L is liquidus temperature of the specific alloy

In the thermal analysis of the "MExpt" series of alloys measurements the heating traces were recorded from below 300 to 1510 °C whereas for the other specimens the temperature program was set to record from 1000 °C. A transformation was observed in the vicinity of 989 and 921 °C. The transformation is similar to the allotropic transformation (α-Co, γ-Fe) to α-Fe in the binary Fe-Co.

The consistency in the DTA traces was validated by carrying out interrupted DTA technique (Wu and Perepezko 2000) through heating and cooling cycles, shown in Figure 4.21 and described earlier in section 2.3.2. The objective was to check whether the appearance of the double peak was due to delayed phase transformations caused by sluggish dissolution of elements that may result in non-equilibrium melting of phases. On reheating the specimen from a ten-minute (interruption period) isothermal temperature set near the onset of melting, the second peak reappeared confirming the occurrence of a secondary peak to be an invariant transformation. An identical trace to the heating trace, except for a drift by a few degrees Celsius, was obtained on cooling the alloy from the liquid phase. This drift is most likely caused by the undercooling effect on cooling the specimen from the liquid phase; a phenomena of thermal analysis. It is for this reason that liquidus temperature determination are carried out on the heating traces rather than cooling traces (Wu and Perepezko 2000). However, it can be concluded from this test that the double peak is caused by phase transformations taking place at 1400 °C during melting.

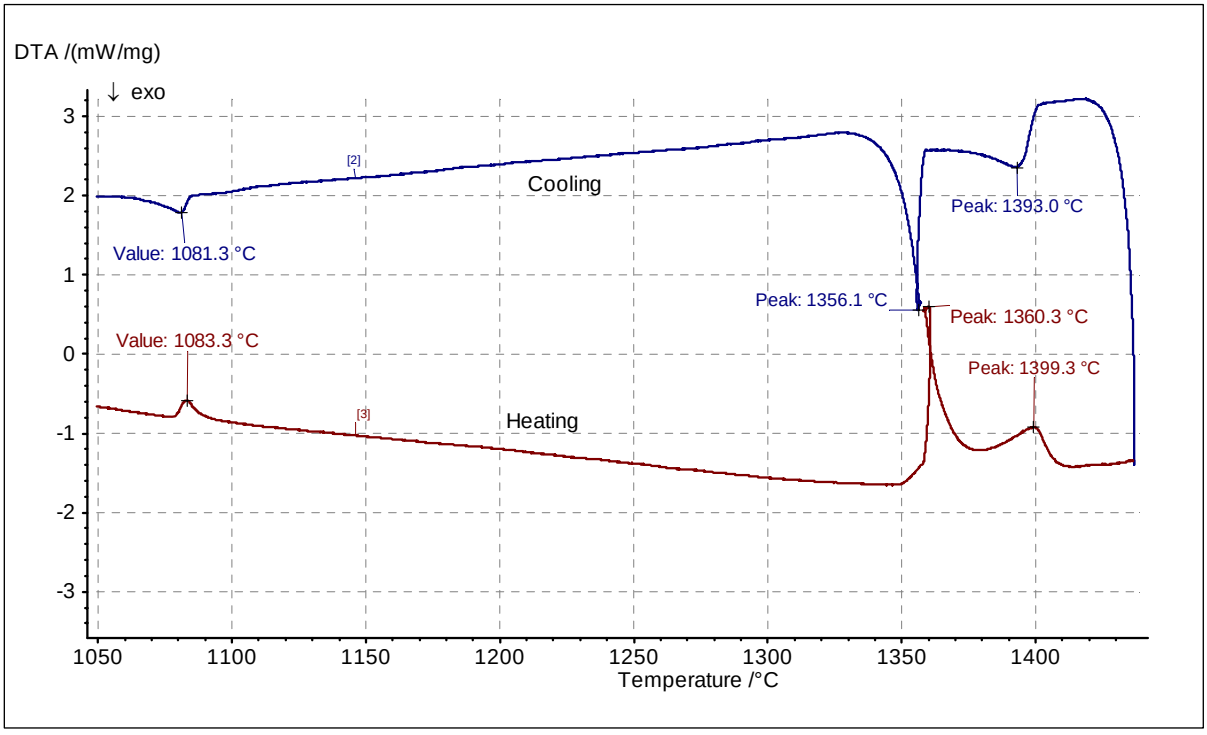

Figure 4.21 DTA heating and cooling traces for specimen C#04 of Fe-Co-Cu-Si system at 10 °C/min an and isothermally held at 1360 °C for 10 minutes using interrupted DTA method (Wu and Perepezko J.H. 2000). There is temperature drift of 2 to 6 °C

It is seen from the results in this section that the liquidus temperatures of the Fe-Co-Cu is lowered when silicon is added. The invariant reactions observed in the ternary systems Fe-Co-Cu

and Fe-Cu-Si persist in the quaternary indicative of the pertinent subsystems to consider when characterising the ferrocobalt defined in the study. The addition of silicon to the Fe-Co-Cu ternary brings about a "double-peak" in the heating traces showing the stabilisation of a second phase. This situation is discussed in the next sections.

It should be mentioned here that in this study the liquidus and solidus temperatures reported refer to the transformation temperatures of complete melting that are represented by the larger peaks in the DTA heating traces. Even though the peritectic transformations yield copper rich liquids, the proportions of this liquid is too small compared to the solid phase that melts at much higher temperatures.

4.2 Phase Equilibria in the Fe-Co-Cu-Si System

A combination of quench and microscopy techniques was used to study phase equilibria in the quaternary Fe-Co-Cu-Si. The model alloys were quenched from temperatures in the proximity of the solidus and liquidus temperatures as determined in section 4.1. The quenched specimens were examined and analysed by scanning electron microscopy.

4.2.1 Validation of Quench Experiments

The quench technique for the experiments was validated by quenching alloys of known composition at predetermined temperatures. The micrographs of binary Fe-30 wt.% Co in Figure 4.22 and Co-40 wt.% Cu in Figure 4.23 show the microstructures in the as-cast specimen and in the quenched specimen. The specimens were quenched at temperatures above the liquidus temperatures. The microstructures evolving on quenching were qualitatively examined by light microscopy. These microstructures when compared to the ones reported by Munitz and Abbaschian (1996) for the Cu-Co binary system and Mingjun *et al*. (1999) for the Fe-Co binary system show similarities that can be deduced to be due to the appropriate quench techniques used. For instance, the microstructure obtained by Li *et al.* (1999) in their studies of the microstructure evolution in the binary Fe-30 wt.% Co system at 200 K/min undercooling is comparable to the microstructure in Figure 4.22 (b) containing granular dendritic microstructures.

A ternary alloy Fe-20wt.% Co-42wt.% Cu, reproduced from the work by Bamberger *et al.* (2002), was examined and the microstructures are shown in Figure 4.24. In the ternary alloy

quenched from 1450 °C the phase separation of two liquids was observed and is shown in Figure 4.23 (b). This liquid phase separation is in agreement with what was reported by Kim and Abbaschian 2000. It is conclusive from these observations that the desired quench temperatures were attained within the experimental limits and that the rate of quenching was sufficiently rapid.

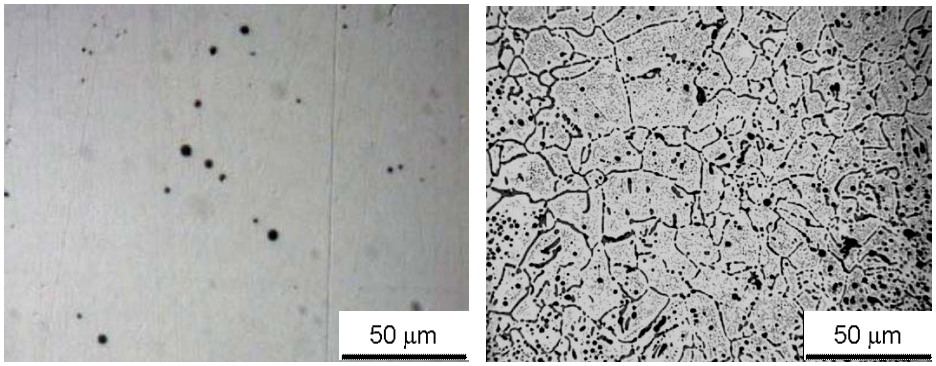

(a) (b)

Figure 4.22 Light micrographs of Fe-30 wt% Co alloy microstructures (a) as cast and (b) quenched from 1450 °C

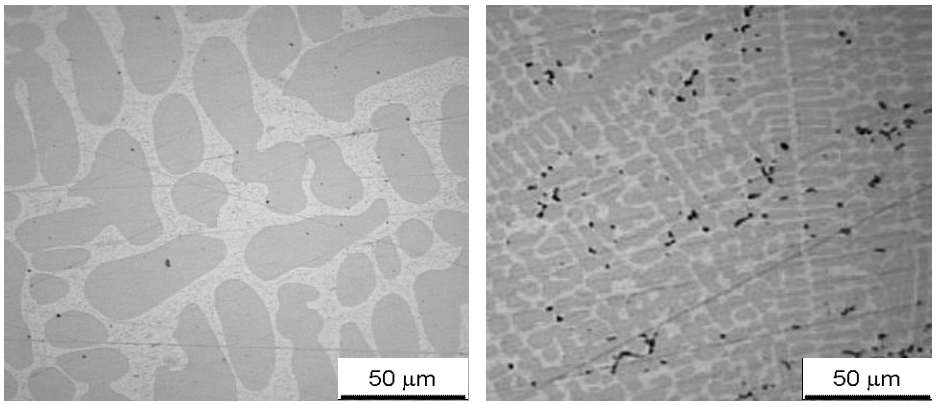

(a) (b)

Figure 4.24 Light micrographs of Co-40 wt% Cu alloy microstructures (a) as cast and (b) quenched from 1450 °C. The light phase is the Cu-rich phase

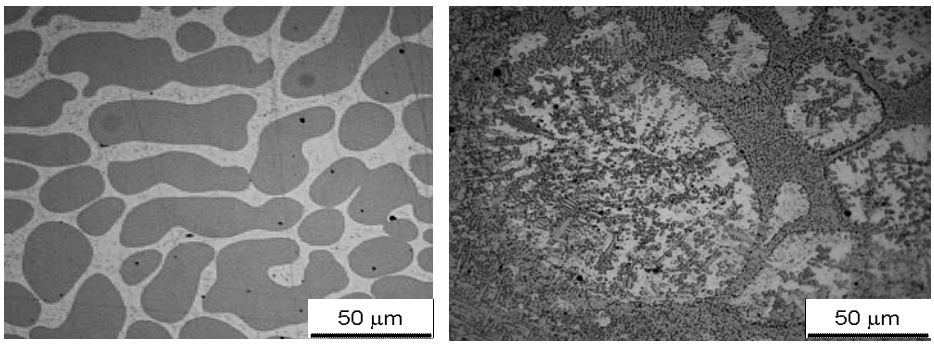

(a) (b)

Figure 4.23 Light micrographs of Fe-20 wt% Co- 40 wt% Cu alloy microstructures (a) as cast and (b) quenched from 1450 °C and etched in $FeCl_3$-HCl-alcohol mixture . The light phase is the Cu-rich phase

Upon a successful validation of quench techniques the alloys designated for phase equilibria studies where quenched. Shown in Figure 4.25, Figure 4.26 and Figure 4.27 are the single-phase and two-phase equilibria microstructures in the quenched alloys. The alloys were quenched at temperatures above the liquidus temperature and between the liquidus and solidus temperatures as described earlier in Table 3.3. The phase constituents for the alloy systems are copper-rich phase, which forms predominantly at the peritectic transformation temperatures, and iron-rich phase which constitutes a large proportion of the system and has a higher melting temperature. The copper-rich liquid coexists with the solid α-Fe rich phase over a wide temperature range up as earlier discussed in DTA results until the onset of melting of the α-Fe rich phase. It is observed that the composition of the phases changes with respect to copper content as temperature increases. This is due to the limited solubility of copper in both solid iron and solid cobalt. However, as the temperature increases the concentration of copper show an apparent decrease because of the dissolution of iron and cobalt in the increasing liquid proportion. On the other hand the ratio of iron to cobalt remains constant over the same temperature range.

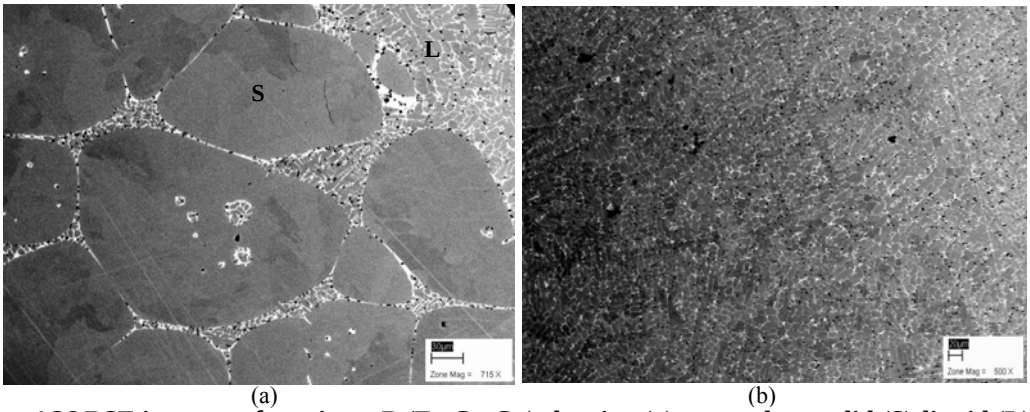

(a) (b)

Figure 4.26 BSE imgages of specimen B (Fe-Co-Cu) showing (a) a two phase solid (S)-liquid (L) formed on quenching from 1445 °C, and (b) a single phase liquid on quenching from 1460 °C

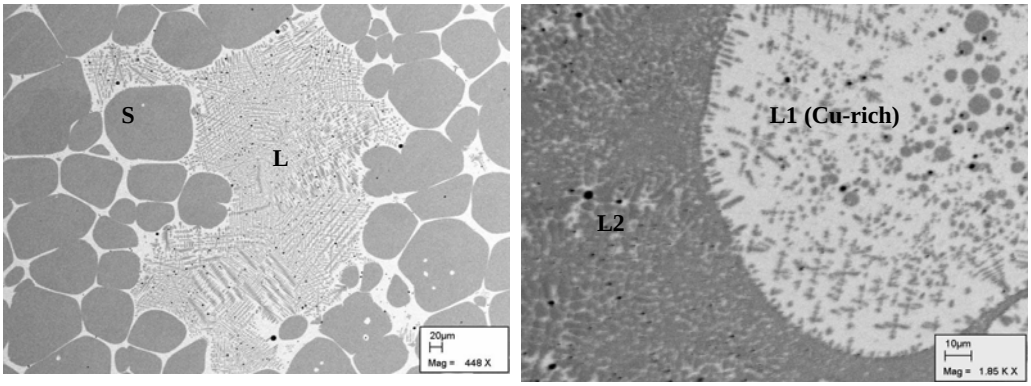

(a) (b)

Figure 4.25 BSE imgages of specimen T (Fe-Co-Cu) showing (a) a two phase solid (S)-liquid (L) formed on quenching from 1390 °C, and (b) a single phase containing two liquids formed on quenching from 1405 °C

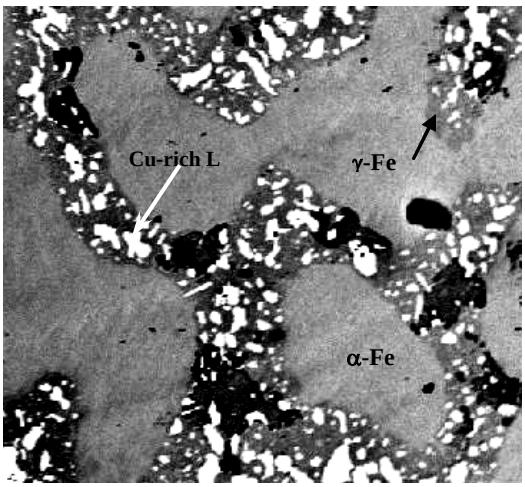

Figure 4.27 A BSE image of specimen C#02 (Fe-Co-Cu-Si) quenched from 1328 °C, showing a three phase region of Cu-rich (light) liquid, two solid phases α-Fe (light grey) and γ-Fe (dark grey)

In the system Fe-Co-Cu-Si, a secondary phase surrounding the copper-rich primary liquid phase (γ-Fe) forms allotropically from α-Fe, (see Figure 4.27). This phase is prominent in the alloys containing about 5 wt.% Si and only appears as a shoulder in less than 5 wt.% Si as discussed in the DTA traces for the quaternary Fe-Co-Cu-Si (see Figure 4.20).

4.2.2 Phase Equilibria in the Fe-Co-Cu System

The results of the phase analysis of the Fe-Co-Cu system are summarised in Table 4.5. The phase equilibria in the Fe-Cu-Si and Co-Cu-Si is derived from the literature resources where available. In particular, the Fe-Cu-Si system has been studied in the temperature range up to 1300 °C (Hino *et al*. 1999; Miettinen 2003; Raghavan 2002b; Rogel and Horstman 1953; Wang *et al*. 2002).

The phase proportions were calculated from the compositions of the components in the liquid and solid phases of the quenched specimen. The lever rule defined by West (1982) was applied in the calculations of the phase proportions. The phenomenal dendritic segregation took place on quenching in the specimen higher in iron content such as specimen B shown in Figure 4.25(a). The dendritic segregation presents difficulties in distinguishing the solid phase from the liquid phase on analysis by EDS (Hasebe and Nishizawa 1980). To resolve this problem the lighter phase was characterised as the liquid phase and the grey phase as the solid phase. This avoided the selection of an area in the dendritic region which gave inconsistent phase compositions

among phases of the same microstructure. This was not the case when a spot (1μm x 1μm) was analysed.

Table 4.11 Equilibrium Composition of ternary system Fe-Co-Cu

Alloy	Alloy Composition, wt%			Quench Temp	Phase Composition, wt.%						Phase Distribution, %	
					Fe-rich Liquid Phase			Solid Phase			Liq	Solid
	Fe	Co	Cu		Fe	Co	Cu	Fe	Co	Cu		
A	79.1	10.6	10.5	1450	71.1	13.6	15.2	79.1	10.2	9.9	11.1	88.9
				1460	77.0	10.1	13.4	82.4	10.1	8.1	45.7	54.3
B	68.5	16.2	15.2	1435	66.5	14.9	18.5	72.2	15.3	11.8	57.8	42.2
D	54.3	27.2	18.2	1390	25.6	15.0	59.5	55.4	31.6	13.0	7.4	92.8
				1400	40.4	20.1	39.6	59.8	27.8	12.4	24.8	75.2
				1410	46.3	22.5	31.2	60.7	27.2	12.15	38.1	61.9
				1420	51.9	24.9	23.3	61.2	27.8	11.0	66.4	33.6
F	64.8	15.2	20.4	1420	46.4	12.5	42.1	69.6	17.0	12.6	23.6	76.4
				1430	60.2	14.1	26.2	72.3	15.8	11.6	61.1	38.8
T	40.3	20.9	38.1	1385	14.9	8.1	73.1	55.6	29.1	14.0	39.2	60.8
				1390	24.7	12.5	63.2	57.5	27.4	13.6	48.4	51.6
				1395	30.2	17.6	51.3	56.8	29.9	13.0	66.8	33.2

4.2.3 Phase equilibria in quaternary Fe-Co-Cu-Si

The results from quench experiments of alloy C#02 are listed in Table 4.12. The specimens were quenched at selected temperatures below transition temperature P1, between P1 and P2, and above transition temperature P2 at 1317, 1328, 1360, and 1369 °C respectively. The micrographs in Figures 4.28 to 4.31 show the evolved microstructures in the quenched specimen. The three phase system was identified as the Cu-rich liquid (white) phase which formed at 1084 °C; the peritectic temperature. The α-Fe solid phase (dark) was identified by the amount of dissolved silicon according to the crystal structure data of the Fe-Si binary system (Massalski 2001). The maximum silicon content in the α-Fe phase is 3.19 at.% Si and in the γ-Fe is 19.5 at.% Si. The darker phase (γ-Fe) coexists with the Cu-rich phase, increasing in volume at 1328 °C before diminishing at 1330 °C. The γ-Fe (darker) phase and the Cu-rich phase are bounded by the dark phase (α-Fe). The microstructures indicate that the alloy system is peritectic (Exner and Petzow 2004; Macchesney and Rosenberg 1970) and match the transformations in the DTA traces in Figure 4.20 and Figure 4.21. At 1360 °C the darker (γ-Fe) phase diminishes leaving only the dark (α-Fe) and the Cu-rich (white) liquid phase.

As mentioned earlier, the transformations in the Fe-Co-Cu-Si system is typical of the ternary systems Fe-Cu-Si and Co-Cu-Si. The studies of the ternary Fe-Cu-Si system by Wang *et al.* (2002) show that α-Fe and γ-Fe phases coexist at 1300 °C in the iron rich section of the Fe-Si side. It should follow then that in melting or cooling of the quaternary Fe-Co-Cu-Si that the

double peak identified in the DTA measurements is the transformation of the γ-Fe phase with a higher silicon concentration to α-Fe phases. The element cobalt has little effect on the phase equilibria in the ternary Co-Cu-Si and thus it must be expected to have less influence on the quaternary Fe-Co-Cu-Si in the respective composition.

Table 4.12 Equilibrium composition of the liquid phases of the Fe-Co-Cu-Si system

Specimen Composition, wt%				Quench Temp	Phase Composition, wt.%			
					Cu-Rich			
Fe	Co	Cu	Si		Fe	Co	Cu	Si
57.8	19.2	19.3	4.8	1317	2.6	0.7	94.6	0.7
				1328	3.4	1.5	93.4	1.3
				1360	5.3	2.5	93.4	0.7
				1369	5.5	2.5	94.3	0.9

Table 4.13 Equilibrium compositions of the solid phases of the Fe-Co-Cu-Si system

Specimen Composition, wt%				Quench Temp	Phase Composition, wt.%							
					α-Phase				γ-phase			
Fe	Co	Cu	Si		Fe	Co	Cu	Si	Fe	Co	Cu	Si
57.8	19.2	19.3	4.8	1317	64.7	20.8	11.0	4.9	62.3	21.9	10.8	6.0
				1328	62.9	20.0	11.5	3.6	62.5	22.6	9.4	6.3
				1360	64.5	20.9	12.2	2.9				
				1369	66.9	21.1	12.0	2.5				

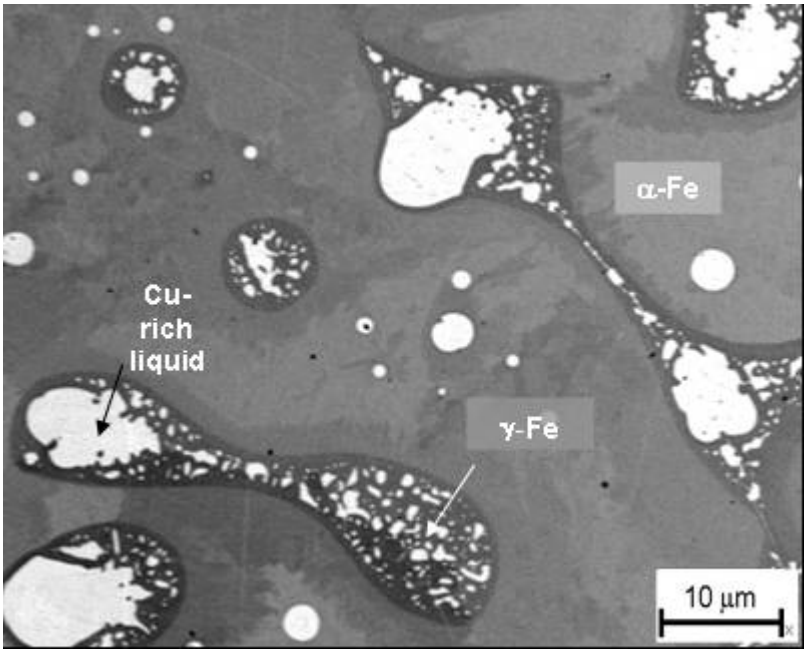

Figure 4.28 A BSE image of specimen C#02: Fe-19Co-19Cu-5Si (wt. %) quenched at 1317 °C

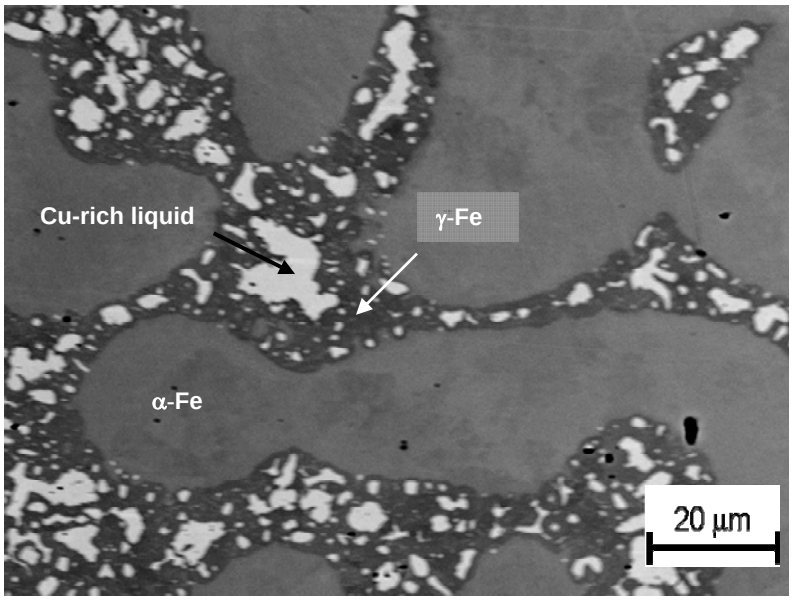

Figure 4.29 A BSE image of specimen C#02: Fe-19Co-19Cu-5Si (wt. %) quenched at 1328 °C

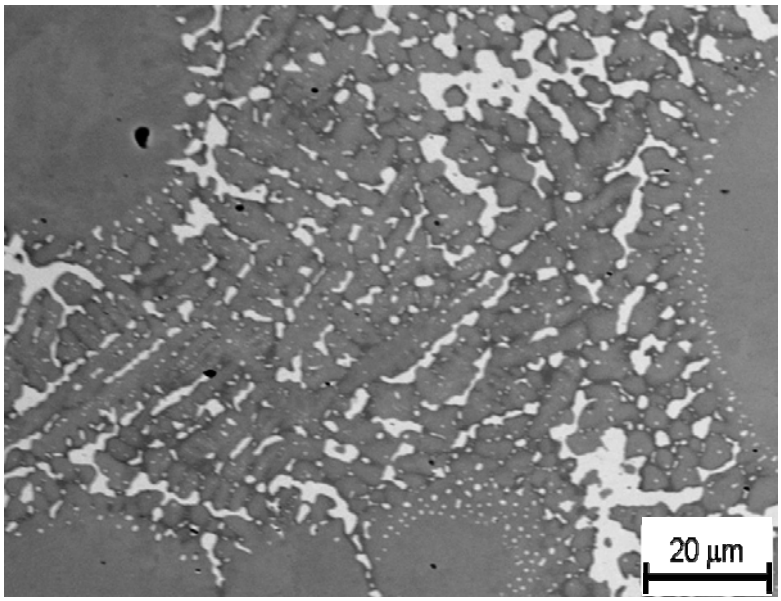

Figure 4.30 A BSE image of specimen C#02: Fe-19Co-19Cu-5Si (wt. %) quenched at 1360 °C

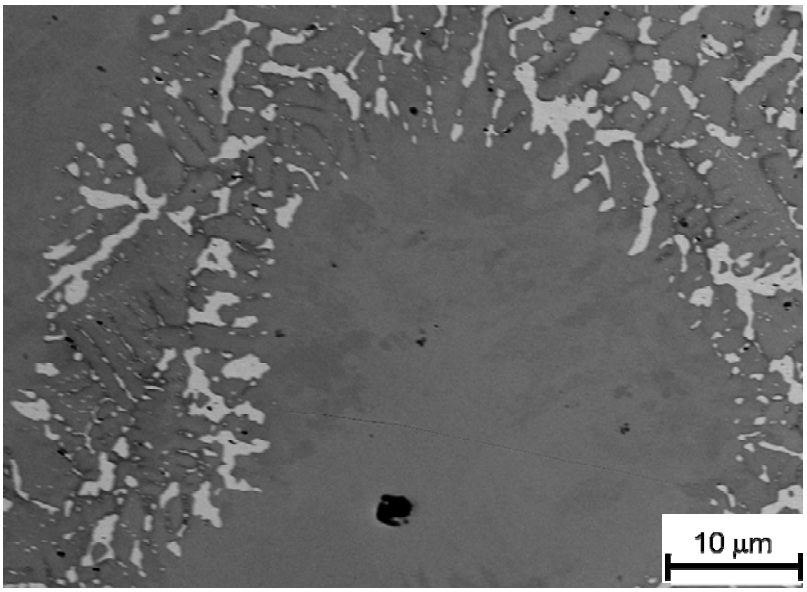

Figure 4.31 A BSE image of specimen C#02: Fe-19Co-19Cu-5Si (wt. %) quenched at 1369 °C

The phase proportions listed in Table 4.14 were calculated using the "centre of gravity" principle for three phases as described by West (1982). The calculations of the proportions for the phases L, α, and γ listed in Table 4.14 are described in Appendix VII. The lever rule was applied on each component of the phases of interest in the system to calculate the phase amount. The arithmetic mean of the sum of the phase amounts based on each element was taken as the phase amount of the system. For example, to calculate the amount of Cu-rich liquid in the alloy quenched at 1317 °C, the proportions were calculated based on copper content in the liquid phase, α-Fe phase and the γ-Fe phases. This was repeated but with iron and silicon as the basis of calculations. Then the reported phase amount was found by taking the arithmetic mean of the three calculations.

As discussed earlier, the significance of the SEM-EDS analytical option used lies in the fact that the metal solutions when quenched tend to produce dendrites (ex-solution). For instance, if an area in the dendritic region is selected, the probability of analysing two different phases is increased due to the intergrowth nature of the dendrites. For this reason, the liquid phase in this study is confined to a copper-rich or an iron-rich phase.

Table 4.14 Phase proportions in the Fe-Co-Cu-Si

Specimen	Specimen Composition, wt%				Quench Temp	Phase proportions.%		
	Fe	Co	Cu	Si		Cu-rich Liquid Phase	α–Fe Phase	γ– Fe phase
C#02	57.8	19.2	19.3	4.8	1317	9.74	61.04	29.22
					1328	10.30	46.87	42.82
					1360	88.7	11.30	
					1369	90.23	9.77	

The element maps generated from SEM images are shown in Figure 4.32. The concentration of each element is indicated by its brightness on the black background. The element distribution among phases shows an association of copper and silicon in the γ-Fe phase, Figure 4.32(a). In this phase silicon is higher in concentration relative to the α-Fe phase Figure 4.32(e), iron is relatively low in this phase, Figure 4.32(b). The element cobalt distributes fairly the same in both the α-Fe and γ-Fe phases. The association of the copper and silicon elements in the γ-Fe phase is due to higher solubility of copper in the presence of silicon in the γ-Fe phase than in the α-Fe phase in which silicon is lower. This is in agreement with the data from the work by Hino *et al.* (1999) at 1300 °C.

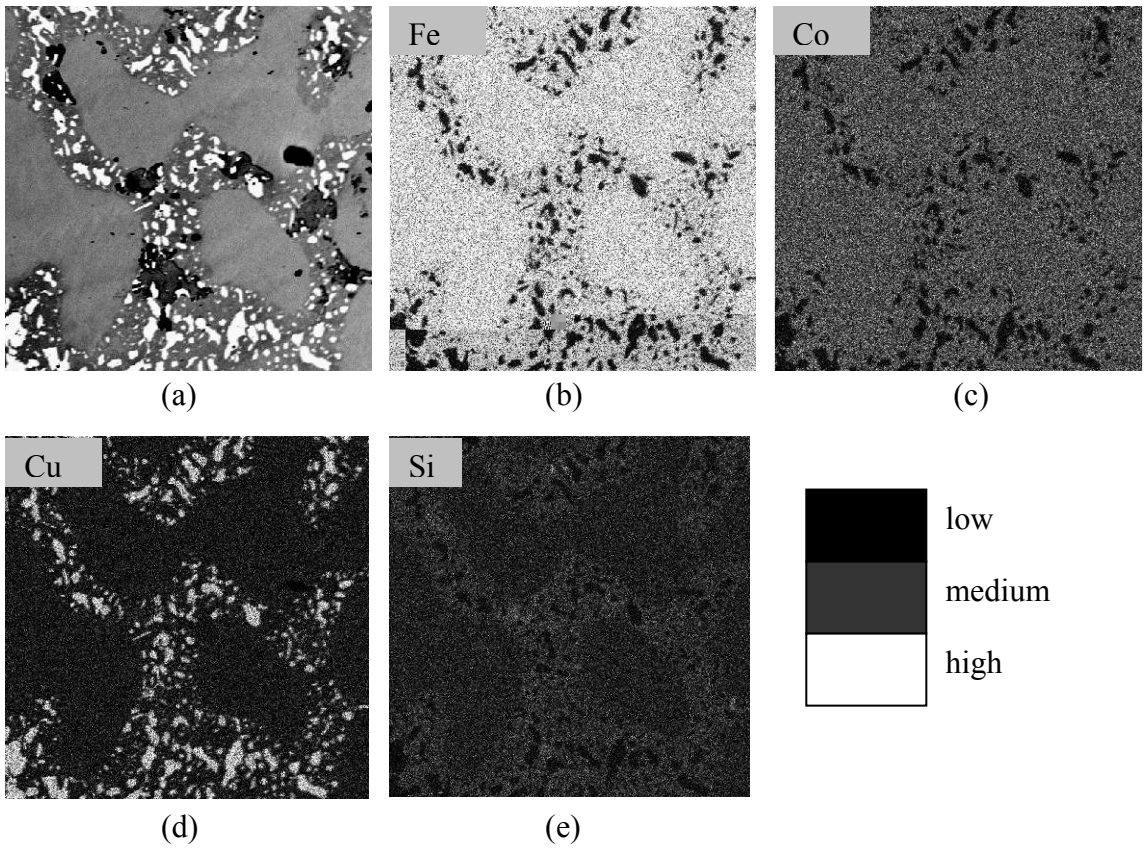

Figure 4.32 Element distribution maps of C#02 quenched from 1328 °C. (a) is BSE image (400x), (b) to (e) are element distribution indicated by intensity of brightness in the greyscale maps

4.3 Gas-Alloy-Silica Equilibria

The results of the experiments where the liquid binary and ternary alloys were equilibrated with solid silica are presented in this section. The activity of silicon in the liquid alloy was determined by chemical equilibration. By using the thermodynamic relationships, the activity coefficient was calculated as a function of temperature and composition.

4.3.1 General Considerations

It has been established that reducing conditions are essential in slag cleaning; the other important aspect of the process is the manipulation of the slag chemistry for an optimum recovery of pay metals. The slag treated in these processes is at near silica saturation and highly oxidised with respect to iron content. Inevitably, the reduction of the slag by carbonaceous materials leads to the partitioning of silicon to the ferroalloy. The behaviour of the silicon as an undesirable element in the liquid alloy can be understood by investigating its thermodynamic activity.

The metals copper and silicon behave differently in liquid iron. Silicon exhibits a strong negative deviation from ideal solution behaviour whereas copper has a positive deviation. The tendency for the miscibility gap in the Fe-Cu system to form is high whereas in the Fe-Si and Cu-Si systems the tendency is towards the formation of intermetallics. An investigation of silicon behaviour in the quaternary Fe-Co-Cu-Si was conducted in reducing conditions controlled by setting the oxygen partial pressure and temperature was either varied or fixed.

Alloys of known composition and liquidus temperatures were equilibrated with pure silica in very low oxygen partial pressure atmosphere as described in section 3.4. The silica (quartz) crucible used to contain the liquid alloy was also a standard reference for the oxide SiO_2 and the only source of silicon in the liquid alloy. The gas composition used for pO_2 buffer was uniquely defined by choosing the temperature, pressure and mixing ratios of the reactant gases. So the five partial pressures for H_2, O_2, CO_2, CO, and H_2O were defined by two equilibrium constants from reaction equations (see appendix VI), the total pressure, and the C/H and C/O ratio were fixed by the chosen CO_2/H_2 ratio for the experiment.

The following assumptions are made about the gas during the experiments in the study;

- the gas cleaning system is effective rendering the gases free of impurities,
- no precipitation takes place due to the formation of H_2O liquid from the species,
- the gases behave ideally at high temperatures,
- equilibrium is achieved among the phases, and
- there is no formation of organic polymers (CH_4) due to high temperatures used.

4.3.2 Activity of silicon in liquid Fe-Co-Cu-Si

The activity of silicon was determined from the amount of silicon in the alloy and by following the reaction for the dissolution of silicon in the liquid alloy from the silica crucible, Equation (4.2). The extent of dissolution of silicon is dependent on temperature and the oxygen fugacity. The reference states for the calculations were the liquid silicon in alloy and the solid (crystobalite) phase for SiO_2.

$$SiO_{2(crystobalite)} = Si(l) + O_2(g) \qquad (4.2)$$

For which the Gibbs free energy of formation, ΔG^o ($J / g.mole.K$) is

$$\Delta G^o = 952,696.94\ J / g.mole - 203.76\ T \qquad (1427\ ^oC < T < 1727\ ^oC) \qquad (4.3)$$

(After Kubaschweski and Alcock 1979)

From Equation (4.2) the equilibrium constant K, is expressed as

$$K = \frac{a_{Si} \cdot pO_2}{a_{SiO_2}} = a_{Si} \cdot pO_2 \qquad (4.4)$$

and

$$K = \exp\left(-\frac{\Delta G^o}{RT}\right) \qquad (4.5)$$

since

$$a_{Si} = \gamma_{Si} \cdot x_{Si} \qquad (4.6)$$

a_{Si} is the activity of silicon in the liquid alloy and γ_{Si} its activity coefficient, x_{Si} the mole fraction of silicon in alloy, pO_2 the equilibrium oxygen fugacity, R the gas constant and T the temperature in Kelvin. Equation (4.5) can be expressed in terms of activity coefficient (γ_{Si}):

$$\gamma_{Si} = \frac{\exp\left(-\frac{\Delta G^o}{RT}\right)}{x_{Si} \cdot pO_2} \qquad (4.7)$$

By using Equation (4.7) and the mole fraction of silicon in the alloy, the activity coefficient of silicon in the liquid quaternary Fe-Co-Cu-Si alloy was calculated. The results of the experiments at isothermal conditions are listed in **Error! Reference source not found.**.

Table 4.15 Measured activity of Si by gas-alloy-silica in liquid Fe-Co-Cu-Si. (a) Quaternary alloys resulting from ternary and/or quaternary equilibration with silica and (b) ternary alloys resulting from binary and/or ternary equilibration with silica

Alloy	CO_2 / H_2 (10^{-3})	equiv. pO_2	T, °C.	Mole fractions				γ_{Si} (10^{-3})	a_{Si} (10^{-5})	error a_{Si} (10^{-6})
				Fe	Co	Cu	Si			
(a) Quaternary alloys										
8.C	0.770	-15	1450	0.55	0.22	0.17	0.06	10.400	58.000	±7.75
T	0.770	-15	1450	0.38	0.17	0.35	0.1	5.990	5.800	±3.21
18.C#5.3	2.193	-14.1	1450	0.6	0.19	0.13	0.08	0.867	0.730	±0.45
10.B1	2.193	-14	1450	0.71	0.14	0.11	0.04	1.370	0.580	±1.35
10.C	2.193	-14	1450	0.58	0.18	0.2	0.04	1.470	0.580	±1.09
4.C	2.193	-14	1450	0.6	0.2	0.16	0.05	1.160	0.580	±0.73
1.C	7.145	-13	1450	0.62	0.2	0.15	0.02	0.297	0.058	±0.41
1.C#3	7.145	-13	1450	0.58	0.19	0.15	0.08	0.072	0.058	±0.04
1.C#7	7.145	-13	1450	0.62	0.2	0.16	0.02	0.268	0.058	±0.37
11.B2	7.145	-13	1450	0.71	0.15	0.12	0.03	0.192	0.058	±0.25
11.D1	7.145	-13	1450	0.53	0.23	0.21	0.03	0.192	0.058	±0.18
2.C	7.145	-13	1450	0.62	0.2	0.15	0.02	0.297	0.058	±0.41
5.C	7.145	-13	1450	0.61	0.21	0.16	0.02	0.240	0.058	±0.27
9.C#5	7.145	-13	1450	0.63	0.19	0.13	0.05	0.109	0.058	±0.07
9.E	7.145	-13	1450	0.53	0.3	0.15	0.03	0.228	0.058	±0.24
(b) Ternary alloys										
4.CoCu	2.193	-14	1450	0	0.78	0.13	0.1	0.594	0.580	±0.422
4.FeCu	2.193	-14	1450	0.77	0	0.18	0.05	1.120	0.580	±0.698
2.CoCu	7.145	-13	1450	0	0.83	0.14	0.03	0.194	0.058	±0.190
2.FeCu	7.145	-13	1450	0.84	0	0.15	0.02	0.328	0.058	±0.539
5.CoCu	7.145	-13	1450	0	0.83	0.14	0.03	0.181	0.058	±0.227
9.CoCuSi	7.145	-13	1450	0	0.74	0.17	0.09	0.065	0.058	±0.046
5.FeCu	7.145	-13	1450	0.82	0	0.16	0.02	0.308	0.058	±0.415

4.3.2.1 Solution thermodynamics of liquid Fe-Co-Cu-Si

The activity of silicon in liquid Fe-Co-Cu-Si is calculated from the measured concentration in the liquid ferrocobalt and is plotted in Figure 4.33 against the mole fraction of silicon. The results show a large negative deviation from ideal solution (Rauoltian) behaviour. This is in agreement with the studies by Wang *et al.* (2002) and it is also an indication of silicon's large chemical interaction with the ternary alloys of the transition metal group (Witusiewicz 1994). The tangent to this line is the activity coefficient. It is in the magnitude of 10^{-3} which is the same magnitude as the activity coefficient of liquid silicon in liquid iron at 1600 °C in dilute concentrations (Rosenqvist 1983). The activity coefficient will approach a constant as the concentration of silicon approaches zero. This sort of behaviour is said to obey Henry's law. However, in real solutions the interactions between species give rise to deviations from ideal behaviour. In the alloy melt with as many components as the ferrocobalt, other methods for describing the behaviour with respect to the activity coefficient of silicon should be considered.

In the descriptions of phase solutions, solid or liquid in the ternary systems Fe-Co-Cu and Fe-Cu-Si, three types of solution models have been applied; the regular solution model (Ohtani *et al*. 1997), the sub-regular solution model (Wang *et al*. 2002) and the substitutional solution model (Hino *et al*. 1999). All the three models take into account the interaction between the components and their dependence on the temperature and composition. The tendency of the solution to deviate from ideal behaviour is described by the excess quantity ($^{E}G^{l}_{mix}$) in the standard Gibbs free energy of mixing for a phase. The Gibbs free energy for the liquid phase of the Fe-Co-Cu-Si can be described by a substitutional subregular solution model (Bratberg and Frisk 2004; Hino *et al*. 1999) expressed as the function of temperature and composition (Equation 4.8).

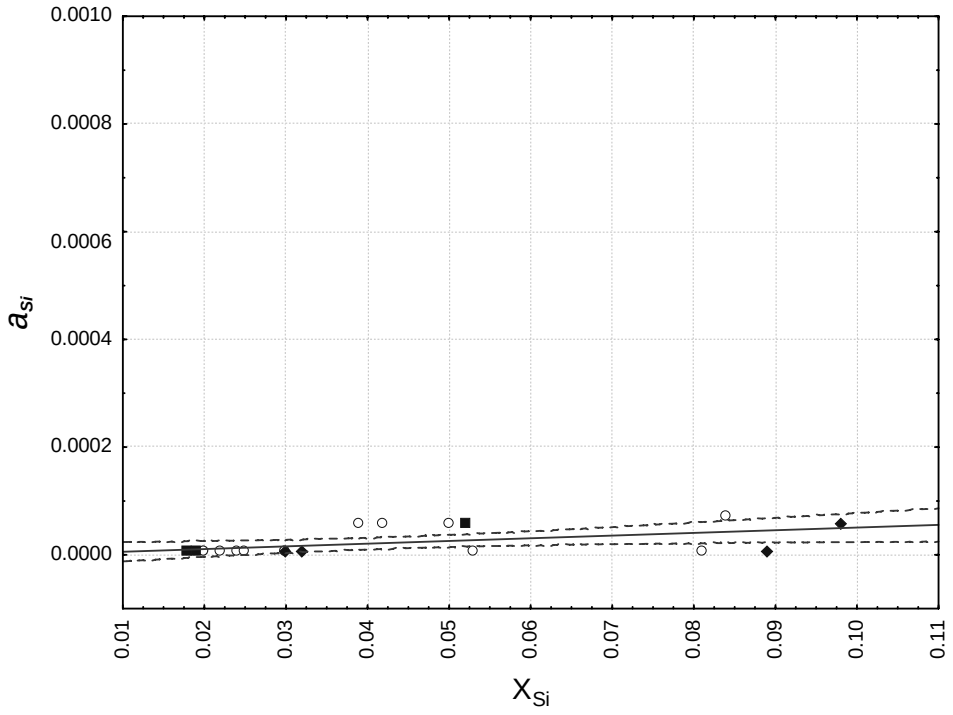

Figure 4.33 Measured activity of silicon in liquid Co-Cu-Si (♦), Fe-Cu-Si (■) and Fe-Co-Cu-Si (o) alloy systems equilibrated at 1450 °C

$$G^{l}_{mix} = x_{Fe}\,{}^{o}G^{l}_{Fe} + x_{Co}\,{}^{o}G^{l}_{Co} + x_{Cu}\,{}^{o}G^{l}_{Cu} + x_{Si}\,{}^{o}G^{l}_{Si} + RT(x_{Fe}\ln x_{Fe} + x_{Co}\ln x_{Co}\,x_{Cu}\ln x_{Cu} + x_{Si}\ln x_{Si}) + {}^{E}G^{l}_{mix} \qquad (4.8)$$

The term $({}^{E}G^{l}_{mix})$ of the liquid (l) is expressed as the sum of the binary, ternary and quaternary interaction parameter contributions expanded on a Redlich-Kister (Redlich and Kister 1948) polynomial:

$$ {}^{E}G^{bin,l}_{mix} = \sum_{i=1}^{c-1}\sum_{j>i}^{c} x_i x_j \sum_{m=0}^{n} {}^{m}L^{l}_{ij}(x_i - x_j)^m \qquad (4.9) $$

$$ {}^{E}G^{tern,l}_{mix} = \sum_{i=1}^{c-2}\sum_{j>i}^{c-1}\sum_{k>j}^{c} x_i x_j x_k \{ {}^{0}L^{l}_{ijk}(x_i + \delta_{ijk}) + {}^{1}L^{l}_{ijk}(x_i + \delta_{ijk}) + {}^{2}L^{l}_{ijk}(x_i + \delta_{ijk})\} \qquad (4.10) $$

$$ {}^{E}G^{quat,l}_{mix} = \sum_{i=1}^{c-3}\sum_{j>i}^{c-2}\sum_{k>j}^{c-1}\sum_{h>j}^{c} x_i x_j x_k x_h \{ {}^{0}L^{l}_{ijk}(x_i + \delta_{ijk}) + {}^{1}L^{l}_{ijk}(x_i + \delta_{ijk}) + {}^{2}L^{l}_{ijk}(x_i + \delta_{ijk}) + {}^{3}L^{l}_{ijk}(x_h + \delta_{ijk})\} \qquad (4.11) $$

where $\delta_{ijk} = (1 - x_i - x_j - x_k)/3$

where L^{l}_{ij}, L^{l}_{ijk}, and L^{l}_{ijkh} are binary, ternary and quaternary interaction parameters between *i* and *j* atoms and among *i, j, k* and *i, j, k, h* atoms respectively (where *i*=Fe, *j*= Co, *k*=Cu and *h*=Si). The number of components in the system is denoted by *c.* The interaction parameters for the Redlich-Kister formalism can be composition or temperature dependent (Redlich and Kister 1948):

$$ {}^{n}L_{ij}, {}^{n}L_{ijk} = {}^{n}A + {}^{n}B \cdot T + {}^{n}C \cdot T \ln T \qquad (4.12) $$

The parameters for the binary terms have been evaluated (Hino *et al*. 1999; Ohtani *et al*. 1997; Palumbo *et al*. 2006; Wang *et al*. 2002) and can readily be used. However the ternary interaction parameters for Fe-Co-Si and Co-Cu-Si are not available as well as the quaternary interaction parameter. These parameters can be set to zero or, if the experimental data is available an optimisation procedure can be carried to generate the interaction parameters. A discussion of the solution models is outlined in Appendix VI.

4.4 Thermodynamic Calculations

The general approach to calculating phase equilibria has been discussed in Chapter 2. In order to draw the phase diagrams a mathematical procedure is required using computer-based numerical methods. The FactSage™ and MTData software were used to calculate and describe the phase equilibria in the Fe-Co-Cu-Si system namely Fe-Co-Cu and Fe-Cu-Si as well as the estimation of

quaternary Fe-Co-Cu-Si. It is shown later in the section that the liquidus temperatures calculated with the FactSage™ equilibrium module (Equilib) were lower than the experimental measured values. This discrepancy is inherent in the optimised database. On the other hand calculations carried out by MTData, using a different database gave close values as the measured ones.

Thermodynamic calculators Factsage™ and MTData™ use databases that are based on optimised experimental information from phase diagram and phase equilibria data and because experimental data is not readily available for the wide composition and temperature ranges, the accuracy of the calculated phase equilibria and diagrams might be compromised and should be treated with caution. In this section, the database used with the FactSage™ is explained in terms of the optimised data from pure components through the binary and the ternary subsystems to the quaternary Fe-Co-Cu-Si. The FactSage™ steel alloy (FSstel) database has been optimised from the iron-rich alloy data comprising most of the systems components and their binary and ternary systems. The optimised binary and ternary systems considered pertinent to the study of the quaternary Fe-Co-Cu-Si are listed in Table 4.16. The characterisation of the database as outlined in the documentation of the software is described in the following paragraphs.

Table 4.16 The FSstel optimised systems

System	Reference
Co-Cu	(Nishizawa and Ishida 1984)
Co-Fe	(Guillermet Fernandez 1988)
Co-Si	(Choi 1992)
Cu-Fe	(Ansara and Jansson 1993)
Cu-Si	(Jantzen and Lukas 2000) (unpublished data)
Fe-Si	(Lacaze and Sundman 1991)
Co-Cu-Fe	(Ohtani *et al*. 1997)
Cu-Fe-Si	(Ohtani *et al*. 1997)

The FSstel database is intended to allow calculations primarily for the iron-rich composition ranges, although the assessed data are also reliable for higher concentrations of alloying components in a number of cases. It is therefore important that when one intends to use this database an assessment of the optimised systems for the temperature and composition ranges is carried out. The database is supposedly valid for the temperature range of approximately 400 ^{o}C to 1800 ^{o}C.

The database is built on assessed information of the phases using simple substitutional solution approach based on the Redlich-Kister-Muggianu polynomial expression for the description of the liquid phase. As for the solid phases the fcc (austenite) and bcc (ferrite) Fe-rich phases have been described using a sub-lattice model with carbon, nitrogen and vacancies on interstitial sites. Lastly the non-stoichiometric intermetallic phases are described using sublattice models. The referenced material for the subsystems optimised in the database is based on the work by Ohtani *et al.* (1997) (Fe-Co-Cu and Fe-Cu-Si); Nishizawa and Ishida (1984) (Co-Cu); Guillermet (1988) (Co-Fe); Choi (1992) (Co-Si); Ansara (1993) (Cu-Fe); Jantzen (2000) (Cu-Si); Lacaze (Lacaze and Sundman 1991) (Fe-Si).

4.4.1 FactSage Calculations: Ternary system

Calculations of equilibrium for the Fe-Co-Cu systems by FactSage™ are in good agreement with measured values at the peritectic transformation temperatures. However, equilibrium calculations at higher temperatures yield lower liquidus temperatures in comparison to the measured values of the same alloy compositions. **Error! Reference source not found.** show the calculated liquidus temperatures compared to the measured liquidus temperatures for FactSage™ and MTData^{TM} software. The FactSage™ results only accounts for 70 % of the measured values whereas the MTData accounts for 81% showing that the database of MTData is extensively optimised than that of the FactSage™ in this regard.

The phase equilibria in the ternary Fe-Co-Cu were calculated with the "Equilib" module of FactSage™ using the FSstel database. The selection of the solution species used from the database was based on the optimised solid and liquid solutions. Since the ternary alloy Fe-Co-Cu has been reported to posses metastable phases, the equilibrium calculations by FactSage™ were set to take into consideration the existence of such metastable phases as well as the occcurence of imscibility within the phases. In the practical sense, however, the metastable phases occur when the liquid alloy is undercooled prior to solidification which is contrary to the approach of this study.

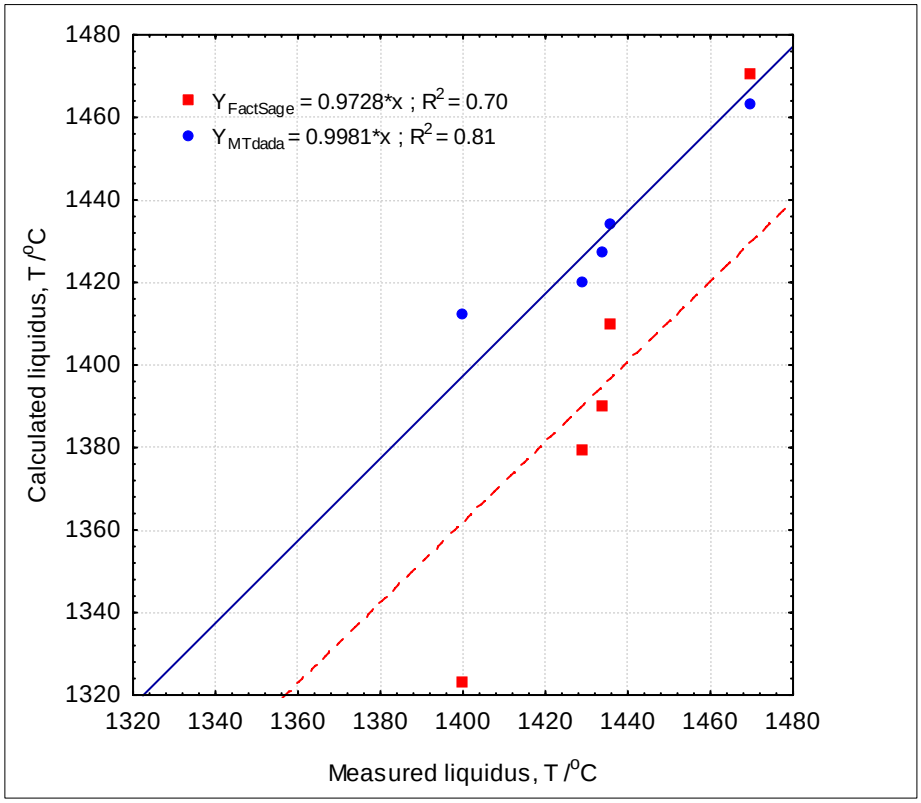

Figure 4.34 The graph shows the relationship between the calculated and measured liquidus temperatures in the Fe-Co-Cu system

The results of euilibria calculations are plotted on the composition-temperature and mass-temperature distribution diagrams shown in Figure 4.35 and Figure 4.36. The calculations with FactSage™ are inaccurate for the alloys outside the iron-rich composition (less than 80 wt. % Fe) region. For instance, the transformations temperatures for alloy A are in agreement with the calculated values whereas, in alloy C the liquidus temperatures do not correspond to the measured temperatures inspite of the lower temperature transformations being in agreement with the calculated values.

In both charts, the formation of the peritectic temperature is in agreement with the measured ones. The mass of the peritectic liquid (Cu-rich) is less than 0.05 g at the formation temperature compared to the iron rich liquid in alloy A (Figure 4.35). In alloy C (Figure 4.32), the mass of the peritectic liquid is relatively more at the temperature of formation, at about 0.1 g, than in alloy A. The peritectic temperature does not have a significant dependence on composition. However, the liquidus temperature does. The melting of the iron-rich (fcc#1 in the Figure) involves a process of incorporating increasing amounts of iron and cobalt into the copper rich liquid phase prior to break of the structure through grain boundary melting. Since alloy A is

richer in iron and going by the observations from the HLSCM measurement its high melting temperature or liquidus temperature can be explained on this basis.

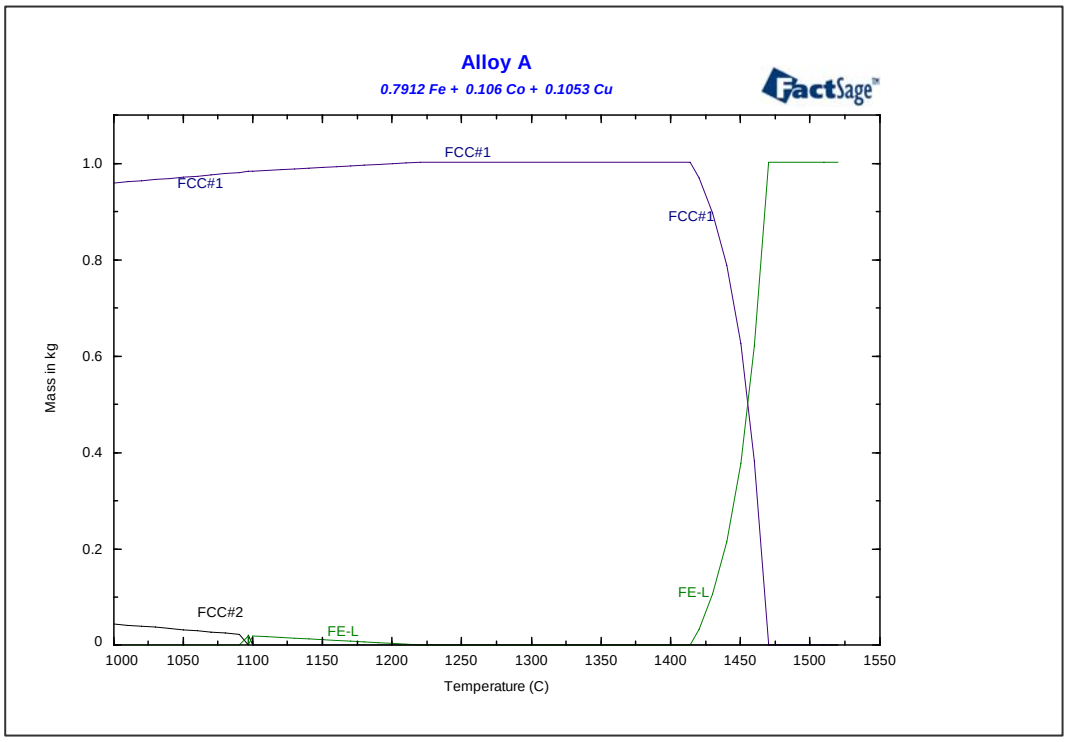

Figure 4.36 Calculated phase distribution by mass in alloy A at indicated composition

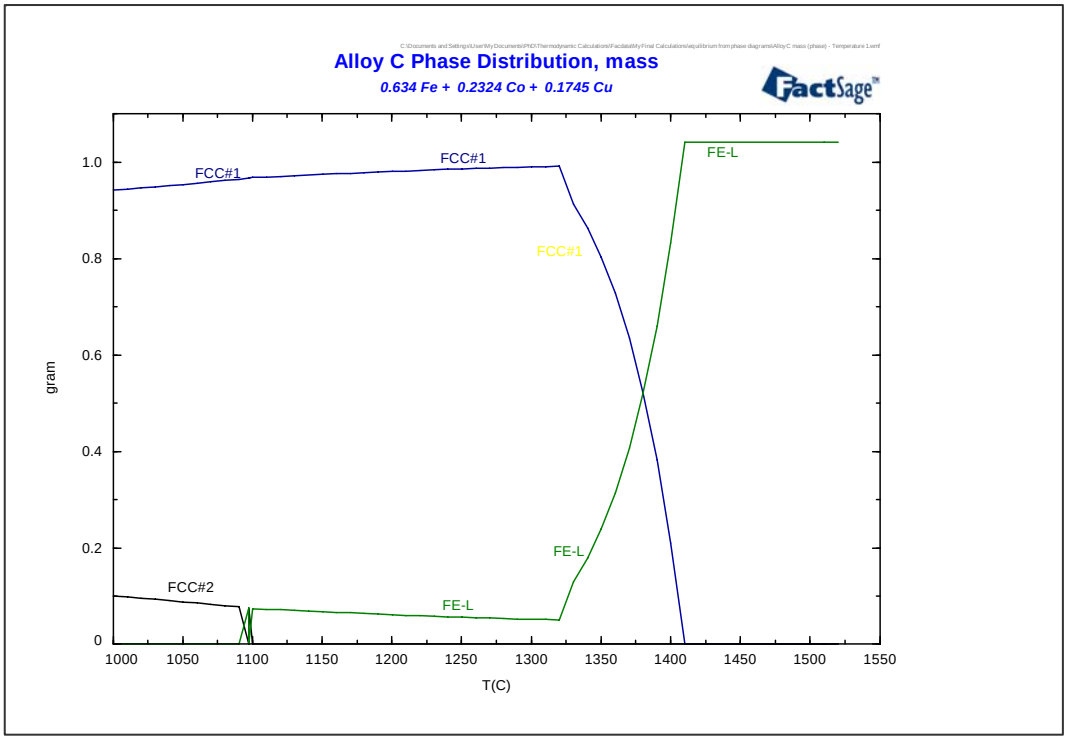

Figure 4.35 Calculated invariant and liquidus transformation by mass in alloy C at indicated composition

However, because of the observed discrepancies between the measured values and the calculated ones, the calculations of the phase equilibria are supplemented with MTData.

4.4.2 MTData Calculations: Ternary Systems

The temperature-phase-composition relationships were calculated for the four alloys submitted to the BHP steel institute. The temperature range for the transformation was 1000 to 1550 °C. The alloy designated T, based on the composition of the alloy reported by Bamberger (2002) in which a phase separation was reported as well as the liquidus temperatures, is included in the calculations. Figure 4.37 to Figure 4.41 show the liquidus transformation temperatures in the alloys A to T. For the values reference should be made to Table 4.5 in section 4.1.2.1.

The phase–temperature–composition diagrams in Appendix VII give a direct measure of the distribution of each of the elements across the phases. The fractions given on the diagrams must be correlated with the total amount of the element present in the system. For example, considering the three diagrams in Appendix VI to alloy A, and choosing a temperature of 1050 °C (for comparison to data given in Table 4.17) the fraction of each element may be determined from the graphs. Table 4.16 demonstrates how the fractional distribution charts may be used to generate the data given in Table 4.17. The fractional distributions were measured directly from the charts using a ruler. It is possible to generate the data contained in the mass of phases vs temperature charts from the fractional distribution charts and the known system concentrations.

Table 4.17 Data generation using fractional distribution charts

Phase	Cu	Co	Fe	
5	0.554	1.000	0.998	measured fractional distribution of elements across phases
6	0.442	0.000	0.002	
mass fraction of each element in each phase is determined by multiplying each element fraction by the total system fraction for that element				
	x0.1	x0.1	x0.8	sum of masses of elements gives mass fraction of phase
5	0.055	0.100	0.798	0.954
6	0.044	0.000	0.002	0.046
composition of each phase (as mass fraction) is determined by dividing the mass fraction of each element in a phase by the total mass fraction of that phase				
5	0.058	0.105	0.837	
6	0.965	0.000	0.035	

Note: 5- FCC (Fe rich) 6- FCC (Cu rich)

Table 4.18 Phase weight percents and compositions for each alloy at a number of temperatures

Alloy	T (C)	Phase	Phase m%	Mass% in each phase			mass% in system		
				Fe	Co	Cu	Fe	Co	Cu
A	1050	FCC1	4.58	2.92	0.32	96.76	0.13	0.01	4.43
	1050	FCC2	95.42	83.7	10.47	5.83	79.87	9.99	5.57
	1150	Lq	2.57	3.36	0.35	96.29	0.09	0.01	2.47
	1150	FCC2	97.43	82.02	10.25	7.73	79.91	9.99	7.53
	1250	Lq	0.77	5.53	0.59	93.88	0.04	0	0.73
	1250	FCC2	99.23	80.58	10.07	9.35	79.96	10	9.27
C	1050	FCC1	15.8	2.41	0.81	96.78	0.38	0.13	15.29
	1050	FCC2	84.2	70.81	23.6	5.59	59.62	19.87	4.71
	1150	Lq	14.01	2.74	0.86	96.4	0.38	0.12	13.5
	1150	FCC2	85.99	69.33	23.12	7.56	59.62	19.88	6.5
	1350	Lq	11.39	7.64	2.5	89.86	0.87	0.29	10.24
	1350	FCC2	88.61	66.73	22.25	11.02	59.13	19.71	9.76
D	1050	FCC1	15.85	2.18	1.07	96.75	0.35	0.17	15.33
	1050	FCC2	84.15	64.95	29.51	5.55	54.65	24.83	4.67
	1150	Lq	14.01	2.46	1.13	96.41	0.34	0.16	13.5
	1150	FCC2	85.99	63.56	28.89	7.55	54.66	24.84	6.5
	1350	Lq	11.24	6.84	3.22	89.94	0.77	0.36	10.11
	1350	FCC2	88.76	61.1	27.76	11.14	54.23	24.64	9.89
E	1050	FCC1	15.85	1.94	1.35	96.7	0.31	0.21	15.33
	1050	FCC2	84.15	59.05	35.4	5.55	49.69	29.79	4.67
	1150	Lq	13.96	2.19	1.42	96.39	0.31	0.2	13.46
	1150	FCC2	86.04	57.76	34.64	7.6	49.69	29.8	6.54
	1350	Lq	11.05	6.09	4.01	89.91	0.67	0.44	9.94
	1350	FCC2	88.95	55.46	33.23	11.32	49.33	29.56	10.06
T	1050	FCC1	35.59	2.14	1.11	96.75	0.76	0.4	34.43
	1050	FCC2	64.41	64.02	30.44	5.54	41.24	19.6	3.57
	1150	Lq	34.26	2.42	1.17	96.41	0.83	0.4	33.03
	1150	FCC2	65.74	62.63	29.81	7.56	41.17	19.6	4.97
	1350	Lq	34.07	6.72	3.34	89.94	2.29	1.14	30.64
	1350	FCC2	65.93	60.23	28.61	11.16	39.71	18.86	7.36
	1450	Lq	15.94	12.35	5.7	81.95	1.97	0.91	13.06
	1450	Lq2	84.06	47.62	22.71	29.67	40.03	19.09	24.94

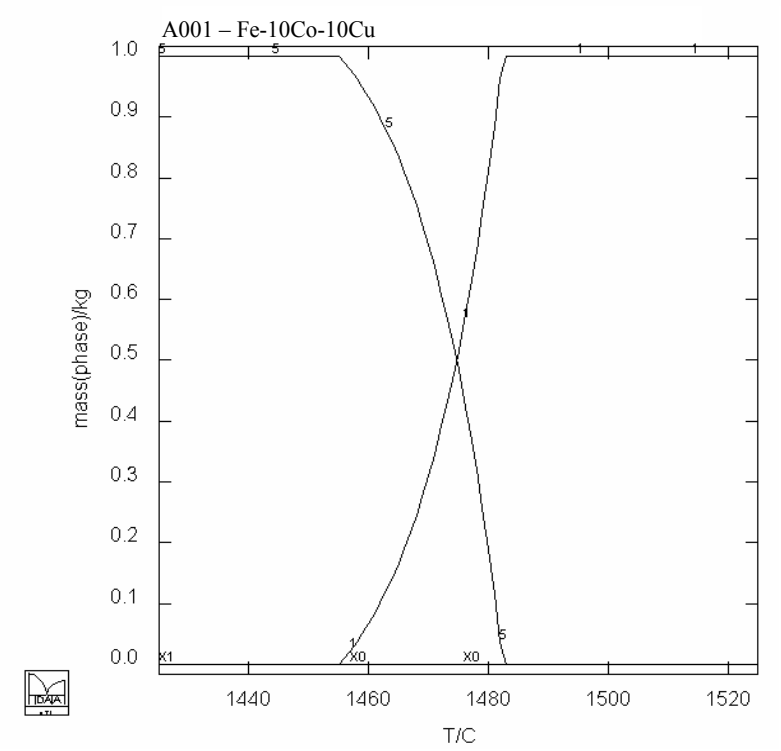

Figure 4.37 Phase equilibria in the Fe-Co-Cu at indicated composition (alloy A)

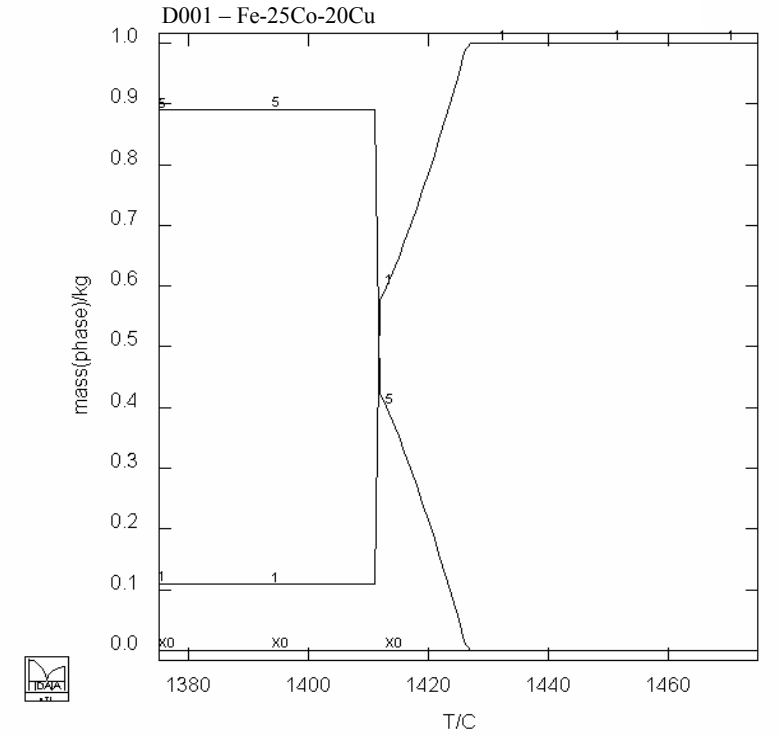

Figure 4.38 Phase equilibria in the Fe-Co-Cu at indicated composition (alloy D)

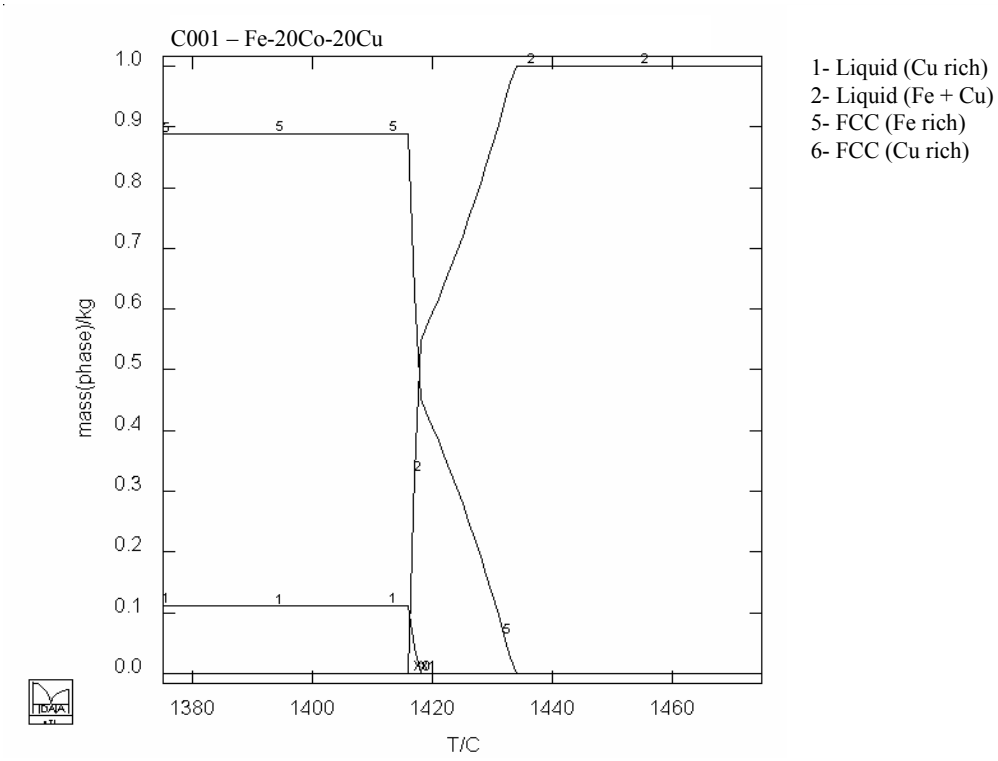

Figure 4.39 Phase equilibria in the Fe-Co-Cu at indicated composition (alloy C)

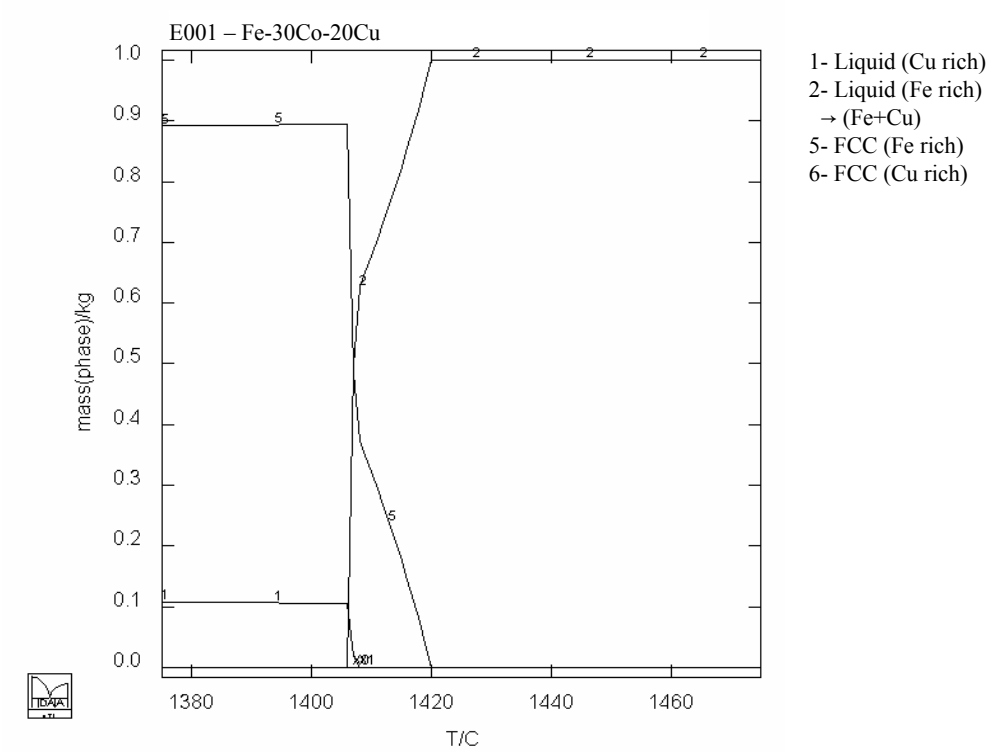

Figure 4.40 Phase equilibria in the Fe-Co-Cu at indicated composition (alloy E)

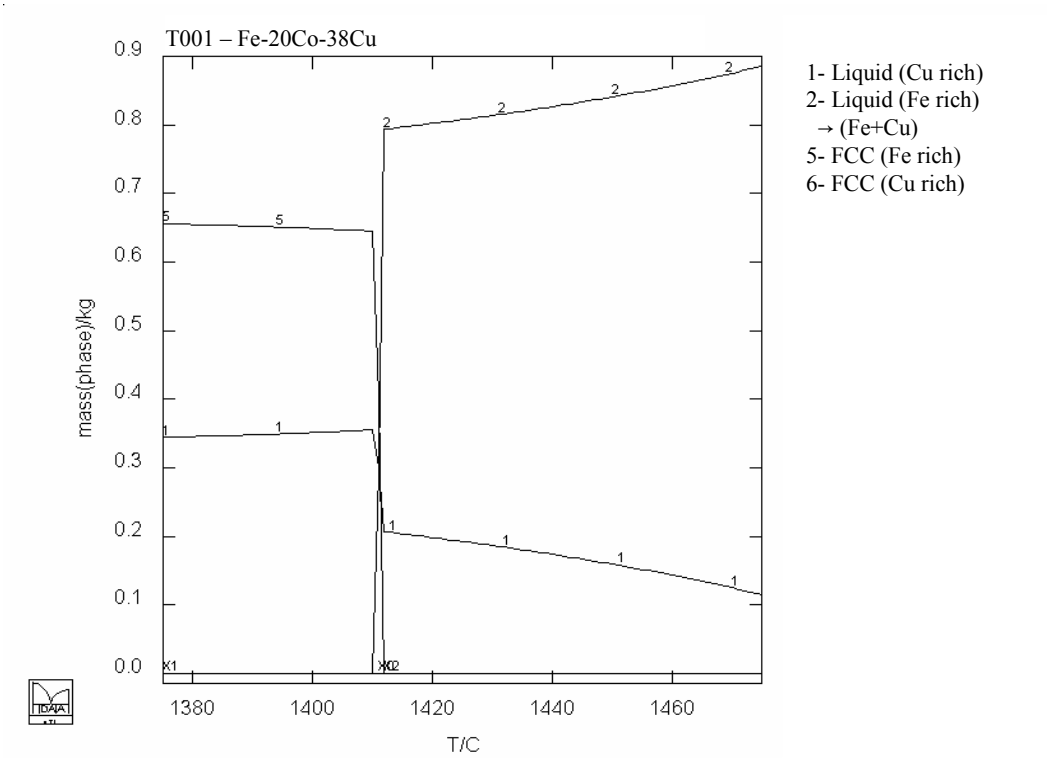

Figure 4.41 Phase equilibria in the Fe-Co-Cu at indicated composition (alloy T)

4.4.3 MTData Calculations: Quaternary Fe-Co-Cu-Si System

The calculation of the phase equilibria in the ternary Fe-Co-Cu using MTData yield plausible results which are comparable to the experimental data. In the absence of optimised data for the entire system, a step towards calculating the phase equilibria in the quaternary Fe-Co-Cu-Si system was taken by using the MTData program. Six alloy compositions on a fixed cobalt to copper ratio and containing silicon up to 5 wt.% were subjected to equilibrium calculations over a temperature range similar to the range discussed for the phase equlibria experiments.

The charts of composition-temperature-phase distribution show the distribution of the components of the Fe-17.5Co-17.5Cu-5Si (in wt. %) system in the equilibrium phases in the temperatures range 800 °C to 1550 °C. Silicon is shown in Figure 4.42, Figure 4.43 shows the distribution of iron and, Figure 4.44 the distribution of copper. The phase mass fraction distribution as function of temperature is shown in Figure 4.45. The distribution of silicon in the fcc-Cu, is negligibly small (Figure 4.42) but slightly more in the L-Cu rich between 1080 and 1225 °C. Within the same temperature range silicon decreases in the fcc-Fe rich until the formation of the L-Fe rich phase when silicon decreases in the L-Cu rich phase. Iron distribution (Figure 4.43) in the fcc-Cu rich or L-Cu rich phases is negligibly small. This is due to the solubility limit of iron in copper. On the other hand the distribution of copper in the fcc-Fe rich

phase (Figure 4.44) increases temperature up to the formation of L-Fe rich liquid at 1225 °C. This increase can be attributed to the presence of silicon because solubility of copper in iron is reportedly very small (Olensiki and Abbaschian 1986) but increases in the presence of silicon (Othani *et al.* 1997). Between 1225 and 1335 °C the two liquids L-Fe rich and L-Cu coexist.

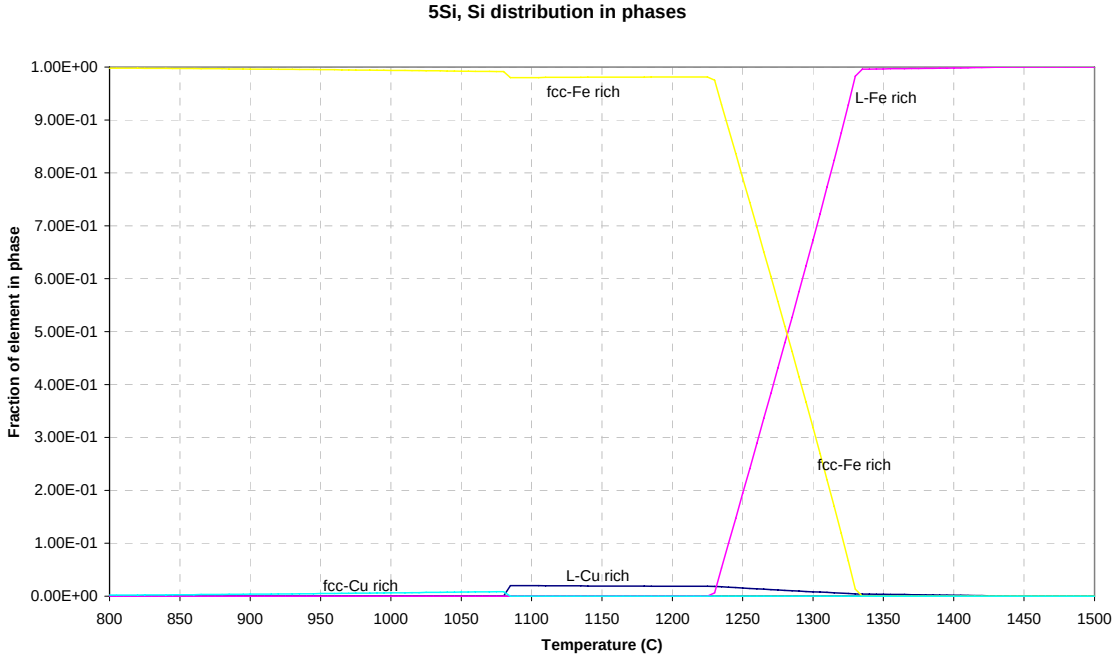

Figure 4.42 Silicon distribution in equilibrium phases of quaternary Fe-17.5Co-17.5Cu-5Si (wt.%) calculated with MTData

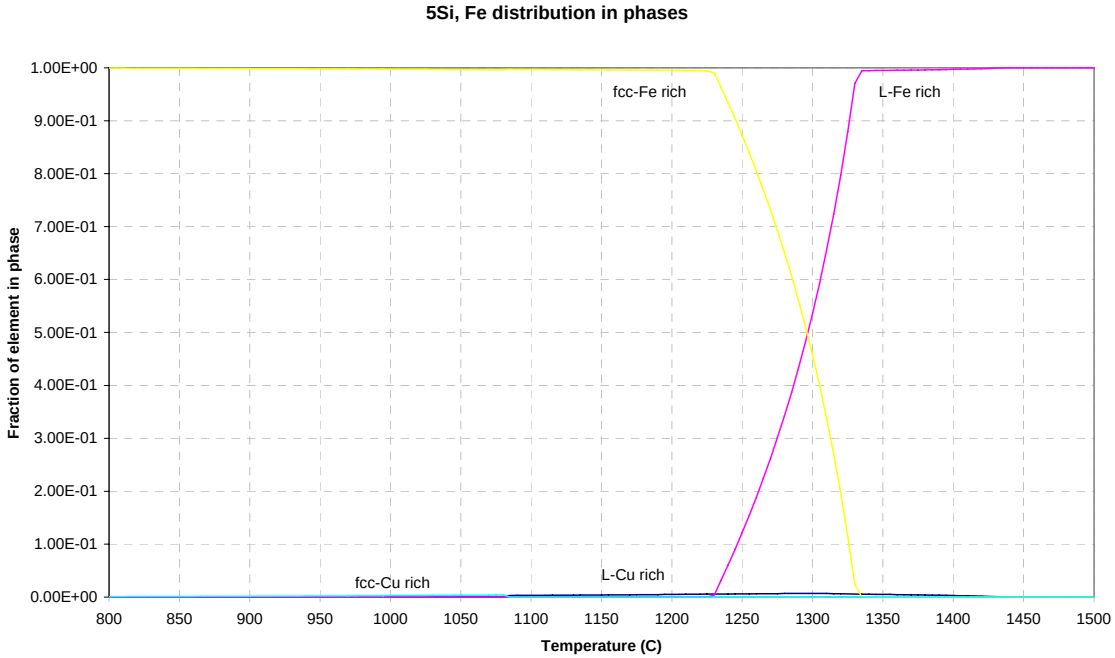

Figure 4.43 Iron distribution in equilibrium phases of quaternary Fe-17.5Co-17.5Cu-5Si (wt.%) calculated with MTData

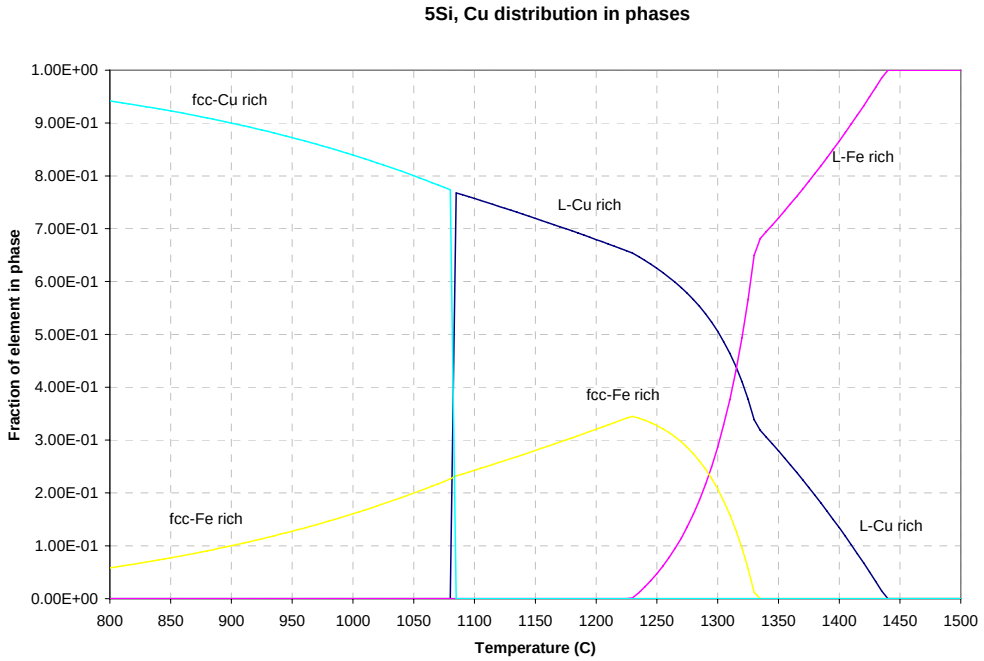

Figure 4.44 Copper distribution in equilibrium phases of quaternary Fe-17.5Co-17.5Cu-5Si (wt.%) calculated with MTData.

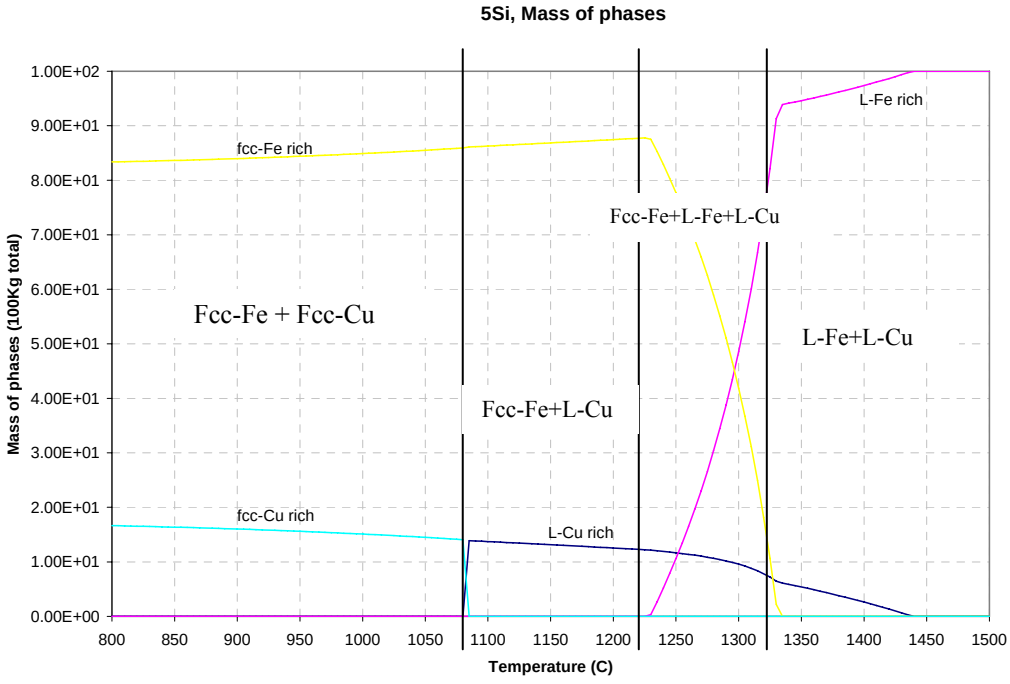

Figure 4.45 MTData calculated phase distribution in quaternary Fe-17.5Co-17.5Cu-5Si (in wt. %)

From Figure 4.45 the transition temperatures for the invariant reactions in the composition range are indicated on the diagram. The appearance of the second iron rich phase is equivalent to the

transitions observed in DTA and dark grey phase in quench experiments. Considering the lack of evidence in the thermodynamic databases used, the calculated phase equilibria at the 5 wt.% Si can be used to describe the Fe-Co-Cu-Si quaternary system.

CHAPTER 5

SUMMARY AND CONCLUSIONS

The liquidus temperatures of the quaternary Fe-Co-Cu-Si system and its subsystems were determined within the experimental errors by DTA and the high temperature phase equilibria by melt-and-quench methods coupled with SEM/EDS. These findings close up the gap of uncertainty about the liquidus temperature of ferrocobalt characterised in chapter 2.

The liquidus temperatures of the subsystems of the quaternary Fe-Co-Cu-Si is

- Compositional dependent on the Fe/Cu ratio. Iron and copper constitute the two dominating phases observed in the ternary Fe-Co-Cu system. The findings are in agreement with the early findings by Maddocks and Claussen (1936) who considered the ternary Fe-Co-Cu as a Φ–Cu binary where Φ represents (Fe-Co). The liquidus surface characteristically drops towards the copper corner of the ternary. The maximum liquidus temperature measured for this alloy system is 1470 °C for iron rich (80Fe-10Co-10Cu) corner and drops to 1436 °C along Co/Cu = 1 line at 60Fe-20Co-20Cu (wt.%).

- In the Fe-Cu-Si system the liquidus temperature on the Fe-Cu side ranged from 1445 °C at 77Fe-20Cu-2.6Si (wt.%) to 1374 °C at 74Fe-20Cu-6Si (wt.%). Similarly, the Co-Cu-Si system exhibits a drop in the liquidus temperature at increased silicon content, from 1420 °C at 84Fe-14.5Cu-1.5Si to 1361 °C at 82.6Fe-14.5Cu-4.9Si. This effect is due to the increased solubility of copper in the γ–Fe which coexists with α–Fe at 1295 °C in the high silicon alloy.

The findings of the study on the phase equilibria in the Fe-Co-Cu-Si System show that

- The physical and thermochemical properties of the multicomponent Fe-Co-Cu-Si system can be studied by examining its subsystems. Characteristics existing in binary and/or ternary systems are extended into the multicomponent system and by that, the quaternary Fe-Co-Cu-Si system exhibit peritectic behaviour in the temperature range 1096 to 1098 °C (within experimental errors) on the iron-rich side. This is typical of the binary systems Co-Cu and Fe-Cu. There was no metastable liquid phase separation (MLPS) observed on heating in the alloys studied confirming that the phenomena of MLPS takes place under supercooling conditions. Whether this condition would exist in the handling of the liquid ferrocobalt will depend on the prevailing condition and precautionary preheating of the

hot-metal channels to prevent rapid change in temperature that would lead to MLPS. In any case the MPLS concept is prevalent in the ternary Fe-Co-Cu and not in the silicon containing ternary systems. Silicon has a stabilising effect on the MLPS and as shown in the DTA and MTData calculations the liquid separation is prevalent in higher contents of silicon.

- The existence of the peritectic reaction in the system signifies that the copper-rich liquid which forms at the peritectic temperature is in equilibrium with the solid iron rich liquid over a wide temperature range over which the iron-rich solid phase melt by dissolution of its components in the copper-rich liquid phase. This was observed in the heating traces of the subsystems, which exhibit a steady and slanting deviation from the baseline before approaching the liquidus temperature.

- The quaternary Fe-Co-Cu-Si behaves like the Fe-Cu-Si ternary with coexisting phases during the melting experiments. Again, this behaviour is inherent in the Fe-Si system where the γ-Fe exists on the iron side and is also observed in the ternary Fe-Cu-Si and Co-Cu-Si systems too. The strong chemical interaction between silicon and copper is evident in the element distribution maps of the three phase system of the Fe-Co-Cu-Si.

The activity of silicon in liquid ferrocobalt was determined at 1450 °C and it was found to have a large negative deviation from Raoult's ideal solution behaviour in the composition range 0.01 to 0.09 mole fractions of silicon. It is deduced from this finding that the solution thermodynamics of the Fe-Co-Cu-Si system can be treated with regular solution model to extend the thermodynamic descriptions to the quaternary provided there is sufficient experimental data to satisfy the degrees of freedom required for optimisation.

The thermodynamic database FSstel used by FactSage™ is inadequate for the calculation of the phase equilibria in the Fe-Co-Cu and Fe-Cu-Si system, let-alone the quaternary Fe-Co-Cu-Si. It is inconsistent when iron concentration is below 80 wt.%. There is a large discrepancy between the experimentally determined liquidus temperatures and the calculated values with FactSage™ (see Figure 4.34). MTData on the other hand, predicted the liquidus temperatures in agreement with the measured values. Therefore, the phase equilibria in the Fe-Co-Cu-Si system can be described with MTData.

The findings of this work, within the experimental errors, conclude that the liquidus temperatures of the Ferrocobalt alloys are composition dependent on copper and silicon. Silicon is readily soluble at the slag cleaning smelting conditions, which are reducing. The chemical interaction of silicon in the liquid ferrocobalt system has a large thermodynamic activity deviation from ideal solution behaviour.

Further more, from the behaviour of ferrocobalt based on the model alloy Fe-Co-Cu-Si it is suggested that:

- as long as silicon can be handled (is not a nuisance) in the subsequent processes, the activity coefficient of silicon in the liquid ferrocobalt must be promoted to lower the liquidus temperatures and in so doing reduce the energy demand for smelting.
- since silicon stabilises the immiscibility gap between the iron-rich and copper-rich liquid phases, the furnace temperature of the ferrocobalt must be operated at temperatures at which no liquid separation exists. Therefore, composition-temperature phase equilibria in the ferrocobalt should be incorporated in the process control algorithms and the operational philosophy of the single electrode dc arc furnace.

Future work that would complement the current study should include:

- The thermochemical data for the Co-Cu-Si and Fe-Co-Si is scarce or unpublished. It is therefore recommended that a study of the thermochemical aspect of these ternary systems be established. This would assist in validating the assessment of the binary systems as well as introduction of the ternary interaction energies. This should further the understanding of the ferrocobalt behaviour pertinent to smelting conditions:
    - Investigate solution behaviour type up to 5 wt.% Si
    - Model the activity coefficient data at different temperatures
    - Build a database that can accommodate the ferrocobalt physicochemical properties
    - Expand the region of composition with respect to Fe and Cu
    - Expand the system to investigate the effect of sulphur and carbon.

APPENDICES

APPENDIX I: LIST OF MATERIALS

Table I.1 Materials used in the experiments

1.0 Reagents		
Chemical	**Purity and quality**	**Supplier**
Co Powder	Puratronic, 99.998% (metals basis), -22 mesh	Alfa Aesar; LOT:23097
Cu Powder	Puratronic, 99.999% (metals basis), -22 mesh	Alfa Aesar; LOT:23171
Fe Powder	99.5%	Sigma-Aldrich
Si Granules	99.999%, Granules, 5-10mm	Unaxis; LOT:02-347865
Argon Gas	UHP	Afrox
	HP	Afrox
Hydrogen Gas	HP	Afrox
Carbon Dioxide	CP	Afrox
2.0 Crucibles	**Description**	**Usage**
Degussit AL23	No. 201-11010-0150 Vol. ~0.7ml	Quench Experiments
	No. 201-1120-0300 Vol. ~6ml	Alloy Preparation
	No.209-11000-0068 Slip-on Crucible	DTA measurements
Quartz	100% SiO_2	Liquid-Solid Equilibria Experiments
Graphite	Le Carbone Grade 2020	Induction Receptor
3.0 Thermocouples	**Type**	**Usage**
	Type B	Tube & Induction Furnaces
	Type S	DTA
4.0 Bubble Alumina	**Granular 1-2mm.**	**Induction Furnace**
5.0 Platinum Wire	**10Rh-Pt, 0.5mm diameter**	**Quench Experiments**
6.0 Molybdenum Wire		**Gas-Liquid-Solid Equilibrium**

APPENDIX II: METALLOGRAPHY AND SEM/EDS - METHODS AND PROCEDURES

The specimens for all SEM/EDS analysis were mounted and polished to 1 micron. The appropriate specimen were cut from the samples using a precision waffle blade cutter. In cases where light microscope was required to validate the microstructures, etching with 2 % Nital or $FeCl_3$.

Imaging of the samples and analysis of the phase compositions was accomplished using a Leo® 1430VP Scanning Electron Microscope at the Stellenbosch University. Prior to imaging or analysis the samples are sputter-coated with either gold or carbon depending on the application. Samples were identified with backscattered electron (BSE) and/or secondary electron images, and phase compositions quantified by EDS analysis using an Oxford Instruments® 133KeV detector and Oxford INCA software. Beam conditions during the quantitative analyses were 20 KV and approximately 1.5 nA, with a working distance of 13 mm and a specimen beam current of -3.92 nA. Despite the relatively low energy of the beam, X-ray counts with the set-up used were typically ~ 5000 cps. The counting time was 50 seconds live-time. Pure metals; iron, cobalt and copper were used for standardization and verification of the analyses. Pure Co, was used periodically to correct for detector drift.

APPENDIX III: ERRORS SOURCES

The errors generated from measurements in DTA and EDS are listed in Table III.1 for the each element analysed in the phases.

Table III.1 Range of errors observed on measurements by EDS

	wt% errors observed			
	Fe	Co	Cu	Si
Fe-rich Phases	0.44	0.27	0.32	0.11
Cu-rich Phases	0.15	0.15	0.79	0.09

All temperatures measured by DTA have an error of ±2 °C as determined from calibration factor.

APPENDIX IV: PARTIAL PRESSURE (FUGACITY) OF OXYGEN BY MIXING CO_2 AND H_2

In principle, the mixture of CO_2 and H_2 constitute the C-O-H system in which oxygen fugacity is uniquely fixed according to the phase rule. The C-O-H system has been reported by Deines (Deines *et al*. 1974), and Naphziger *et al.* (1971) in which they reported that the oxygen fugacity and partial pressure of oxygen are treated likewise at 1 atmosphere at high temperatures typically employed in pyrometallurgical research. The method depends strongly on the high temperature dissociation equilibria of suitable gases (in the current study CO_2 and H_2) to produce the desired oxygen fugacity to be used to control the oxidation-reduction reactions in the involved condensed phase. They achieved the desired fugacity at a desired temperature by controlling the gas mixing ratio at room temperature. The Gibbs free energies of formation and the corresponding equilibrium constants of reaction equations (1) to (3) can subsequently, be used to calculate the fugacities at the furnace temperatures.

$$CO_2(g) \Leftrightarrow CO(g) + \tfrac{1}{2}O_2(g) \quad \text{(IV.1)}$$

$$H_2(g) + \tfrac{1}{2}O_2(g) \Leftrightarrow H_2O(g) \quad \text{(IV.2)}$$

$$H_2(g) + CO_2(g) \Leftrightarrow H_2O(g) + CO(g) \quad \text{(IV.3)}$$

The reaction equation yield three degrees of freedom expressed by equation 4 as follows.

$$F = (N\text{-}r\text{-}t)\text{-}p+2 = (5\text{-}2\text{-}1)\text{-}1+2 = 3 \quad \text{(IV.4)}$$

F: degrees of freedom = 3; p: number of phases-gas = 1; N: number of species = 5; r: number of independent reactions = 2; t: stoichiometric constraints = 1; for a fixed mixing ratio of CO_2/H_2 molar ratios of C/H and C/O are also fixed, assuming that no solids deposit.

The work by Nafziger *et al.* (1971), has shown that the reaction of interest at high temperatures in the CO_2-H_2 mixture is

$$nH_2(g) + CO_2(g) \Leftrightarrow nH_2O(g) + CO(g) + \tfrac{(1-n)}{2}O_2 \quad \text{(IV.5)}$$

$$0 < n \leq 1$$

From which the equilibrium constant is expressed as

$$K_{(2.5)} = \frac{(pCO \cdot pH_2O^n \cdot pO_2^{\frac{(1-n)}{2}})}{(pCO_2 \cdot pH_2^n)} \quad \text{(IV.6)}$$

If the pO_2 desired is very small compared to the total pressure then it can be assumed that n is very close to one (n= 1) since there will be very little free oxygen present at equilibrium. The exact partial pressures for the gases will depend on the choice of n.

$$P_{total} = pCO + pH_2O + pCO_2 + pH_2 + pO_2 = 1 \qquad \text{(IV.7)}$$

For n = 1, Equations 3 to 7 are justified and lead to an expression for the calculation of the volume percent of CO_2 in a CO_2-H_2 mixture to obtain any desired oxygen potential (pO_2) at any desired temperature by Equation8.

$$\%CO_2 = 100 \cdot \frac{1 + pO_2^{1/2}}{\left(2 + \frac{pO_2^{1/2}}{K_{2.1}} + \frac{K_{2.2}}{pO_2^{1/2}}\right) \cdot K_{(2.1)}} \qquad \text{(IV.8)}$$

Deines *et al.* (1971) tabulated the values of volume percent CO_2, temperature and corresponding log pO_2 based on Equation 8. The tables have been used in the study to proportion gases for the gas-alloy-silica equilibrium experiments described in Chapter 3.

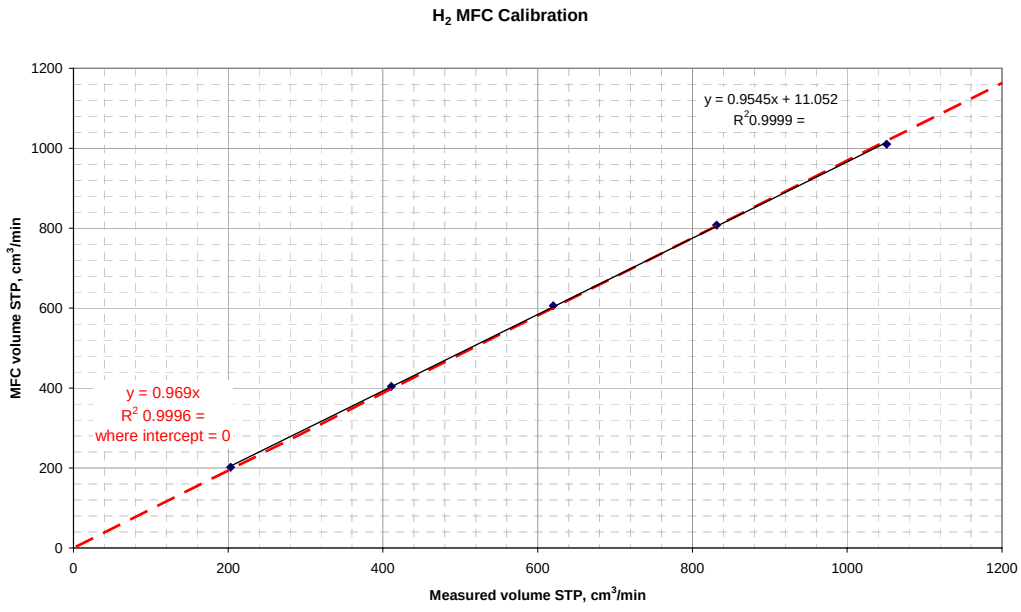

Figure IV.1 Correction Chart for CO2 gas mass flow controller

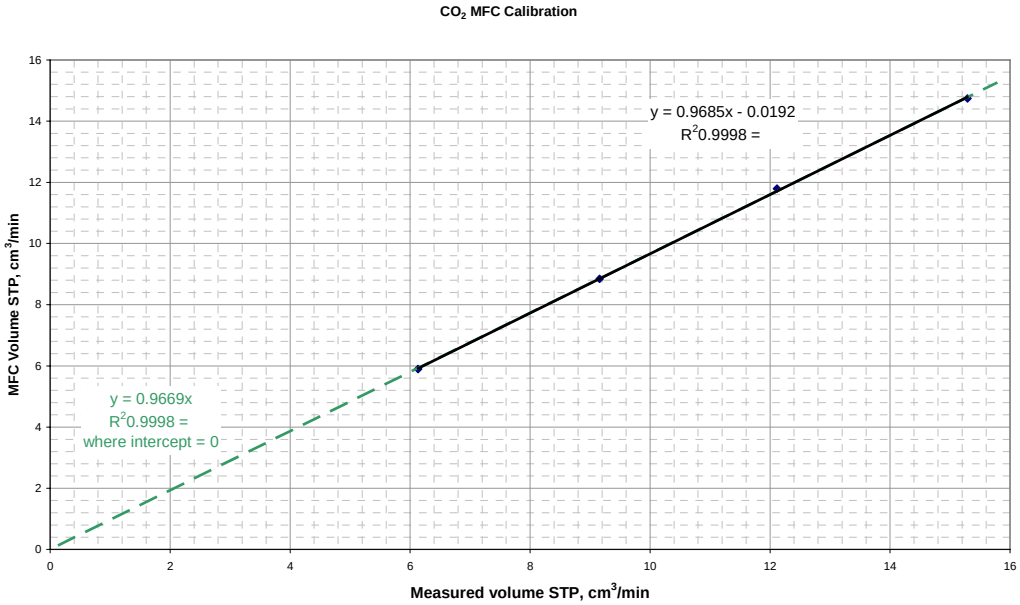

Figure IV.2 Correction Chart for H_2 gas mass flow controller

APPENDIX V: NOTES ON SOLUTION MODELS

The Gibbs free energy of mixing in a liquid phase is expressed at equilibrium as

$$G^{l}_{mix} = x_{Fe}\,{}^{o}G^{l}_{Fe} + x_{Co}\,{}^{o}G^{l}_{Co} + x_{Cu}\,{}^{o}G^{l}_{Cu} + x_{Si}\,{}^{o}G^{l}_{Si} + RT(x_{Fe}\ln x_{Fe} + x_{Co}\ln x_{Co}\,x_{Cu}\ln x_{Cu} + x_{Si}\ln x_{Si}) + {}^{E}G^{l}_{mix} \quad \text{(V.1)}$$

The term $({}^{E}G^{l}_{mix})$ of the liquid (l) is expressed as the sum of the binary, ternary and quaternary interaction parameter contributions expanded on a Redlich-Kister polynomial (Redlich and Kster 1948):

$${}^{E}G^{bin,l}_{mix} = \sum_{i=1}^{c\text{-}1}\sum_{j>i}^{c} x_i x_j \sum_{m=0}^{n} {}^{m}L^{l}_{ij}(x_i - x_j)^m \quad \text{(V.2)}$$

$${}^{E}G^{tern,l}_{mix} = \sum_{i=1}^{c\text{-}2}\sum_{j>i}^{c-1}\sum_{k>j}^{c} x_i x_j x_k \{{}^{0}L^{l}_{ijk}(x_i + \delta_{ijk}) + {}^{1}L^{l}_{ijk}(x_i + \delta_{ijk}) + {}^{2}L^{l}_{ijk}(x_i + \delta_{ijk})\} \quad \text{(V.3)}$$

$${}^{E}G^{quat,l}_{mix} = \sum_{i=1}^{c\text{-}3}\sum_{j>i}^{c\text{-}2}\sum_{k>j}^{c-1}\sum_{h>j}^{c} x_i x_j x_k x_h \{{}^{0}L^{l}_{ijk}(x_i + \delta_{ijk}) + {}^{1}L^{l}_{ijk}(x_i + \delta_{ijk}) + {}^{2}L^{l}_{ijk}(x_i + \delta_{ijk}) + {}^{3}L^{l}_{ijk}(x_h + \delta_{ijk})\} \quad \text{(V.4)}$$

where $\delta_{ijk} = (1 - x_i - x_j - x_k)/3$

where L^{l}_{ij}, L^{l}_{ijk}, and L^{l}_{ijkh} are binary, ternary and quaternary interaction parameters between i and j atoms and among i, j, k and i, j, k, h atoms respectively (where i=Fe, j= Co, k=Cu and h=Si). The number of components in the system is denoted by c. The interaction parameters for the Redlich-Kister formalism can be composition or temperature dependent (Redlich and Kster 1948):

$${}^{n}L_{ij}, {}^{n}L_{ijk} = {}^{n}A + {}^{n}B\cdot T + {}^{n}C\cdot T\ln T \quad \text{(V.5)}$$

The parameters for the binary terms have been evaluated (Hino *et al*. 1999; Ohtani *et al*. 1997; Palumbo *et al*. 2006; Wang *et al*. 2002) and can readily be used. However the ternary interaction parameters for Fe-Co-Si and Co-Cu-Si are not available as well as the quaternary interaction parameter. These parameters can be set to zero or, if the experimental data is available an optimisation procedure can be carried to generate the interaction parameters.

It is noted that when $c = 3$ the term $\delta_{ijk} = 0$ and in a quaternary the same term $\delta_{ijk} \neq 0$. If the solution exhibits a regular solution behaviour the ternary interaction parameters are assumed equivalent (Janz and Schmid-Fetzer 2005), that is, ${}^0L^l_{ijk} = {}^1L^l_{ijk} = {}^2L^l_{ijk} = L^l_{ijk}$.

Then the expansions of equations V.1 to V.4 lead to the following expression, equation V.5

$$\begin{aligned}
{}^E G^l_{mix} &= x_{Fe}x_{Cu}[{}^0L^l_{Fe,Cu} + {}^1L^l_{Fe,Cu}(x_{Fe} - x_{Cu})^1 + {}^2L^l_{Fe,Cu}(x_{Fe} - x_{Cu})^2] \\
&+ x_{Co}x_{Fe}[{}^0L^l_{Co,Fe} + {}^1L^l_{Co,Fe}(x_{Co} - x_{Fe})^1 + {}^2L^l_{Co,Fe}(x_{Co} - x_{Fe})^2] \\
&+ x_{Cu}x_{Co}[{}^0L^l_{Cu,Co} + {}^1L^l_{Cu,Co}(x_{Cu} - x_{Co})^1 + {}^2L^l_{Cu,Co}(x_{Cu} - x_{Fe})^2] \\
&+ x_{Fe}x_{Si}[{}^0L^l_{Fe,Si} + {}^1L^l_{Fe,Si}(x_{Fe} - x_{Si})^1 + {}^2L^l_{Fe,Si}(x_{Fe} - x_{Si})^2] \\
&+ x_{Co}x_{Si}[{}^0L^l_{Co,Si} + {}^1L^l_{Co,Si}(x_{Co} - x_{Si})^1 + {}^2L^l_{Co,Si}(x_{Co} - x_{Si})^2] \\
&+ x_{Cu}x_{Si}[{}^0L^l_{Cu,Si} + {}^1L^l_{Cu,Si}(x_{Cu} - x_{Si})^1 + {}^2L^l_{Cu,Si}(x_{Cu} - x_{Si})^2] \\
&+ x_{Fe}x_{Co}x_{Cu} \cdot L^l_{Fe,CoCu} + x_{Fe}x_{Co}x_{Si} \cdot L^l_{Fe,CoSi} + x_{Fe}x_{Cu}x_{Si} \cdot L^l_{Fe,Cu,Si} \\
&+ x_{Co}x_{Cu}x_{Si} \cdot L^l_{Co,Cu,Si}
\end{aligned} \qquad \text{(V.6)}$$

The activity coefficient of silicon can be calculated from equation V.6 by differentiating with respect to silicon concentration, x_{Si}. The terms without x_{Si} in the equation will drop out leading to Equation V.7.

The interaction parameters L_{ij} for binary have been assessed except for the Co-Si system. The ternary interaction parameters for Fe-Co-Si and Co-Cu-Si systems are not available in literature. The missing interaction parameters can be generated by calculations, commonly referred to as optimisation if the experimental data were available for the phase diagrams as well as thermochemical quantities. This would require a critical analyses of the experimental data of the binary subsystem and extrapolated to the ternary and higher order systems.

$$\begin{aligned}
RT \ln \gamma_{Si} &= {}^0L_{Fe,Si}(x_{Fe}) + {}^1L_{Fe,Si}(x_{Fe}^2) - {}^1L_{Fe,Si}2(x_{Fe}x_{Si}) + {}^2L_{Fe,Si}(x_{Fe}^3) - {}^2L_{Fe,Si}4(x_{Fe}^2x_{Si}) \\
&+ {}^2L_{Fe,Si}3(x_{Fe}x_{Si}^2) + {}^0L_{Cu,Si}(x_{Cu}) + {}^1L_{Cu,Si}(x_{Cu}^2) - {}^1L_{Cu,Si}2(x_{Cu}x_{Si}) + {}^2L_{Cu,Si}(x_{Cu}^3) \\
&- {}^2L_{Cu,Si}4(x_{Cu}^2x_{Si}) + {}^2L_{Cu,Si}3(x_{Cu}x_{Si}^2) + {}^0L_{Co,Si}(x_{Co}) + {}^1L_{Co,Si}(x_{Co}^2) - {}^1L_{Co,Si}2(x_{Co}x_{Si}) \\
&+ {}^2L_{Co,Si}(x_{Co}^3) - {}^2L_{Co,Si}4(x_{Co}^2x_{Si}) + {}^2L_{Co,Si}3(x_{Co}x_{Si}^2) + L_{Fe,Co,Si}(x_{Fe}x_{Co}) \\
&+ L_{Fe,Cu,Si}(x_{Fe}x_{Cu}) + L_{Co,Cu,Si}(x_{Co}x_{Cu})
\end{aligned} \qquad \text{(V.7)}$$

On the other hand Chuang *et al.* (Chuang *et al*. 1984) expressed the excess Gibbs energy in form that can readily be applied and in conformity with the Margules-type of equation when a forth power term in composition is included. Equations V.8 and V.9 show the formula for the partial excess free energy and the activity coefficient respectively.

$$\frac{{}^{E}G^{l}}{RT} = RT\,\tfrac{1}{2}\sum_{j=1}^{n}\sum_{i=1}^{n}[w_{ij}^{l} + (w_{ij}^{l} - w_{ji}^{l})x_j - 4v_{ij}^{l}x_i x_j]x_i x_j \qquad \text{(V.8)}$$

and

$$\ln\gamma_p^{l} = \sum[(w_{ip}^{l} + w_{pi}^{l})/2 + (w_{ip}^{l} - w_{pi}^{l})(x_p - x_i/2) - 8v_{ij}^{l}x_i x_j]x_i$$

$$-\sum_{j=1}^{n}\sum_{i=1}^{n}[w_{ij}^{l}/2 + (w_{ij}^{l} - w_{ji}^{l})x_j - 6v_{ij}^{l}x_i x_j]x_i x_j \qquad \text{(V.9)}$$

When $v_{ij} = v_{ji} = 0$, $w_{ij} \neq w_{ji}$, Equation V.8 reduces to that for a subregular solution. When $v_{ij} = v_{ji} = 0$, and $w_{ij} = w_{ji}$ the same equation reduces further to a regular solution model as

$$\frac{{}^{E}G^{l}}{RT} = \tfrac{1}{2}\sum_{j=1}^{n}\sum_{i=1}^{n}w_{ij}^{l}\cdot x_i x_j \qquad \text{(V.10)}$$

and

$$\ln\gamma_p^{l} = \sum(w_{ip}^{l})x_i - \sum_{j=1}^{n}\sum_{i=1}^{n}(w_{ij}^{l}/2)\cdot x_i x_j \qquad \text{(V.11)}$$

The parameters w_{ij} and w_{ji} are linear and are expressed as a function of $1/T$ as

$$w_{ij}^{l} = A + B/T \qquad \text{(V.12)}$$

$$w_{ji}^{l} = C + D/T \qquad \text{(V.13)}$$

and

$$v_{ij} = v_{ji} = E + F/T \qquad \text{(V.14)}$$

As mentioned earlier the solution models must be used to estimate the parameters by an optimisation procedure of the experimental data.

V.1 Regression of experimental data – activity coefficient of silicon in Fe-Co-Cu-Si

The experimental data in Table 4.14 is used in the building the regression model. A forward stepwise method is opted for at statistical significance value (p) set at 0.05 (5%) and confidence limit at ±95%.

A typical statistical approach is used to model the experimental results. This arises from the fact that the proposed solution models yield poor descriptions of the data. The poor description is due to the limited data sets for a system with four components. By using a Pareto chart to test the significance of the regressors (component concentration) on the dependent variable ($RT \ln \gamma_{Si}$) the following model was regressed to fit the data.

Table 1 Parameter Estimates Sigma-restricted parameterization

Parameter Estimates (Spreadsheet2 in Workbook - New Activity table) Sigma-restricted parameterization					
Regressor	**Comment**	***RT* ln γ_{Si} Parameter**	***RT* ln γ_{Si} Std Err.**	**-95.00% Confid. Limit**	**+95.00% Confid. Limit**
X_{Fe}^2		-1.308975E+07	2.550413E+06	-2.017083E+07	-6.008671E+06
X_{Co}^2		-6.912752E+08	6.087709E+07	-8.602971E+08	-5.222533E+08
X_{Cu}^2		2.615551E+09	2.858545E+08	1.821891E+09	3.409210E+09
X_{Si}^2		-5.472349E+08	4.405836E+07	-6.695606E+08	-4.249093E+08
$X_{Fe}*X_{Co}$		2.134385E+09	3.128550E+08	1.265761E+09	3.003010E+09
$X_{Co}*X_{Cu}$		2.749263E+07	6.443123E+07	-1.513971E+08	2.063824E+08
$X_{Fe}*X_{Cu}$		-3.192445E+09	3.495216E+08	-4.162872E+09	-2.222017E+09
$X_{Fe}*X_{Si}$		2.437413E+09	2.049467E+08	1.868390E+09	3.006437E+09
$X_{Co}*X_{Si}$		-5.827603E+09	6.673760E+08	-7.680536E+09	-3.974670E+09
$X_{Cu}*X_{Si}$		1.479526E+09	2.545197E+08	7.728656E+08	2.186185E+09
$X_{Co}*X_{Fe}^2$		-2.280805E+09	3.170809E+08	-3.161162E+09	-1.400447E+09
$X_{Cu}*X_{Fe}^2$		3.562968E+09	3.868507E+08	2.488898E+09	4.637037E+09
$X_{Si}*X_{Fe}^2$		-2.422664E+09	1.995962E+08	-2.976832E+09	-1.868496E+09
$X_{Fe}*X_{Co}^2$		-5.942921E+08	2.684269E+08	-1.339565E+09	1.509804E+08
$X_{Si}*X_{Co}^2$		1.134130E+10	1.278732E+09	7.790968E+09	1.489163E+10
$X_{Cu}*X_{Cu}^2$		-3.083561E+09	3.210786E+08	-3.975019E+09	-2.192104E+09
$X_{Si}*X_{Cu}^2$		-2.982476E+09	5.144530E+08	-4.410827E+09	-1.554126E+09
$X_{Fe}*X_{Si}^2$	Pooled				
$X_{Cu}*X_{Si}^2$	Pooled				

Table 2 Test of Whole Model, Adjusted for the Mean

	Multiple	Adjusted	SS	MS	SS	MS	F	p
$RT \ln \gamma_{Si}$	0.994778	0.973891	1.242241E+10	730729933	65207782	16301946	44.82471	0.001073

Design Effects:
Continuous effects:
"XFe2"
"XCo2"
"XCu2"
"XSi2"
"XFe"*"XCo"
"XCo"*"XCu"
"XFe"*"XCu"
"XFe"*"XSi"
"XCo"*"XSi"
"XCu"*"XSi"
"XCo"*"XFe2"
"XCu"*"XFe2"
"XSi"*"XFe2"
"XFe"*"XCo2"
"XSi"*"XCo2"
"XCu"*"XCu2"
"XSi"*"XCu2"
"XFe"*"XSi2"
"XCu"*"XSi2"

Model specifications:
General Regression Model;
DEPENDENT = "RT ln gSi";
COVARIATE = "XFe" "XCo" "XCu" "XSi" "XFe2" "XCo2
" "XCu2" "XSi2";
DESIGN = "XFe2" + "XCo2" + "XCu2" + "XSi2" + "
XFe"*"XCo" + "XCo"*"XCu" + "XFe"*"XCu" + "XFe"*"
XSi" + "XCo"*"XSi" + "XCu"*"XSi" + "XCo"*"XFe2"
+ "XCu"*"XFe2" + "XSi"*"XFe2" + "XFe"*"XCo2" + "
XSi"*"XCo2" + "XCu"*"XCu2" + "XSi"*"XCu2" + "
XFe"*"XSi2" + "XCu"*"XSi2";

Prediction equation for: "RT ln gSi"
"RT ln gSi"=-13089751.*"XFe2"-6912752E2*"XCo2"+26155507E2
"XCu2"-5472349E2"XSi2"+21343854E2*"XFe"*"XCo"+
27492628.2*"XCo"*"XCu"-3192444E3*"XFe"*"XCu"+24374135E2
"XFe""XSi"-5827603E3*"XCo"*"XSi"+14795255E2*
"XCu"*"XSi"-2280805E3*"XCo"*"XFe2"+35629676E2*"XCu"*"XFe2"
-2422663E3*"XSi"*"XFe2"-5942920E2*"XFe"*"XCo2"+11341299E3
"XSi""XCo2"-3083562E3*"XCu"*"XCu2"-2982476E3*"XSi"*"XCu2"

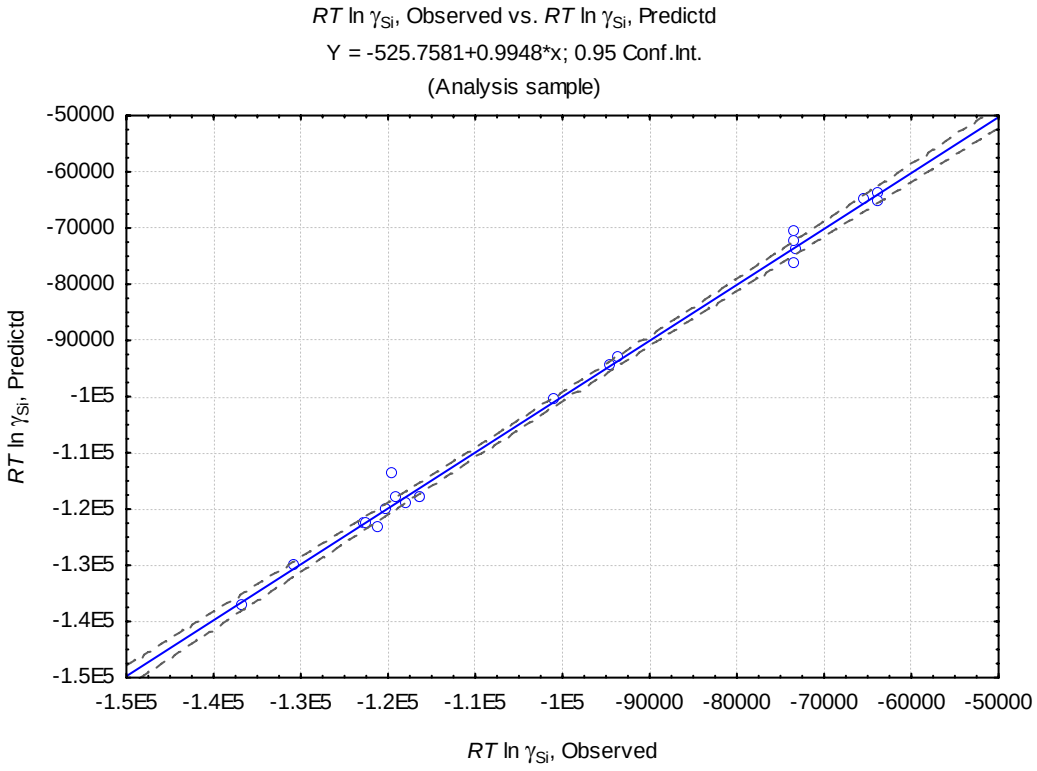

Figure 1 Predicted versus calculated $RT \ln \gamma_{Si}$

Table V.1 Summary of results of activity determination in the Fe-Co-Cu-Si system

1.0Determination of Activity of Si in alloy: Equilibrium determination

Expt#	Specimen	log pO^2	Temperature	Time, hrs	Remarks
2	C	1.00E-12	1450	16	Equilibrium reached
2	Co-Cu	1.00E-12		16	
2	FeCu	1.00E-12		16	
5	C	1.00E-12	1450	8	Equilibrium reached
5	CoCu	1.00E-12		8	
5	FeCu	1.00E-12		8	
1	C	1.00E-12	1450	24	Equilibrium reached, repeat of expt#2 specimen C
1	C+4.5wt%Si	1.00E-12		24	
1	C+1.5wt%Si	1.00E-12		24	Reverse of Expt# 1specimen C
4	C	10e-14.1	1450	16	Equilibrium reached
4	CoCu	10e-14.1		16	
4	FeCu	10e-14.1		16	

2.0 Experiments

Expt#	Specimen	log pO^2	Temperature	Time, hrs	Remarks
6	T-powder				not successful
7	T-powder				not successful
8	C	1.00E-14	1450	8	
9	C	1.00E-12	1450	14	Rpeat on C
9	E	1.00E-12	1450	14	
9	C+2.5wt%Si	1.00E-12	1450	14	Reverse of expt 4 Specimen C
10	C	1.00E-13	1453 (1450)	8	Rpeat on C
10	B1	1.00E-13	1453 (1450)	8	
11	B2	1.00E-12	1453 (1450)	14	
11	D1	1.00E-12	1453 (1450)	14	
12	A	10e-14.1	1470 (1461)	8	Temperature after experiment drops
13	A	1.00E-14	1470 (1461)	8	Temperature dropped on remeasuring after expts gas composition as determined for 1450 equilib. Initially Tsv = 1402 (Texpt = 1420) for 8hrs, corrected and expt continued at (1460) 1422+28 for 14hrs
13	C	1.00E-14	1470 (1461)	8	
14	A	1.00E-14	1495 (1486)	8	
15	FeCo	1.00E-14	1500	14	SiO2 crucible fusing with furnace tube. Problem resolved by working with Si-containing alloys at lower liquidus temps (in expts 16 to 20)

3.0 Temperature effect on Activity Coefficient of Si in alloy

Expt#	Specimen	log pO2	Temperature	Time, hrs	Remarks
16	C#5.1	10e-14.1	1500	8	CO2/H2 composition kept constant at 0.35%CO2-H2 wich equlibrates at 1450. In expts 17 carbon deposition was observed, this was the case for expts 19 and 20 (even if it may be difficult to quantify)
17	C#5.2	10e-14.1	1475 (1470)	8	
18	C#5.3	10e-14.1	1450 (1451)	8	
19	C#5.4	10e-14.1	1425 (1422)	8	
20	C#5.5	10e-14.1	1400 ()	8	

4.0 Notes

Temperature for the experiments was measured at gas compositions/mixtures for the experiments taking into account the difference between the set point and the actual measurement of the hot zone.

APPENDIX VI: ELEMENT DISTRIBUTION ACROSS PHASES IN THE FE-CO-CU SYSTEM CALCULATED WITH MTDATA

A001-Cu (Fe-10Co-10Cu)

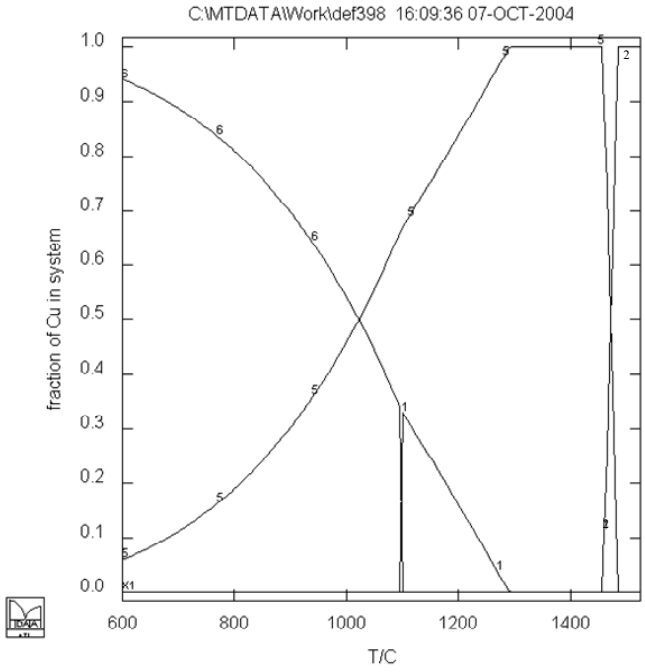

1- Liquid (Cu rich)
2- Liquid
5- FCC (Fe rich)
6- FCC (Cu rich)

A001-Co (Fe-10Co-10Cu)

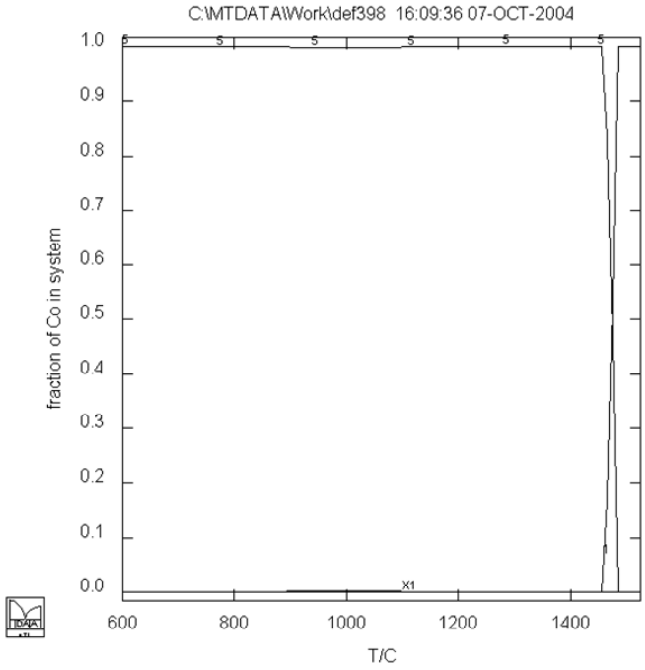

1- Liquid
5- FCC (Fe rich)
X1- FCC, Liquid (Cu rich)

A001-Fe (Fe-10Co-10Cu)

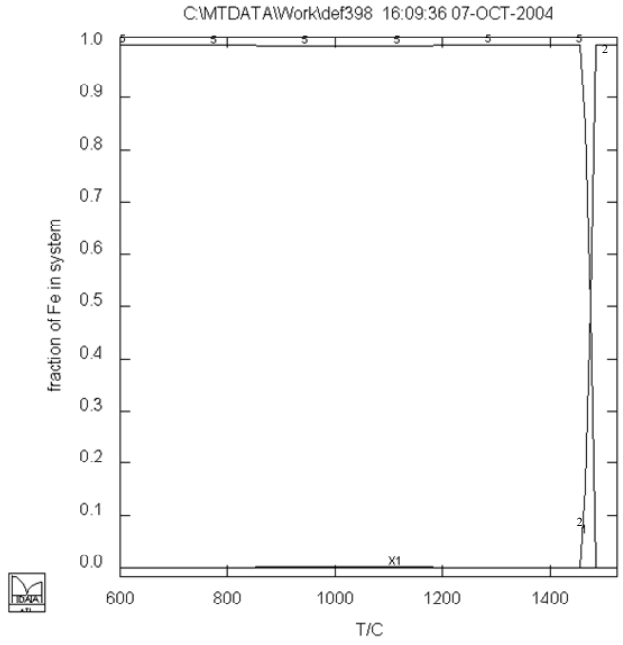

X1- FCC, Liquid (Cu rich)
2- Liquid
5- FCC (Fe rich)

C001-Fe (Fe-20Co-20Cu)

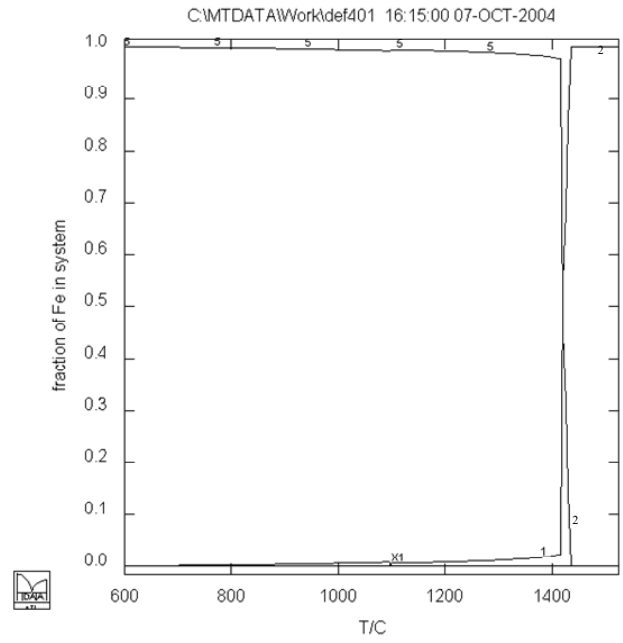

X1- FCC, Liquid (Cu rich)
2- Liquid
5- FCC (Fe rich)

D001-Cu (Fe-25Co-20Cu)

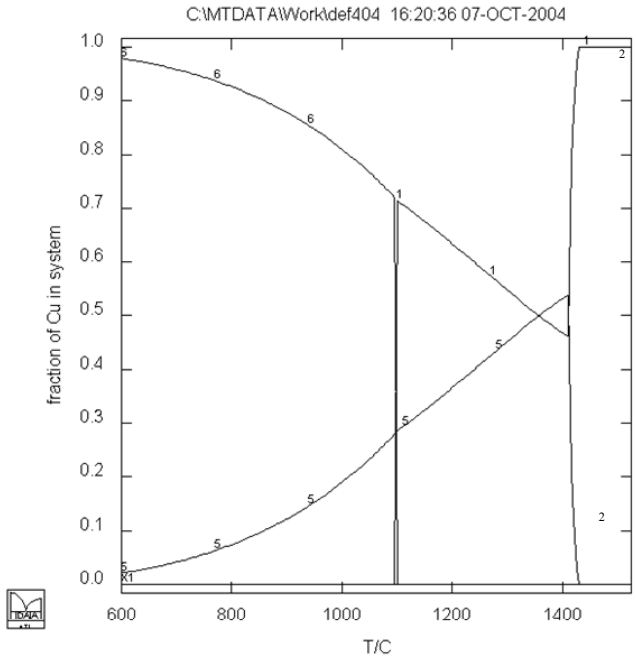

1- Liquid (Cu rich)
2- Liquid
5- FCC (Fe rich)
6- FCC (Cu rich)

D001-Co (Fe-25Co-20Cu)

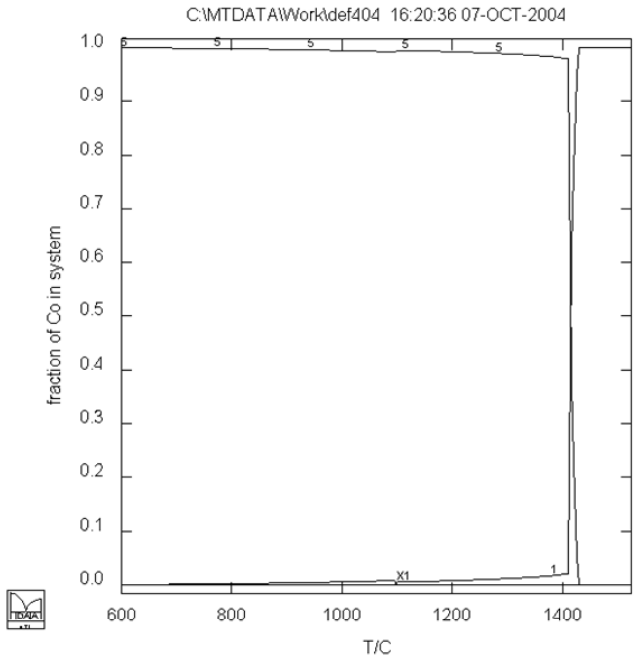

1- Liquid
5- FCC (Fe rich)
X1- FCC, Liquid (Cu rich)

D001-Fe (Fe-25Co-20Cu)

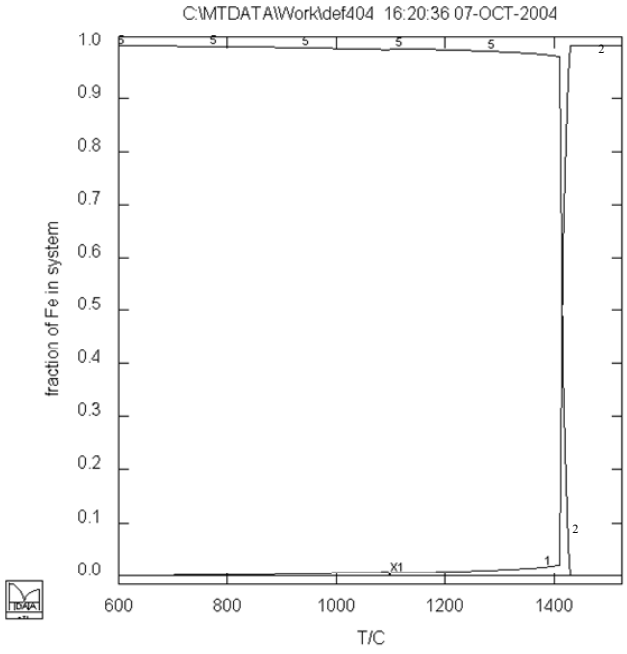

X1- FCC, Liquid (Cu rich)
2- Liquid
5- FCC (Fe rich)

E001-Fe (Fe-30Co-20Cu)

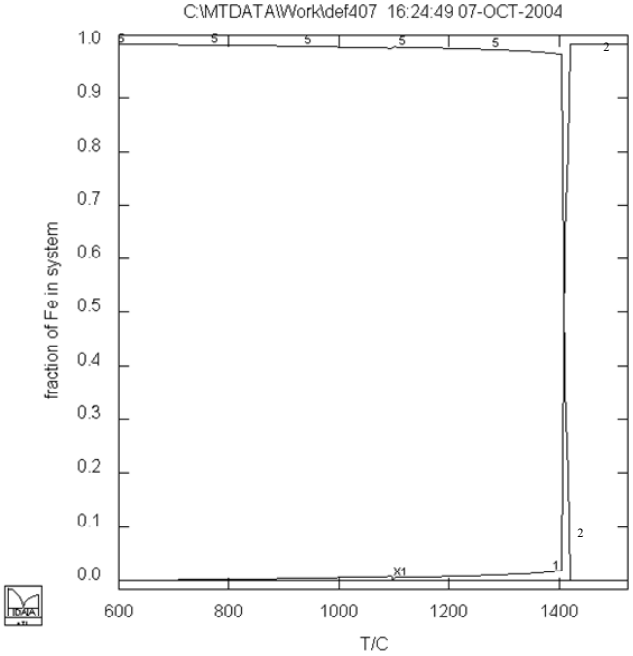

X1- FCC, Liquid (Cu rich)
2- Liquid
5- FCC (Fe rich)

E001-Cu (Fe-30Co-20Cu)

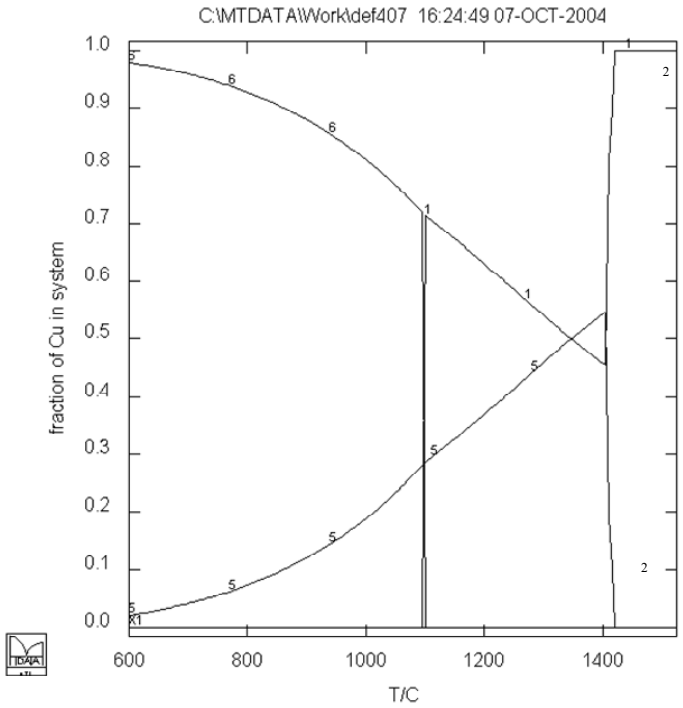

1- Liquid (Cu rich)
2- Liquid
5- FCC (Fe rich)
6- FCC (Cu rich)

E001-Co (Fe-30Co-20Cu)

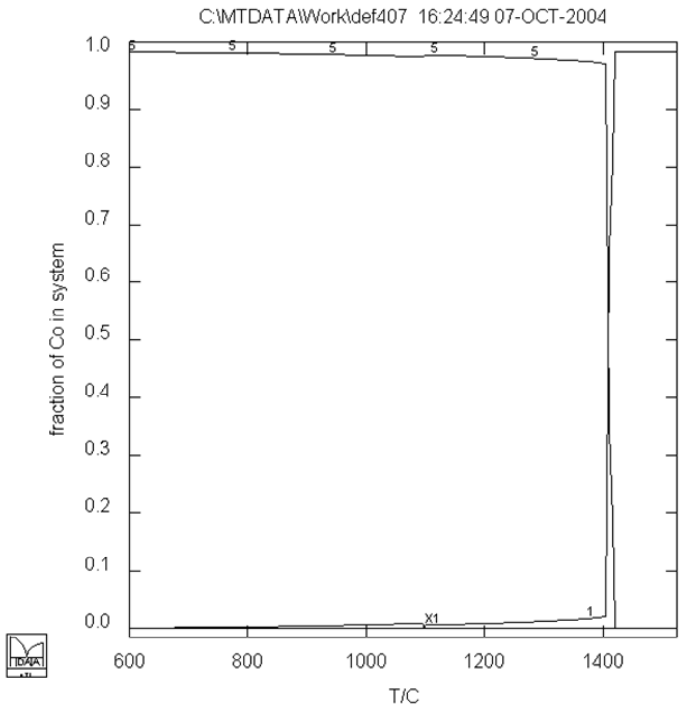

1- Liquid
5- FCC (Fe rich)
X1- FCC, Liquid (Cu rich)

T001-Cu (Fe-20Co-38Cu)

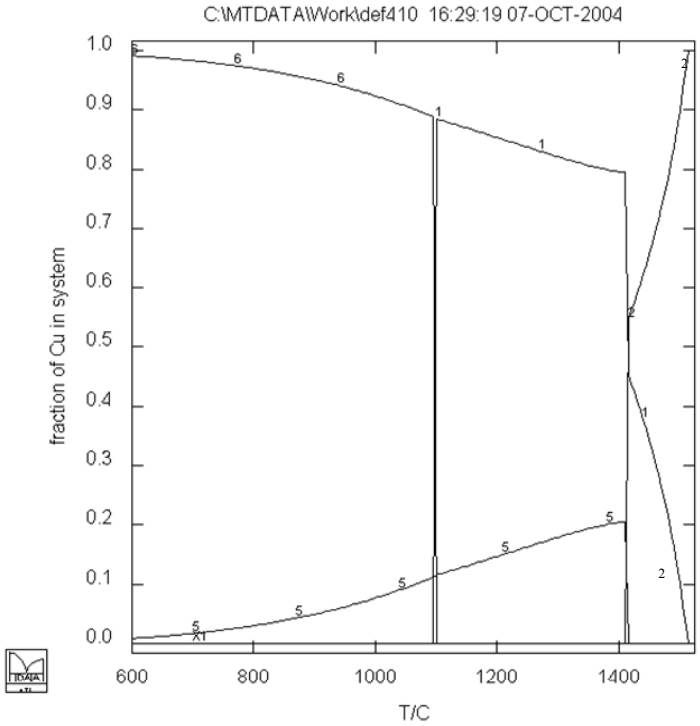

1- Liquid (Cu rich)
2- Liquid
5- FCC (Fe rich)
6- FCC (Cu rich)

T001-Co (Fe-20Co-38Cu)

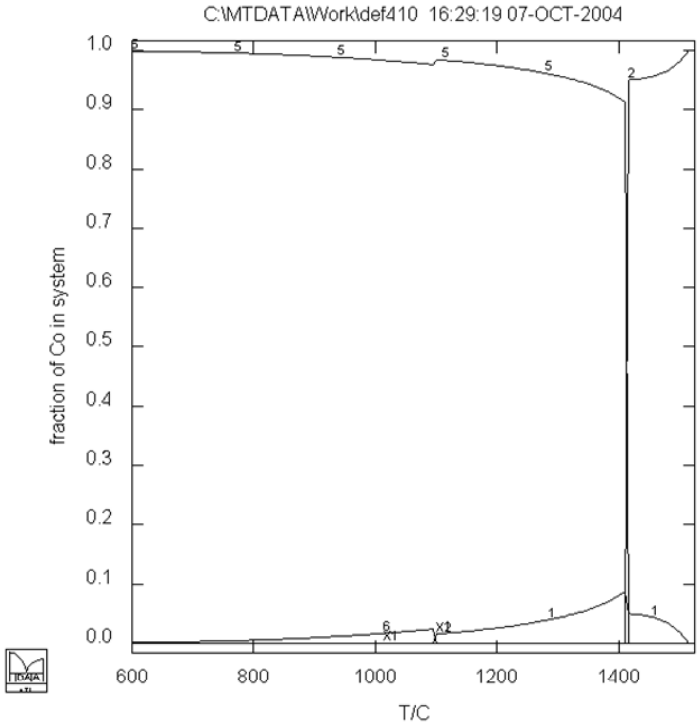

1- Liquid
5- FCC (Fe rich)
X1- FCC, Liquid (Cu rich)

T001-Fe (Fe-20Co-38Cu)

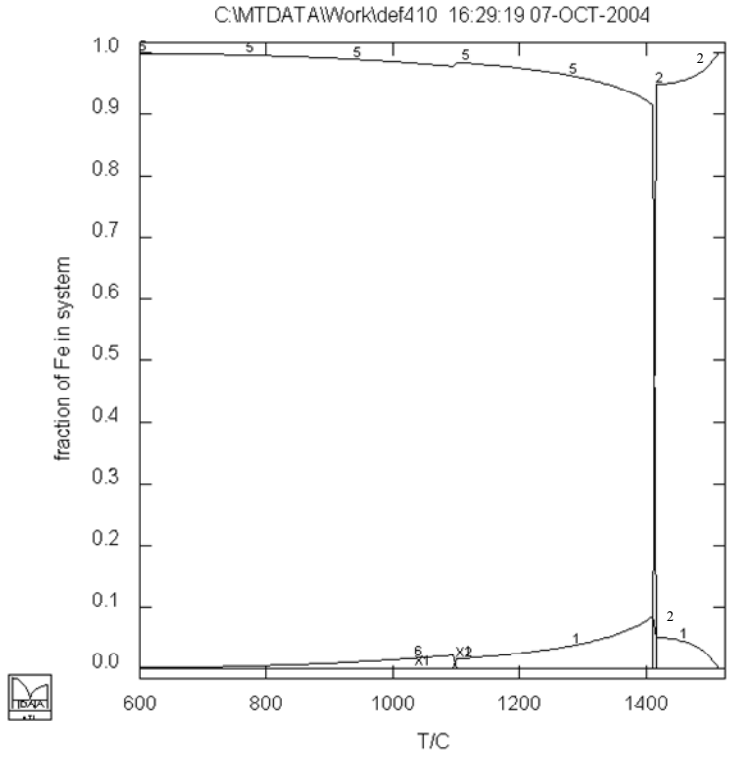

1- Liquid (Cu rich)
2- Liquid (Fe rich)
5- FCC (Fe rich)
6- FCC (Cu rich)

APPENDIX VII: CALCULATION OF PHASE PROPORTIONS IN THE FE-CO-CU-SI SYSTEM

Two phases; liquid and Solid

$$\%\text{solid}\ (\alpha) = \frac{\alpha X}{\alpha L} \times 100 \qquad \text{(VII.1)}$$

$$\%\text{liquid}\ (L) = \frac{LX}{\alpha L} \times 100 \qquad \text{(VII.2)}$$

where X is the composition of the alloy, αL is the distance of the tie lines joining the liquid and solid phases, αX and LX are the distances of the lines between the the alloy compsition and the phases.

Three Phases; liquid and two solids

The centre of gravity principle entails the construction of a tie triangle using the compositions of the three phases. An illustration of the tie triangle is shown in Figure VII-1.

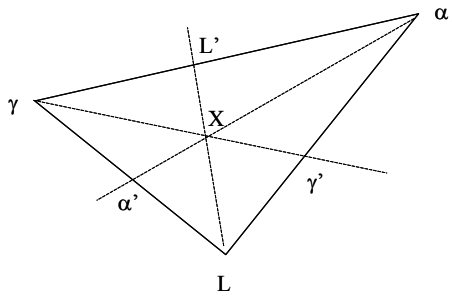

Figure VII-1 The tie triangle illustrating the centre of gravity principle.

The intersection points α', γ', and L', are calculated by solving intersecting lines in Figure VII-1 with the Matlab function:

```
function [x,y]=linesintersect(a,b,c,d)
% find intersection of two straight lines given two points on each of the
% lines [(x1,y1),(x2,y2)] and [(x3,y3),(x4,y4)]
% -----------
% OUTPUT
% -----------
% (x,y) - intersection point

dy1=b(2)-a(2); % a1 = y2 - y1;
dx1=a(1)-b(1); % b1 = x1 - x2;
c1=b(1)*a(2) - a(1)*b(2); %c1 = x2*y1 - x1*y2; %% a1*x + b1*y +c1 = 0 is line
1

dy2=d(2)-c(2); %a2 = y4 - y3;
dx2=c(1)-d(1); %b2 = x3 - x4;
c2=d(1)*c(2) - c(1)*d(2); %c2 = x4*y3 - x3*y4;% a2*x + b2*y +c2 = 0 is line 1
```

```
denom=dy1*dx2 - dy2*dx1; %denom = a1*b2 - a2*b1;
if denom == 0,
    error('parallel lines')
else
    x = (dx1*c2 - dx2*c1)/denom; % x = (b1*c2 - b2*c1)/denom;
    y = (dy2*c1 - dy1*c2)/denom; % y = (a2*c1 - a1*c2)/denom;
end
```

The points of intersection and the, the compositions of the phases are used to calculate the phase proportions from the following expressions.

$$\%\alpha = \frac{X\alpha'}{\alpha\alpha'} \times 100 \qquad \text{(VII.3)}$$

$$\%\gamma = \frac{X\gamma'}{\gamma\gamma'} \times 100 \qquad \text{(VII.4)}$$

$$\%L = \frac{XL'}{LL'} \times 100 \qquad \text{(VII.5)}$$

where X is the composition of the alloy.

GLOSSARY

Congruent Phase Transformations	a transformation in which the phase composition does not change as in allotropic transformation of α-Fe to γ-Fe or the melting or solidification of a pure compound.
Equilibrium Phase	a phase which minimizes a system's free energy for a specified combination of temperature, pressure, and composition – therefore, by definition, a phase diagram contains **only** equilibrium phases.
Free Energy	a thermodynamic quantity which represents the internal energy of a system, in addition to the randomness or disorder of its atoms and/or molecules (a.k.a. entropy).
Intermediate Compounds (Or Stoichiometric Compounds)	a compound that has a distinct chemical formula, and therefore, is represented by a vertical line on a binary phase diagram.
Intermediate Solid Solutions (or Intermediate Phases)	in addition to the two solid solutions at either side of a phase diagram, it is possible to have single-phase regions located fully within the diagram's interior.
Liquid Solution	phases are denoted as L
Liquidus Line	the line separating the liquid (L) region from the two-phase α+L region. The liquid phase is present for all temperatures and compositions above this line.
Metastable (or Non-Equilibrium) Phase	a phase that can be produced by a very rapid change in system conditions (i.e. temperature or pressure) – in some cases, the metastable state may persist indefinitely, as the movement towards equilibrium is virtually imperceptible over long periods of time – metastable phases can be extremely important in the processing of materials, e.g. Quenching of austenitic steel to produce martensite.
Microstructure	the ***micro***scopic ***structure*** of an alloy (i.e. spatial arrangement of phases), as viewed using an optical or electron microscope – of note, the term microstructure refers to features on the scale of micrometers, **not** those at the atomic level.
Peritectic Reaction	an invariant point – this reaction refers to the formation of one solid phase upon cooling from a solid plus a liquid phase.
Phase	a homogeneous portion of a system that has uniform physical and chemical characteristics – i.e. every pure metal

	is a phase, as is any particular solid solution.
Phase Amounts	this refers to the relative amounts (or percentages) of equilibrium phases that are present at a given temperature and composition If the temperature-composition point is in a single phase region, that phase comprises 100% of the structure.
Phase Composition	this refers to the composition of each equilibrium phase present at a given temperature and composition if the temperature-composition point is in a single phase region, the corresponding composition is simply read from the x-axis.
Phases Present	any temperature-composition point on the phase diagram indicates the **equilibrium** phase(s) within the material for those conditions.
Solid Solution	A mixture of two (or more) types of atoms in which the solute atoms occupy either *substitutional* or *interstitial* positions within the solvent lattice and the crystal structure of the solvent is maintained. phases are designated by lower-case Greek letters, for example, α, β, γ, δ.
Solidus Line	separates the α region from the α+L region – i.e. only solid phases are present below this line.
Solubility Limit	The maximum concentration of solute atoms that can dissolve in a solvent to form a single phase – ie. if this limit is exceeded, another solid solution or compound of different composition will form
System	A series of possible metal mixtures (called alloys) consisting of the same components, but without regard to alloy composition.

REFERENCES

Ansara, I. and Jansson, Å. *Trita-Mac-0533,* KTH, Stockholm, 1993.

Balitchev, E., Jantzen, T., Hurtado, I., and Neuschutz, D. "Thermodynamic Assessment of The Quaternary System Al-Fe-Mn-Si in the Al-Rich Corner." *Computer and Coupling of Phase Diagrams and Thermochemistry*, vol. 27, 2003, pp. 275-278.

Bamberger, M., Kaufman, L., Abbaschian, R., and Munitz, A. "Evaluation of the Stable and Metastable Cu-Co-Fe Phase Diagram." *CALPHAD*, vol. 26, no.3, 2002, pp. 375-384.

Banda W, Morgan N, and Eksteen J J, "Role of Slag Modifiers on the Selective Recovery of Cobalt and Copper from Waste Smelter Slags", *Minerals Engineering*, vol. 15, no.11 (supplement), 2002, pp. 889-907.

Banda W., Beukes N.T., and Eksteen J.J. "Factors Influencing Base Metal Recovery from Waste Reverbaratory Furnace Slags in A 50 kVA Laboratory DC Plasma Arc Furnace." *Journal of the South African Institute of Mining and Metallurgy,* vol. 104, no.3, 2004. pp. 201-207.

Bratberg, J. and Frisk, K. "An Experimental and Theoretical Analysis of the Phase Equilibria in the Fe-Cr-V-C System." *Metallurgical and Materials Transactions A*, vol. 35A December, no.04, 2004, pp. 3649-3663.

Cao, C. D., Gorler, G. P., Herlach, D. M., and Wei, B. "Liquid-Liquid Phase Separation in the Undercooled Co-Cu Alloys." *Materials Science and Engineering*, vol. A325, 2002, pp. 503-510.

Chang Y Austin, Shuaglin Chen Fan Zhang, Xiyan Yan Fanyou Xie, Rainer Schmid-Fetzer, and W.Alan Oats "Phase Diagram Calculation: Past, Present and Future." *Progress in Materials Science*, vol. 49, 2004, pp. 313-335.

Chen, Q. and Jin, Z. "The Fe-Cu System: A Thermodynamic Evaluation." *Metallurgical and Materials Transactions A*, vol. 26A, 2005, pp. 417-426.

Choi, S.-D. "Thermodynamic Analysis of Co-Si System." *CALPHAD*, vol. 16, no.2, 1992, pp. 151-159.

Chuang, Y., Schmid, R., and Chang, Y. A. "Thermodynamic analysis of the Iron-Copper System I: The Stable and Metastable Phase Equilibria." *Metallurgical and Materials Transaction A*, vol. 15, 1984, pp. 1921-1930.

Curr, T. R., Barcza, N. A., Maske, K. U., and Mooney, J. F., "The design and Operation of Transferred-arc Plasma Systems for Pyrometallurgical Applications", ISPC 6th edn, Montreal, 1983, pp. 175-180.

Deines, P., Nafziger, R., Ulmer, G. C., & Woerman, E. 1974, *Temperature-Oxygen fugacity tables for selected gas mixtures in the system C-H-O at 1atm total pressure*, Bulletin of the Earth and Mineral Sciences Experiment Station, The Pennsylvania State University, University Park, Pennsylvania.

Dippenaar R. and Reid M. *Pers. Comm*. 2004.

Dippenaar, R. J. and Phelan, D. J. "Delta-Ferrite Recovery Structures from Low-Carbon Steels." *Metallurgical and Materials Transactions*, vol. 34B, 2003, pp. 495-501.

Exner, H. E. and Petzow, G. 2004, "Peritectic Structures," in *ASM Handbook*, ASM, pp. 675-680

Grimsey, E. J. and Toguri, J. M. "Cobalt in Silica Saturated Fayalite Slags." *Canadian Metallurgical Quarterly*, vol. 27, no.4, 1988, pp. 331-333.

Gronostajski, J. "Partial Equilibrium Diagram in the Co-Cu-Si System." *Rudy I Metale Niezelazne*, vol. 13, 1968, pp. 164-167.

Guillermet Fernandez, A., "High Temperature High Pressure", pp. 477-499.

Hansen, M. and Anderko, K. 1958, *Constitution of Binary Alloys* McGraw-Hill Book Company.

Hanson, D. and West, E. G. *J. Inst. Met.*, vol. 54, 1934, p. 229.

Haschimoto, U. *J. Inst. Met.*, vol. 1, 1937, pp. 135-143.

Hasebe, M. and Nishizawa, T. "Calculation of Phase Diagram of the Iron-Copper and Cobalt-Copper Systems." *CALPHAD*, vol. 4, no.2, 1980, pp. 83-100.

Haworth, C. W. and Hume-Rothery, W. "The Constitution of Molybdenum-Rhodium and Molybdenum-Palladium Alloys." *Journal of the Institute Metals*, vol. 87, 1958-59, pp. 265-272.

Hino, M., Nagasaka T, and Washizu T "Phase Diagram of Fe-Cu-Si Ternary System above 1523 K", *Journal of Phase Equilibria*, vol. 20, no.3, 1999, pp. 179-186.

Hume-Rothery, W., Christian, J. W., & Pearson, W. B. 1952, "General Principles and Choice of Method," in *Metallurgical Equilibrium Diagrams*, The Institute of Physics, London, pp. 165-174.

Imriš I "Cobalt Distribution in Rokana Smelter", *Transactions C: Mineral Processing and Extractive Metallurgy IMM*, vol. 91, 1982, pp. C153-C161.

Jantzen, T. and Lukas, H. L. Cu-Si. (unpublished data) 2000.

Janz, A. and Schmid-Fetzer "Impact of Ternary Parameters." *Computer and Coupling of Phase Diagrams and Thermochemistry*, vol. 29, 2005, pp. 37-39.

Jones, R. T., Denton, G. M., Reynolds, Q. G., Parker, J. A. L., and van Tonder, G. J. J. "Recovery of Cobalt from Slag in a DC arc Furnace at Chambishi, Zambia." *The Journal of the Institute of Mining and Metallurgy*, vol. 102, no.5, 2001, pp. 5-9.

Kattner, U. R. "The Thermodynamic Modelling of Multicomponent Phase Equilibria." *JOM*, vol. 49, no.12, 1997, pp. 14-19.

Kaufman, L. and Bernstein, H. 1970, *Computer Calculation of Phase Diagrams with SpecialReference to Refractory Metals,* Academic press,

Kaye, M. H., Jaansalu, K. M., and Thompson, W. T. "Phase Equilibrium in Metallic Systems", *Canadian Metallurgical Quarterly*, vol. 42, no.4, 2003, pp. 393-410.

Kim, D. I. and Abbaschian, R. "The Metastable Liquid Miscibility Gap in Cu-Co-Fe Alloys." *Journal of Phase Equilibria*, vol. 21, no.1, 2000, pp. 25-31.

Kongoli, F., Grimsey, E., and Pelton, A. D., "Model Predictions of the Liquidus Surface of Multi-component iron Silicate Smelting Slags Containing Magnesia and Calcia", Proc EPD Congress 98 Editor Mishra B., TMS-AIME, Warrendale, PA, 1998, pp. 821-845.

Kongoli, F. and Pelton, A. D. "Model Prediction of the Thermodynamic Properties of Co-Fe-Ni-S mattes." *Metallurgical and Materials Transactions B*, vol. 30B, 1999, pp. 443-450.

Kubaschweski, O. "Iron-Silicon", *Iron-Binary Phase Diagrams,* 1982, pp. 136-139.

Kubaschweski, O. and Alcock, C. B. 1979, *Metallurgical Thermochemistry*, 5th edn.

Kubišta, J. and Vrešťál, J. "Thermodynamics of Liquid Co-Cu System and Calculation of Phase Diagram." *Journal of Phase Equilibria*, vol. 21, no.2, 2000, pp. 125-129.

Kuo, C.-K., Lin, Z.-X., & Yan, D.-S. 1990, *High Temperature Phase Equilibria and Phase Diagrams* Pergamon Press.

Lacaze, J. and Sundman, B. "An Assessment of Fe-C-Si System." *Metallurgical and Materials Transactions A*, vol. 22A, 1991, pp. 2211-2223.

Lee, S. K. and Lee, D. N. "Calculation of Phase Diagrams using Partial Phase Diagram Data." *CALPHAD*, vol. 10, no.1, 1985, pp. 61-76.

Macchesney, J. B. & Rosenberg, P. E. 1970, "The Methods of Phase Equilibria Determination and their Associated Problems," in *Refractory Materials*, Editor Margrave L. John, Academic Press, New York and London, pp. 113-165.

Mackey, P. J. "The Physical Chemistry of Copper Smelting Slags - A Review." *Canadian Metallurgical Quarterly*, vol. 21, no.3, 1982, pp. 221-260.

Maddocks, W. R. and Clausen, G. E. "Part-III The Fe-Cu-Co System." *Iron and Steel Institute, London, First report of the Alloy Steels Research Committee* no.14, 1936, pp. 116-124.

Massalski, T. B. 2001, *Binary Alloy Phase Diagrams*, Editors: Okamoto, H, Subramanian, P. R., and Kacprzak, L. vol.2, 2nd-edn, William W. Scott, Jr. ASM Internation pp 1771.

Miettinen, J. "Thermodynamic description of the Cu-Fe-Si system at the Cu-Fe side." *Computer Coupling of Phase Diagrams and Thermochemistry*, vol. 27, 2003, pp. 389-394.

Mingjun, L., Xin, L., Guangshen, S., Gencang, Y., and Yaohe, Z. "Microstructure Evolution and Metastable Phase formation in the Undercooled Fe-30 at% Co", *Materials Science and Engineering*, vol. A268, 1999, pp. 90-96.

Munitz A and Abbaschian, R. "Microstructure of Cu-Co Alloys Solidified at Various Supercoolings." *Metallurgical and Materials Transactions A*, vol. 27A, 1996, pp. 4049-4057.

Nafziger, R. H., Ulmer, G. C., & Woerman, E. 1971, "Gaseous Buffering for the Control of Oxygen Fugacity at One Atmosphere," in *Research Techniques for High Pressure and High Temperature,* Editor Ulmer G. C., Springer-Verlag, New York.

Nelson, L. R., Sullivan, R., Jacobs, P., Munik, E., Lewarne, P., Roos, E., Uys, M. J. N., de Vries, M., McKenna, K., Voermann, N., and Wasmund, B. O. "Application of a High-Intensity Cooling System to DC-arc Furnace Production of Ferrocobalt at Chambishi." *The Journal of the Institute of Mining and Metallurgy*, vol. 104, no.9, 2004, pp. 551-561.

Nikolaenko, I. V. and Turchanin, M. A. "Enthalpies of Formation of Liquid Binary (Cu+Fe, Co, and Ni) Alloys." *Metallurgical and Materials Transactions B*, vol. 28B, December, 1997, pp. 1119-1129.

Nishizawa, T. and Ishida, K. "Co-Cu Phase Diagram." *Bulletin of Alloy Phase Diagrams*, vol. 5, 1984, pp. 161-165.

Ohtani, H., Suda, H., and Ishida, K. "Solid/Liquid Equilibria in Fe-Cu Based Ternary Systems", *ISIJ International*, vol. 37, 1997, pp. 207-216.

Okamoto, H. "Cu-Si (Copper-Silicon)", *Journal of Phase Equilibria*, vol. 23, no.3, 2002, pp. 281-282.

Olesinski, R. W. and Abbaschian, G. J. "The Cu-Si System." *Bulletin of Alloy Phase Diagrams*, vol. 7, no.2, 1986, pp. 170-178.

Palumbo, M., Curiotto, S., and Battezzati, L. "Thermodynamic Analysis of the Stable and Metastable Co-Cu and Co-Cu-Fe Phase Diagrams." *Computer and Coupling of Phase Diagrams and Thermochemistry*, vol. 30, 2006, pp. 171-178.

Phelan, D., Reid, M., and Dippenaar, R. 2005, "Experimental and Modelling Studies into High Temperature Phase Transformations", In Press .

Pirard E. "Quantitative Mineralogical Analysis of Co and Cu Distribution in Historical Slags from Küre (Turkey)." *CIM Bulletin*, vol. 84, no.9, 1991, pp. 87-91.

Raghavan, V. "Co-Cu-Fe (Cobalt-Copper-Iron)." *Journal of Phase Equilibria*, vol. 23, no.3, 2002a, pp. 253-256.

Raghavan, V. "Cu-Fe-Si (Copper-Iron-Silicon)." *Journal of Phase Equilibria*, vol. 23, no.3, 2002b, pp. 267-270.

Redlich, O. and Kister, T. "Algebraic Representation of Thermodynamic Properties and the Classification of Solutions." *Industrial and Engineering Chemistry*, vol. 40, no.2, 1948, pp. 345-348.

Revina, N. I., Nikolayev, A. K., and Rozenberg, V. M. "The Constitution Diagram of Copper-rich Cu-Co-Si Alloys." *Russian Metallurgy Translated from Izvestiya Akademi Nuak SSSR, Metally*, vol. 1, 1975, pp. 182-185.

Rogel, R. and Horstman, G. "Das Zustandsschaubild Einsen-Eisensilizi-Kupfersilizid-Kupfer", *Arch.für das Eisenhüttenwes*, vol. 24, 1953, pp. 435-440.

Rosenqvist, T. 1983, "Melts and Solutions," in *Principles of Extractive Metallurgy*, 2nd edn McGraw-Hill Book Company, pp. 66-100.

Schlesinger, M. E. and Xiang, Q. "Enthalpy of Mixing in Fe-C-Si Melts." *Journal of Alloys and Compounds* no.321, 2001, pp. 242-247.

Schwendt, G. 1997, "Thermal Analytical Methods," in *The Essential Guide to Analytical Chemistry*, John Wiley & Sons, pp. 73-76.

Stein, F., Sauthoff, G., and Palm, M. "Experimental Determination of Intermetallic Phases, Phase Equilibria, and Invariant Reaction Temperatures in the Fe-Zr System", *Journal of Phase Equilibria*, vol. 23, no.6, 2002, pp. 480-494.

Teague K C, Swinbourne D R, and Jahanshahi, S. "Activity Coefficient of Cobalt Oxide in Non-Ferrous Smelting Slags- A Review." *Proceedings Australian Institute of Mining and Metallurgy*, vol. 33, no.1, 1999, pp. 1-6.

Turchanin, M. A., Agraval, P. G., and Nikolaenko, I. V. "Thermodynamics of Alloys and Phase Equilibria in Copper-Iron System." *Journal of Phase Equilibria*, vol. 24, no.4, 2003, pp. 307-319.

Villars, P., Prince, A., and Okamoto, H. 1991, *Ternary Phase Diagram Handbook* ASM International.

Vogel, R. and Rosenthal, K. *Arch. für das Eisenhüttenwes*, vol. 12, 1934, p. 689.

Vogel, R. and Rosenthal, K. "Das System Eisen-Kobalt-Kobaltsilizid-Eisensilizid." *Arch. für das Eisenhüttenwes*, vol. 9, 1935, pp. 293-299.

von Jellinghaus, W. "Das System Eisen-Kobalt-Kupfer." *Arch. für das Eisenhüttenwes*, vol. 10, no.3, 1936, pp. 115-118.

Wang, C. P., Liu, X. J., Ikuo, J. L., Rouseki, O., and Ishida, K. K. "Phase Equilibria in Fe-Cu-X (X: Co, Cr, Si, V) Ternary Systems." *Journal of Phase Equilibria*, vol. 23, no.3, 2002, pp. 236-245.

Warczok, A. and Utigard, T. A. "Fayalite Reduction by Solid Graphite." *Canadian Metallurgical Quarterly*, vol. 37, no.1, 1997, pp. 27-39.

Waterstrat, R. M. "The Chromium-Platinum Constitution Diagram." *Metallurgical and Materials Transaction*, vol. 4, 1973, pp. 1585-1592.

West, D. R. F. 1982, *Ternary Equilibrium Diagrams*, 2nd edn, Chapman and Hall, New York.

Whyte, R. M., Orjans, J. R., Harris, G. B., and Thomas, J. A. "Development of a Process for the Recovery of Electrolytic Copper and Cobalt from Rokana Convertor Slag." *Advances in Extractive Metallurgy (London institute of Mining and Metallurgy)* 1977, pp. 57-68.

Witusiewicz, V. T. "Thermodynamic Properties of Liquid Alloys of 3-d Transition Metals with Metalloids (Si, C and B)." *Journal of Alloys and Compounds*, vol. 203, 1994, pp. 103-116.

Wu, R. I. and Perepezko J.H. "Liquidus Temperature Determination in Multicomponent Alloys by Thermal Analysis." *Metallurgical and Materials Transactions A*, vol. 31, February, 2000, pp. 497-501.

Yakowitz, H., Ruff, A. W., & Michaelis, R. E. *Preparation and Homogeneity Characterisation of an Austenitic Fe-Cr-Ni alloy: Special Publication 260-43*, National Bureau of Standards Special Publication, Washington D.C., 1972, 260-43.

Yan, X. and Chang, Y. A. "A Thermodynamic Analysis of the Cu-Si system." *Journal of Alloys and Compounds*, vol. 308, 2000, pp. 221-229.

Yucel O., Addemir O., Teking A., and Nizamoglu S. "Recovery of Cobalt from Copper Slags." *Mineral Processing and Extractive Metallurgy Review*, vol. 10, 1992, pp. 99-107.